Maren Johanne Mood

Reconstruction of whitewater kayak waves in Nidelva

Master's thesis in Civil and Environmental Engineering
Supervisor: Elena Pummer
June 2022

Master's thesis

NTNU
Norwegian University of Science and Technology
Faculty of Engineering
Department of Civil and Environmental Engineering

Kunnskap for en bedre verden

Maren Johanne Mood

Reconstruction of whitewater kayak waves in Nidelva

Master's thesis in Civil and Environmental Engineering
Supervisor: Elena Pummer
June 2022

Norwegian University of Science and Technology
Faculty of Engineering
Department of Civil and Environmental Engineering

NTNU
Norwegian University of Science and Technology

Abstract

Due to changes on the river bed, kayakers in Trondheim lost two popular waves. This thesis aims to reconstruct one of the kayak waves by studying the ideal hydraulic jump for whitewater kayaking. The field that is studied is the Nidelva river, in Trondheim.

A suitable wave for kayaking would be steep, and the water should have a rough surface. Therefore, it is desirable to construct an oscillating jump with a Froude number between 2.5 - 4.5.

The study investigated the correspondence between a physical and numerical model of the hydraulic jump. The physical model was built in a 1 m wide flume, and scaled 1:50. The numerical model was simulated in Open FOAM. The simulations for this experiment were done with Reynolds-Averaged Navier-Stokes (RANS) equations, utilising the k-ϵ turbulence model.

Discharge data over the last nine years have been analysed. The discharges 40, 140, 200, 289 and 400 m^3/s were chosen to represent the situation in the river and were run in the physical and numerical model. Q $=$ 40 m^3/s was too small for testing in the physical model.

A hydraulic jump was induced for all tested discharges. Comparing the different results, it appears to be several errors with the physical model. Therefore, data from the numerical model was used to calculate the weir height necessary to induce a satisfying hydraulic jump for given discharges. The calculated weir height shows that a weir with 0.82 $<$ Δh $<$ 1.42 will induce a wave for the four tested discharges with a Froude number between 2.5 and 4.5.

Further research aims to use these results to decide whether it is desired to adjust the river bed as the desired wave is established.

Keywords: Hydraulic jump, OpenFOAM, physical model, whitewater kayak

Sammendrag

Etter å ha endret elvebunnen i Nidelven mistet kajakkpadlere i Trondheim to populære bølger. Denne masteroppgaven tar sikte på å rekonstruere en av kajakkbølgene ved å studere det ideelle vannstandsspranget for kajakkpadling. Området som studeres er Nidelva, i Trondheim.

En bølge for kajakkpadling vil være bratt, og vannet bør ha en ru overflate i en ideell situasjon. Derfor er det ønskelig å konstruere et oscillerende vannstandssprang med et Froude-tall mellom 2,5 - 4,5.

Studien undersøkte samsvaret mellom en fysisk og numerisk modell av vannstandsspranget i Nidelva. Den fysiske modellen ble bygget i en 1 m bred renne, skalert 1:50. Den numeriske modellen ble simulert i OpenFOAM. Simuleringene for dette eksperimentet ble gjort med Reynolds-Averaged Navier-Stokes (RANS) ligninger, ved å bruke k-ϵ turbulensmodellen.

Vannføringer fra de siste ni årene ble analysert. Vannføringene 40, 140, 200, 289 og 400 m^3/s ble valgt for å representere situasjonen i elven og ble kjørt i den fysiske og numeriske modellen. Q = 40 m^3/s var for lav for testing i den fysiske modellen.

Et vannstandssprang ble indusert for alle vannføringer. Ved å sammenligne resultatene, ser det ut til å være flere feil ved den fysiske modellen. Derfor ble data fra den numeriske modellen brukt til å designe overløpshøyden som er nødvendig for å indusere et tilfredsstillende vannstandssprang for gitte vannføringer. Den beregnede overløpshøyden viser at et overløp med en høyde på 0,82 $< \Delta$h $<$ 1,42 vil indusere en bølge med et Froude-tall mellom 2,5 og 4,5 for de fire testede vannføringene.

Videre forskning tar sikte på å bruke disse resultatene til å justere elvebunnen for å etablere den ønskede bølgen. Elvebunnen bør optimaliseres i den numeriske modellen før den fysiske modellen brukes som prototype.

Nøkkelord: Vannstandssprang, OpenFOAM, fysisk modell, elvekajakk

Acknowledgements

This research would not have been possible without the great support of many.

I wish to express my gratitude to my supervisor, Elena Pummer. Thank you for your feedback and guidance. It has been a pleasure combining leisure activities and hydraulics.

My deepest gratitude also to Asli Bor Türkben, who has guided and supported me during the physical experiments. Thank you for everything you have shared of your knowledge. I have really enjoyed working with you.

I want to thank NTNU for the laboratory facilities and Trondheim kommune for financing the physical model. Thank you for the opportunity.

Jeg vil gjerne takke Thai Mai og Geir Tesaker for støtte på lab. Takk for all hjelp, og svar på alle spørsmål, selv de dumme. Prosjektet hadde ikke latt seg gjennomføre uten deres hjelp.

En stor takk til Nils Solheim Smith som har hjulpet med faglige diskusjoner og den numeriske delen av oppgaven. Det har vært til stor hjelp.

Jeg er takknemlig for all kunnskapen jeg har fått tilegne meg på NTNU. Vel så takknemlig er jeg for mulighetene H.M. Aarhønen - Bygnignslinjens forening og UKA har gitt meg. Her har jeg fått ansvar, tillitt og mulighet til personlig utvikling. Studietiden hadde ikke vært den samme uten studentfrivilligheten.

Tusen takk til kjæresten min, Tor Henry, for støtte. Takk for at du har vist en entusiasme uten like for prosjektet. Jeg er veldig takknemlig.

Takk til familien min som har støttet meg. Selv om de er langt unna føles de alltid nærme. Takk for at dere har engasjert dere i min studietid.

Sist vil jeg takke min beste venn og familie de siste seks årene, Ida. Du har gjort hverdagen i Trondheim til en fryd. Tusen takk for støtte i tunge perioder og fjasing på de gode dagene. Min tjoms!

Contents

List of figures

List of tables

1 Introduction

Hydraulic engineering has been a central part of society since its inception. Since the earliest societies, water has been an essential factor when settling. Historically, humans have chosen to settle close to rivers because of agricultural and domestic water supply (Fang and Jawitz, 2019). Even though our primary needs induce the choice of settling close to water, as a side product, hydraulic engineering has also been used in the service of aesthetic design and leisure activities. There are several examples of how earlier societies used water for cultural use; there are ruins of decorative fountains from ancient Greece. In Vietnam, traditional theatre uses water as the main element (Gaboriault, 2009).

The kayak is also an example of ancient hydraulic engineering. The Inuits and Aleuts have been practising the kayaking skill since the first migrants settled in Eastern Arctic around 1250 AD (Walls, 2016). The skill has rapidly grown from an essential part of the Inuit lifestyle for hunting and transport. Today advanced hydraulic engineering has been used to optimize kayaks' speed, design, and equipment used in competitions and championships, such as the Olympic Games.

As the world keeps getting industrialized, we have a greater need for recreational activities, and there are constant developments in water sports. The attainment of the skill of Eskimo roll, which was first completed by a European in 1927 but is an old Inuit skill, brought a new dimension of safety to whitewater kayaking (Nickel, 1996). Today this technique is taught as a primary safety method, making kayaking more available.

Because people settled close to water resources years ago, several European cities have a river in the city centre. In several cities, people use these city rivers for water sports. Also, in Trondheim, Nidelva is used for recreational activities. Several sports teams use the river to practice sports, like whitewater kayaking and surfing.

Before 2017, there were primarily two waves in Nidelva that stood out among whitewater kayaking enthusiasts; under the Sluppen bridge and further upstream: the Drop of Death. Elevation differences in the river bed would induce a hydraulic jump in both these areas. This type of wave dissipates a significant amount of energy, creating severe erosion on the river bed and bridge piers. Because of this challenge, the area was filled with course material to minimize the scouring effect. The filling changed the flow pattern in the river, and the kayakers lost two popular waves.

This thesis aims to study the possibility of reconstructing the river's kayak wave. The kayak wave should be optimized as a hydraulic jump for a wide range of flows and must satisfy the shape conditions for whitewater kayaking. The possibilities of reconstructing the kayak wave will be addressed according to the following research objectives: exploring literature on the topic, simulations in a numerical model, building a physical model, and a recommendation for placing a weir.

The thesis aims to give a recommendation for the changes needed to be made to reconstruct one of the whitewater kayak waves in Nidelva for a wide range of flows.

2 Literature review

2.1 Physical models

Before the Olympic Games in Athen in 2004, the slalom water course for kayaking was modelled mathematically. To validate the model Christodoulo et al. (2004) built a physical model. These results led to significant modifications of the initially suggested water course. It is concluded that a 1D mathematical model is not sufficient for complex flows.

Lemmin and Rolland (2005) used an ADV in hydraulic research in two laboratory open channels with smooth and gravel beds. The measurement results compare favourably with established laws, for instance, velocities and turbulence. The ADV instrument is a good tool for hydraulic research.

Sweet (2009) used the patent from McLaughlin Whitewater Design Group called Waveshaper to generate waves in a 1:4 scaled physical model. The Waveshaper's use of adjustable vanes induced a robust non-retentive wave for a great variation of flows.

Babaali et al. (2015) compared a numerical simulation of a hydraulic jump with a built physical model. The numerical model was conducted in the commercial software Flow3D and was applied to solve the Navier-Stokes equation. The standard k-ϵ and RNG model was used to study the turbulence. The physical model and CFD results showed promising results, and Babaali recommends further comparisons of numerical and physical models to understand the flow situation better.

Adjustable flaps have been shown to stabilise the surf wave because they will decrease tailwater flow depths. Fuchs (2017) conducted physical laboratory experiments to quantify the effect of adjustable flaps on generated river surf waves. In a small flume, parameters such as discharge, flow depth, drop height, flap length, and angle were varied until favourable surf wave properties were found. The flap significantly increases the wave height for most discharges and mounting of flaps. However, flaps with a slight angle led to a wave height reduction.

Asiaban et al. (2021) introduced a new mechanism for inducing a hydraulic jump on flat river beds. The mechanism is a construction consisting of a ramp, downfall, transition and finally, a kicker. The structure is found by adjusting a numerical model before the physical model is built as a prototype.

2.2 Numerical simulations

Famiglietti (2010) did a numerical simulation where the aim was to create a kayaking-surfing standing wave for a wide range of flows on the Isar River in Munich, Germany. The geometry was modelled using HEC-RAS and Flow 3D. The thesis reached its' aim of constructing a wave by using two different geometries; one that gives a wave with Froude number 1.7 for each discharge and one geometry that gives a wave for Froude numbers over 1.7 for two hundred days per year. For further research, it is recommended to check the numerical simulations against a physical model.

Borman et al. (2014) used a numerical model of three-dimensional transient two-phase RANS CFD-VOF to predict the position of hydraulic jumps within a complex geometry and flow environment. The environment tested was a recreational whitewater course with significant variations in flow rates. The results demonstrated that this type of CFD reliably can predict hydraulic jumps in open channel flow conditions.

Bayon and López-Jiménez (2015) did a numerical model of a hydraulic jump in an open channel. The study addressed the increase of shear stress because of hydraulic jumps and how this affects erosion on the river bed. Turbulence was modelled using RANS. Bayon created a model using OpenFOAM that can be used to study hydraulic jumps with complex geometries.

2.3 Field experiments

Lane et al. (1998) wrote a paper describing the use of instruments for determinating three-dimensional flow velocities in rivers; the ADV included a method for positioning and orienting such measurements relative to the local coordinate system to relate flow velocity vectors with the bed and water surface. With this discovery, it was possible to create velocity profiles of the river area.

Laboratory experiments and field investigations Fujita et al. (1998) showed that the LSPIV is a reliable and economically efficient flow diagnostic tool. The output of the

LSPIV analysis is a velocity profile that can be used to calculate, for instance, the Froude number.

Lester et al. (2012) did his master thesis of landscape architecture about Whitewater park design. He identified seven design principles for constructing whitewater through interviews with whitewater designers. The conclusion is that adjustability is the essential principle to allow stakeholders to influence the decisions.

3 Theory

3.1 Whitewater kayaking

Whitewater kayaking is not much like peaceful ocean kayaking. After dialogue with different kayak enthusiasts from among others, Trondheim kayakklubb, it is stated that practising whitewater kayaking is about finding a perfect wave. In the wave, the kayakers will perform other acrobatics or technical moves. Therefore, river kayaking is about finding a perfect wave where the kayaker can stay and play for a more extended time.

Eddies are essential to do the same wave over again. When doing a wave, kayakers aim for eddies from hydraulic jumps. If they manage to flow with the eddies, they will get some time to rest and the possibility to do the same wave again. This environment, a steep wave with a rough water surface and eddies, is the ideal kayak situation.

3.1.1 The hydraulic jump

A hydraulic jump occurs when the flow regime changes rapidly from supercritical to subcritical. The rapid change of flow regimes dissipates a significant amount of energy. Hydraulic jumps are therefore used either as energy dissipation below hydraulic structures or are unwanted because they contribute to erosion on the river bed. (Ghaderi et al., 2020). In the case of whitewater kayakers, hydraulic jumps are highly wanted. Figure 3.1 shows an example of a hydraulic jump.

Figure 3.1: A hydraulic jump in the Drop of Death, Nidelva, taken 23. February 2022. Q = 102.4 m^3/s

Hydraulic jumps occur in different shapes, depending on, i.e. cross-section, discharge, bathymetry and bed roughness. The different hydraulic jumps are best expressed by the inlet Froude number (Chow, 1959).

- **Pre-jump Fr=1**

  To induce a hydraulic jump, the flow must transition from supercritical to subcritical flow; it then transits through the critical flow where the Froude number is 1. This jump is the smallest and has a smooth water surface.

- **Undular jump 1<Fr<1.7**

  The surface of the water is rotating, creating small, steady waves. There is little energy loss in this wave, practically zero. Illustrated in figure 3.2.

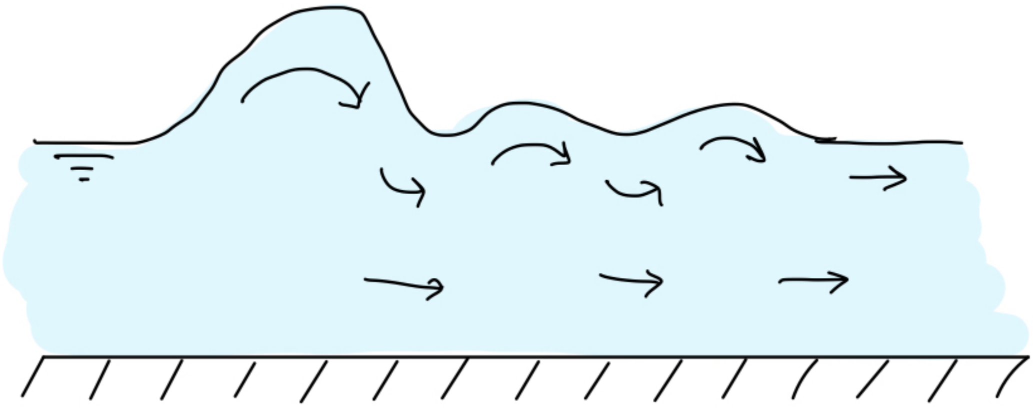

Figure 3.2: Illustration of an Undular jump (Chow, 1959)

- **Weak jump 1.7<Fr<2.5**

  Small rollers are created on the water surface. Downstream of the jump, the water surface is smooth. This jump occurs when the velocity of the water is rather low. Illustrated in figure 3.3.

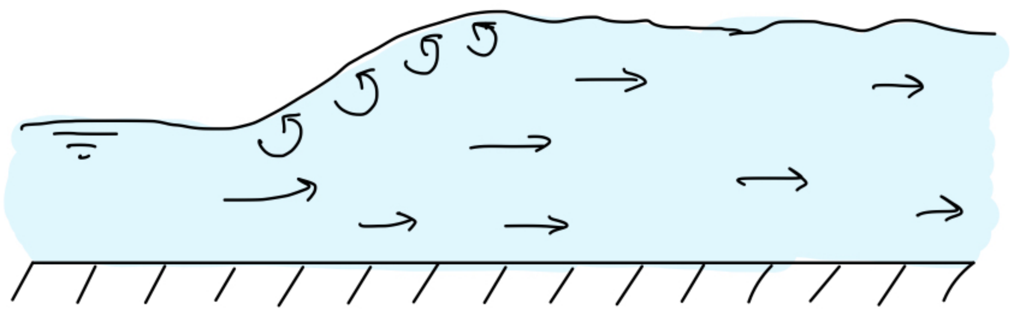

Figure 3.3: Illustration of a Weak jump (Chow, 1959)

- **Oscillating jump 2.5<Fr<4.5**

  Oscillating jets enter the jumps; this creates large waves of irregular periods. Downstream of the jump, relatively large waves are created, making a rougher water surface. Illustrated in figure 3.4.

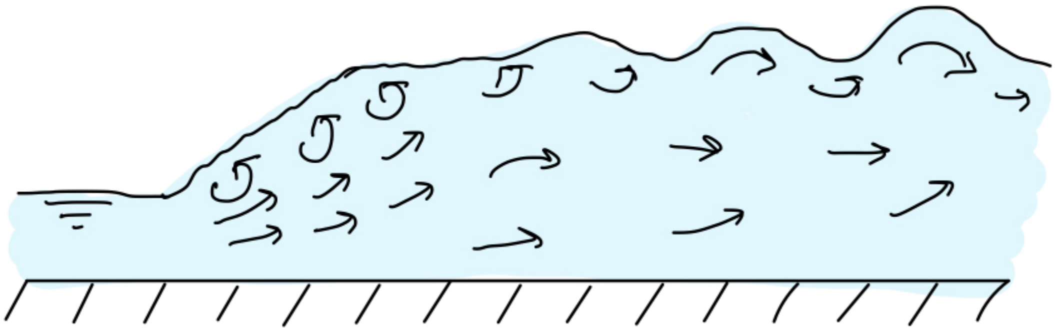

Figure 3.4: Illustration of an Oscillating jump (Chow, 1959)

- **Steady jump 4.5<Fr<9**

  These waves are created in stable conditions, a clear static hydraulic jump. The wave creates an energy dissipation. The water surface is rough. Illustrated in figure 3.5.

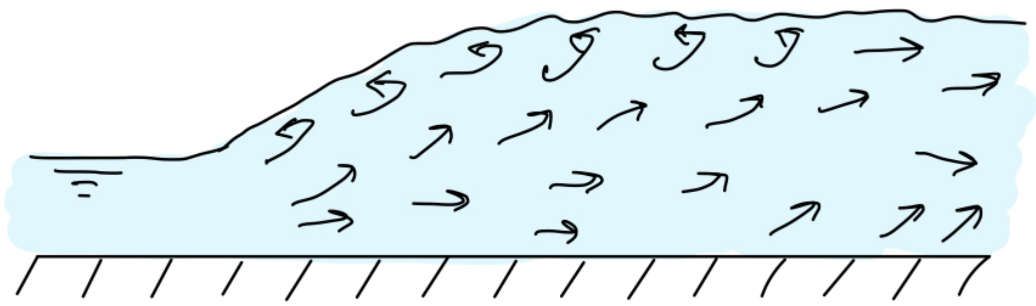

Figure 3.5: Illustration of a Steady jump (Chow, 1959)

- **Strong jump 9<Fr**

  The water surface is rough, and the waves continue for a long distance downstream of the jump. Therefore, this substantial jump creates strong forces at the bed bottom and is often to be avoided because of bed erosion. Special about this jump is that the water flow changes from supercritical to subcritical in a shorter length than the other jumps. Illustrated in figure 3.6.

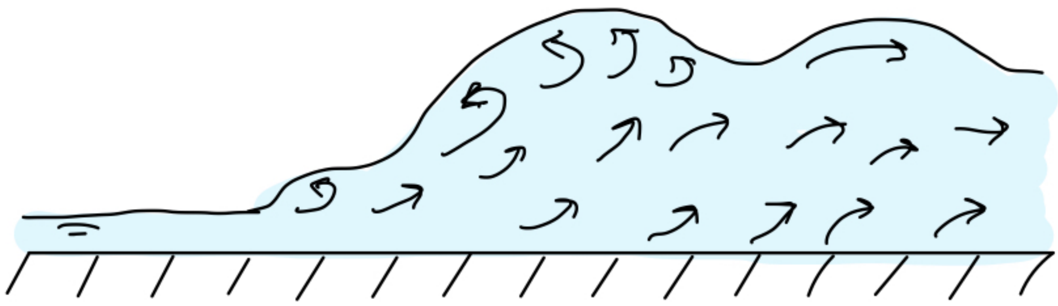

Figure 3.6: Illustration of a Strong jump (Chow, 1959)

The kayak is first to be analyzed when studying the perfect kayak wave. Unlike ocean kayaking, the kayaks used for river kayaking are short. Therefore, these kayaks are suitable for steeper waves than surfers, with longer boards. The undular jump is the steepest of the waves, but the water surface is too smooth downstream of the jump (Chow, 1959). Therefore, the desired wave is the oscillating jump. This wave is steep, and downstream it has several smaller waves and a rough water surface, a whitewater effect. Consequently, it is ideal for constructing a wave with a Froude number between 2.5 and 4.5 that will induce varied discharges in Nidelva.

3.1.2 Standing surfing waves in Europe

The popularity of surfing and kayaking is growing, as is the availability of standing surfing waves. Across Europe, several countries construct multiple standing surfing waves in city centres by changing the river bed or introducing adjustable weirs in the rivers. This method has been implemented in several inland countries, where the shoreline and surfing waves are distant. In Nidelva, it would be ideal to change the river bed to induce a hydraulic jump.

For some years, leisure hydraulics have been practised in great pools where a mechanical device or a pump will induce the waves which travel across the pool. This solution gives an environment and a water surface close to what a surfer would experience along the shore. An example of this is shown in figure 3.7 where an artificial surf lake is built in

Queensland, Australia.

Figure 3.7: Photo of a artificial surf lake in Queensland (SurfLakes, 2020)

It is a popular method, but the challenge is to dedicate enough area for these significant installations. Especially in urban areas, it is desired to create area-efficient solutions. As a result, the concept of surfing on a simple standing wave was created. These waves can be made in artificial environments using the natural components and slope of the river.

International Association for Hydro-Environment Engineering and Research's member Magazine, Hydrolink, dedicated in February 2018 an issue to leisure hydraulics, focusing on the standing surfing waves. These installations, made to induce the standing waves, have the same purpose as this thesis; to create a standing kayak/surfing wave for a wide range of flow by using the natural components in the river. In addition, some of the solutions also include a weir or a ramp that is placed in the river.

Figure 3.8: Photo of surfers on the Eisbach river. Photo from Steven A. Martin (Martin, 2019)

The February issue of Hydrolink describes several solutions and approaches for creating an artificial leisure hydraulic area. One of the most well-known is the Eisbach River in Munich, Germany, as shown in figure 3.8. In this river, a standing wave of 1 m forms. The waveforms are due to optimizing the up-and downstream characteristics and the river bed geometry, which adjusts itself according to the discharge (Fuchs, 2017). Since its installation in 1980, the wave has become a popular attraction for surfers and tourists. Because of this success, several European cities have adopted this form of constructing a standing surf wave in the middle of the town. Projects like this are also brought up in Norway. Akerselva, Numedalslågen and Evje are examples of places where studies are made to examine the possibilities of constructing kayak waves. Unfortunately, these were not available for comments.

3.2 Study area

The river examined in this thesis is Nidelva, located in Trondheim, Norway, as shown in figure 3.9. The river's discharge varies greatly because three upstream hydropower stations regulate it; Øvre Leirfossen, Nedre Leirfossen and Bratsberg power station. The river originates in Trondheimsfjorden, approximately 8,7 km north of the studied area. The tide affects the northern part of the river, closest to the fjord. However, the tide does not influence the water depth in the cross-sections examined in this thesis because of the far distance to the fjord.

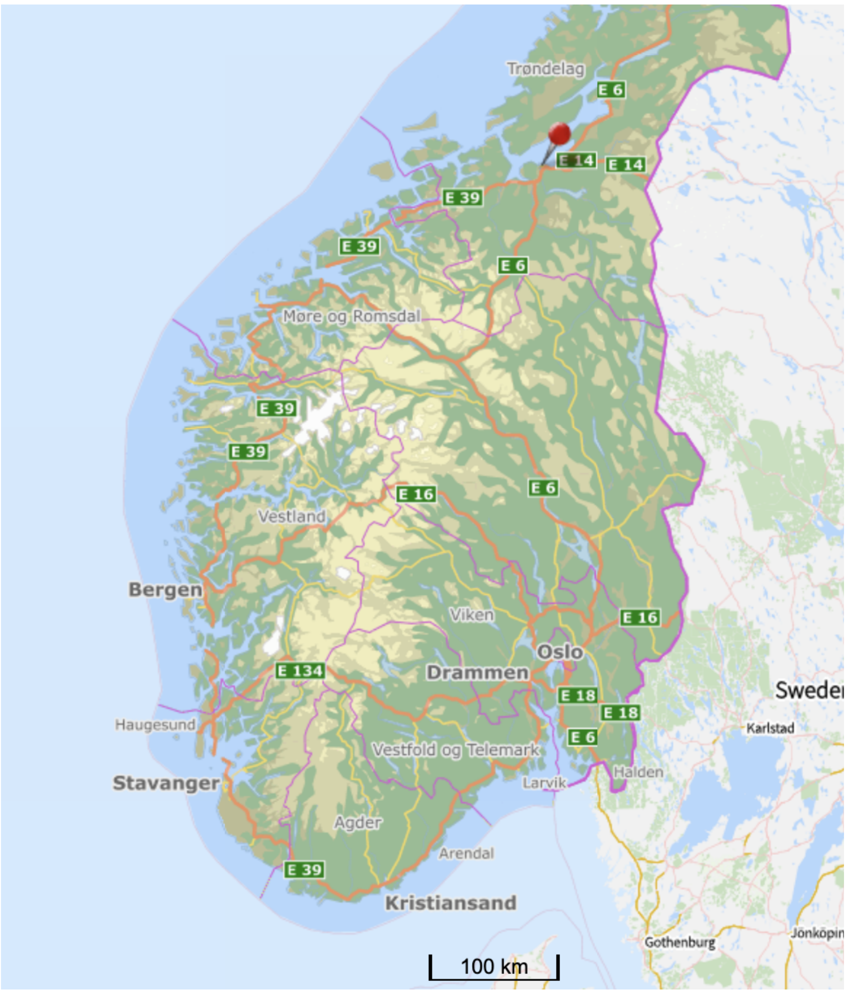

Figure 3.9: The placing of the study area can be seen as the red dot on the map, Nidelva in Trondehim.

3.2.1 Discharge

Because of the regulation from the upstream hydropower plants, the discharge in Nidelva highly varies. According to Statkraft, which controls the plants and monitors the river, there is no "normal" discharge in the river. The day-to-day differences create a challenge when designing a weir whose purpose is to generate a hydraulic jump. Therefore, the weir, or river bed, must satisfy conducting a wave for several discharges. By analyzing discharge data from the last nine years, it is possible to get a mapping of the discharges that dominate the river. The dominated discharge is found by looking at the 40th percentile every day for the last nine years. The 40th percentile corresponds to approximately 150 days a year. These values are presented in figure 3.10, while the minimum, average and maximum of these values are presented in table 3.1.

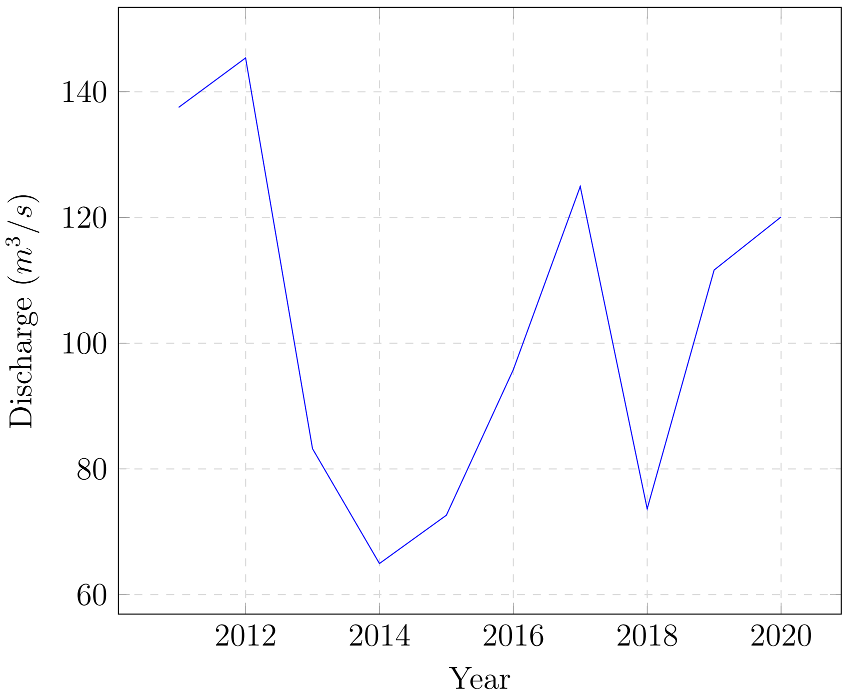

Figure 3.10: Over a perspective of nine years, this represent the 40th percentile of discharge in Nidelva.

Variation in 40th percentile	
Value	Discharge [m^3/s]
Q_{min}	64.95
Q_{middle}	102.98
Q_{max}	145.38

Table 3.1: Flow duration in Nidelva, presented by minimum, middle and maximum of the 40th percentile values the last nine years.

3.2.2 Changes in river bed and possible solutions

The flow changes due to the erosion under the bridge are represented in a report from Sweco. Before the filling, the waves in the area attracted many people. In 2015 the Norwegian Championship in slalom kayak was arranged by Trondheim kajakklubb in this area. According to Sweco, three main changes in the rived bed affect the hydraulic jumps.

- The depth between the bridge pillars is decreased. The rived bed has been increased 0.5 - 1.0 m.
- The difference between before and after the filling can be up to 3 m.
- Before the filling, there was a variation in the depth between the pillars. After the filling, they are all the same.

It is possible to construct an adjustable weir that can be modified for different discharges to facilitate the hydraulic jump. These weirs are a popular solution for similar installations in Southern Europe (Aufleger and Neisch, 2018). This type of weir will be too complex to build and expensive for this project. The preferred solution will be to build a classic weir. Another solution is to remove sediments downstream of the bridge to increase the water depth, but this can be risky considering erosion on the river bed. Because of erosion challenges, Trondheim kommune has forbidden removing sediments under the bridge. The preferred solution is, therefore, to construct a weir. The shape of the weir will be found and optimized by analyzing the water stream in a physical and numerical model of Nidelva.

3.2.3 Popular whitewater kayak waves in Nidelva

The kayakers from Trondheim kajakklubb have suggested several areas in the river where a kayak wave is desired.

Figure 3.11: Screenshot of the relevant area between Sluppen and Kroppan bridge in Nidelva.

The first solution is to create a weir downstream of the Sluppen bridge, as shown in figure 3.11 and 3.12. The width of the river channel in this area is 62.3 m, and the distance between the bridge piers is approximately 10 m.

Figure 3.12: Downstream Sluppen bridge, taken 23. February 2022.

Further upstream of the Sluppen bridge, downstream of Kroppan bridge, there is a popular kayak area called "Dødens drop", which translates to "The Drop of Death". A kayak wave in the shape of a hydraulic jump already exists in this area, as shown in 3.13. Before the filling under the bridge, the wave was even steeper and better fitted for whitewater kayaking than it is today. After the filling under the bridge, the tailwater of the hydraulic jump rose and downscaled the jump's effect. Today, the kayakers are still enthusiastic about the wave in the Drop of Death, but it is still possible to optimize the wave, make it even stepper, and adjust it to the kayaker's desires.

Figure 3.13: "The Drop of Death", taken 23. February 2022.

In addition to these two river areas, several smaller drops and rapids can be examined and modelled. For this thesis, "the Drop of Death" will be the main study.

3.3 Hydraulics

A numerical model will be simulated to study and validate the desired wave, and a physical model will be built. This subchapter explains the hydraulic principles on which the models are based.

3.3.1 The continuity equation

The quantity of water flow will be constant as water flows down a river because it is an incompressible fluid. Therefore, the water must adjust its velocity to be compiled to changes on the river bed and cross-section changes. Since the quantity is constant, so is the product of the velocity and the cross-section area.

$$Q = UA \tag{3.1}$$

This equation describes the conservation of mass and forms the basis for many further calculations in hydraulics. It is called the continuity equation. (Chow, 1959)

3.3.2 Froude number

The Froude number is very relevant when looking at hydraulic jumps. The number is defined as the square of the ratio of the flow's internal and external forces. U is the flow velocity, and g and y are the gravitonial influence and the water depth.

$$Fr = \frac{U}{\sqrt{gy}} \tag{3.2}$$

The Froude is dimensionless and represents the effect of gravity on the state of flow in a stream (Chow, 1959). The number determines the flow regime, whether subcritical, critical or supercritical. The number also determines the direction the disturbances travel. Therefore, the Froude number determines what type of hydraulic jump will occur.

- Fr<1 sub-critical flow regime
  The flow is downstream controlled
- Fr=1 critical flow
- Fr>1 supercritical flow
  The flow is upstream controlled.

3.3.3 Reynolds number

The Reynolds number represents the ratio of internal forces to viscous forces within a fluid. When calculating the Reynolds number, the internal forces are the product of the hydraulic radius and the fluid velocity, while the viscous forces are the kinematic viscosity of the water. The ratio determines whether the flow is turbulent or laminar (Chow, 1959).

- Re > 2000 = Turbulent flow
- Re < 500 = Laminar flow

- All values between are transition stages

$$Re = \frac{UR_h}{v} \tag{3.3}$$

3.3.4 Manning's formula

Manning's equation is the most common formula for average velocity in a channel with uniform flow. (Olsen, 2017)

$$U = \frac{1}{n} R_h^{2/3} I^{1/2} \tag{3.4}$$

Here, n is Manning's coefficient, representing the roughness of the channel bed. R_h is the hydraulic radius, which is the cross-section area divided by the wetted perimeter. Lastly, I is the slope of the bed.

3.3.5 Flow over weir

The Norwegian directorate regarding rivers and water distribution, subordinate to the oil and energy ministry, has published guidelines for designing weirs. (NVE, 2020) For the weirs, the discharge is to be calculated on the following method:

$$Q = CL_{eff} H_O^{3/2} \tag{3.5}$$

Here the following parameters are:

- Q is the total water capacity, discharge
- C is the weir coefficient, which is calculated from several empirical formulas. Here, H is the water height above the weir, and B is the width of the weir.
- L_{eff} is the efficient length of the weir. Which is the length when side contraction is taken into account.
- H_O is the designed water height above the weir

3.3.6 The height of hydraulic jump

The water level is higher downstream than upstream the hydraulic jump. (Chow, 1959) defines this height ratio and relates it to the Froude number. The ratio is expressed like this:

$$\frac{y_2}{y_1} = \frac{1}{2}(\sqrt{1 + 8Fr^2} - 1) \tag{3.6}$$

3.3.7 Critical flow

When a hydraulic jump is induced, the water transitions from super to subcritical flow. This transmission forces the water through a critical flow situation. Therefore, identifying the critical water depth and velocity can indicate whether or not a hydraulic jump will induce.

The critical flow depth is derived from the sum of energy, also called the specific energy height of water flow in a channel, and is expressed:

$$y_c = \sqrt[3]{\frac{q^2}{g}} \tag{3.7}$$

By using the continuity equation, 3.1 on this equation, 3.7 the critical velocity can be expressed:

$$u_c = \sqrt{g y_c} \tag{3.8}$$

3.3.8 The Energy equation

Looking at water flow in an open channel, there are two types of energy; Kinematic energy due to the water velocity and pressure energy due to the weight of the water and the water depth. (Olsen, 2017)

$$E = E_k + E_p = y + \frac{u^2}{2g} \tag{3.9}$$

Over a weir, the water will go through a critical flow regime before transitioning to supercritical flow downstream. (Olsen, 2017) Therefore, the energy over the weir can be defined as the critical energy, which is denoted:

$$E_{weir} = E_c = \frac{3}{2} y_c \tag{3.10}$$

As energy is conserved, the energy over a weir will be the same downstream. The different parameters are illustrated in figure 3.14, meaning that

$$E_1 = E_c + \Delta h \tag{3.11}$$

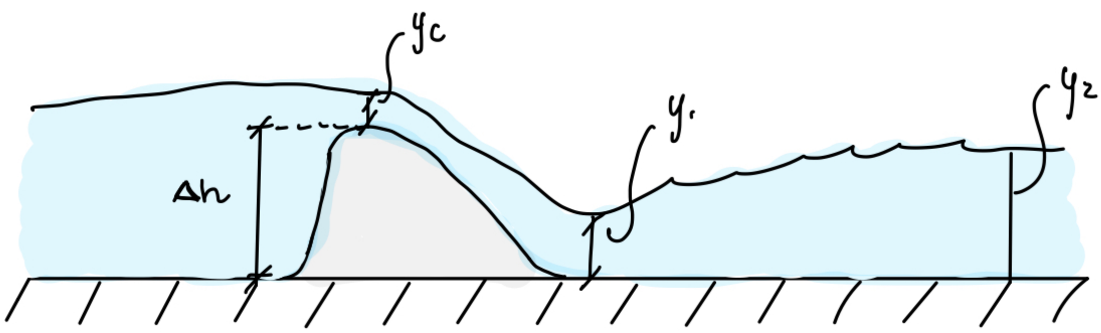

Figure 3.14: Illustration of the different parameters occurring in the energy equation.

3.3.9 Bed shear stress

The hydraulic jump is often avoided because of its energy dissipation and erosion challenges. The bed shear stress is calculated to validate a wave's scouring effect on the river bed. This is done by calculating the forces induced on a particle in the water flow (Olsen, 2017). The forces induced are illustrated in 3.15.

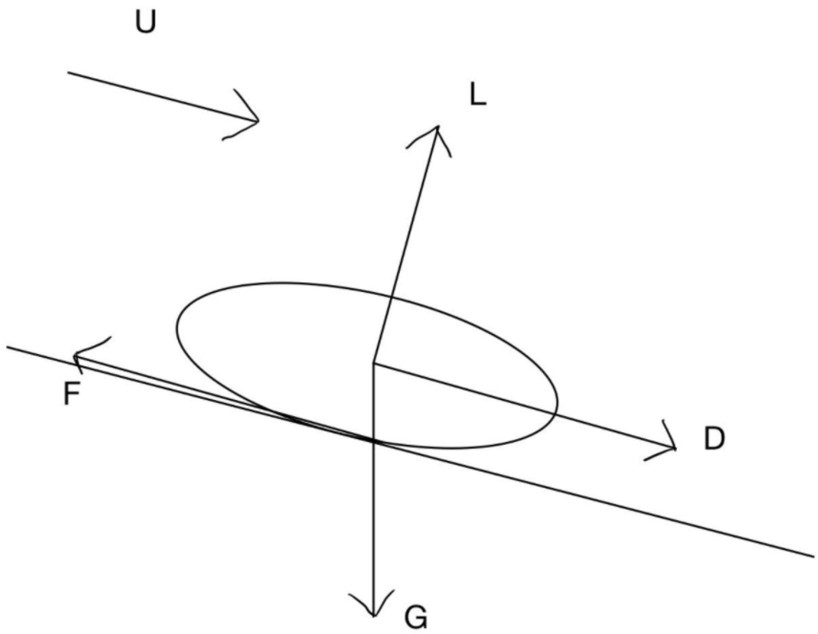

Figure 3.15: Illustration of the different forces working on a particle in the river. There is assumed that the particle has a diameter, d.

There are four forces induced on the particle:

- Drag forces, D

$$D = k_2 \tau_0 d^2 \tag{3.12}$$

  The drag force is the water suction and pressure parallel with the river bed. Here τ_0 is the bed shear stress.

- Friction forces, F

$$F = (G - L) tan(\alpha) \tag{3.13}$$

- Gravity forces, G

$$G = k_1 (\rho_s - \rho_w) g d^3 \tag{3.14}$$

- Lifting forces, L

$$L = k_3 \tau_0 d^2 \quad (3.15)$$

The lifting force is due to the difference in pressure because of local velocity differences in the sediment.

The friction force works parallel with the river bed. The α is the angle of repose of the particle.

The coefficients k_1, k_2 and k_3 are coefficients for the geometry for different particles. By combining the equations of the forces working on the particle and the equilibrium of forces along the direction of the bed, the expression of Shields number is derived.

$$F = D \quad (3.16)$$

$$tan(\alpha)[k_1 g(\rho_s - \rho_w)d^3 - k_4 \tau d^2] = k_3 \tau d^2 \quad (3.17)$$

The equation is solved for d to find the diameter of the sediment that will be eroded.

$$d = \frac{\tau_c}{g(\rho_s - \rho_w)[\frac{k_1 tan(\alpha}{k_3 + k_4 tan(\alpha}]} = \frac{\tau_c}{g(\rho_s - \rho_w)\tau^*} \quad (3.18)$$

The parameter τ^* was originally found experimental by Shields (Olsen, 2017) and can be found in Shields diagram 3.16:

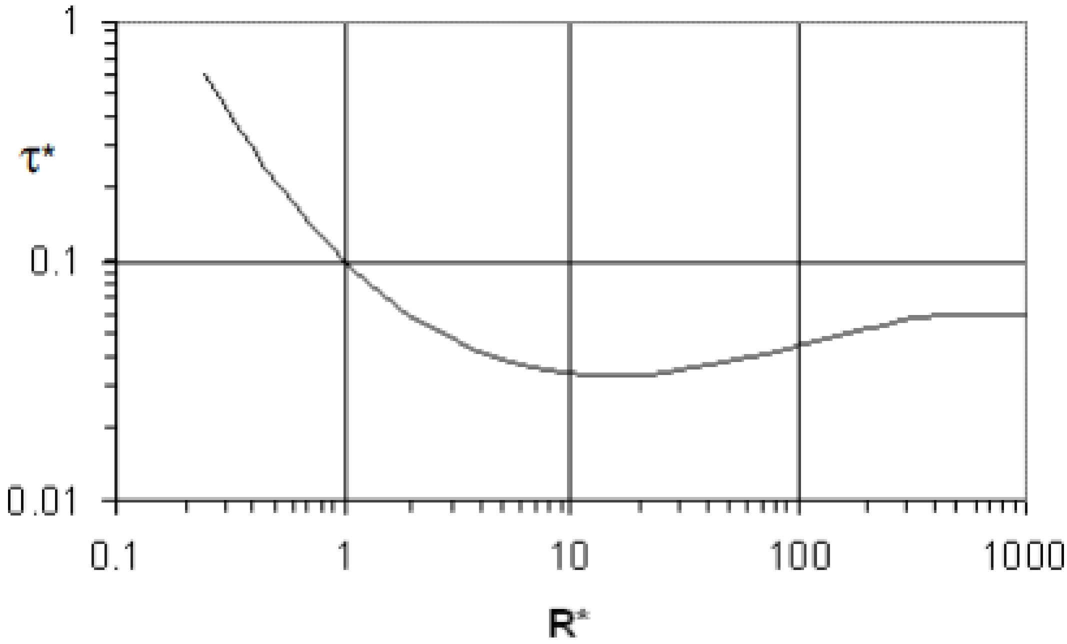

Figure 3.16: Shields diagram giving the critical shear stress for movement of a sediment particle from Numerical Modelling and Hydraulics (Olsen, 2017)

The x-axis in the diagram represents the Reynolds number and is denoted as:

$$Re_* = \frac{v_* d}{v} = \frac{d\sqrt{\frac{\tau}{\rho_w}}}{v} \tag{3.19}$$

Here, v_* is the sheer velocity of the water, d is the sediment diameter, and v is the viscosity of water. v_* can be described as the square root of the ratio between the bed shear stress, τ and the density of water. The bed shear stress is relevant for solving this equation and is expressed as:

$$\tau = \rho g h I \tag{3.20}$$

The critical bed shear stress can be calculated from Equation 3.18 when the diameter of the sediments is known. Then it can be validated whether there will be erosion or not on the river bed. The critical bed shear stress results can be compared to actual bed shear stress, equation 3.20 and it can be validated whether there will be erosion or not.

3.3.10 The Navier-stokes equation

The Navier-Stokes equation describes the water velocity, U, in the river, and is expressed:

$$\frac{\partial U_i}{\partial t} + U_j \frac{\partial U_i}{\partial x_j} = \frac{1}{\rho} \frac{\partial}{\partial x_j} (-P\delta_{ij} + \rho v(\frac{\partial U_i}{\partial x_j} + \frac{\partial U_j}{\partial x_i}) \tag{3.21}$$

P is the pressure, t is the time, v is the kinematic energy, ρ is the water density and δ_{ij} is the Kronecker delta. The Kronecker delta is 0 unless when i=j, then $\delta_{ij} = 1$.

Because the flow in the river is turbulence, there is a need to use Reynold's averaged version of the Navier-Stokes equation, also called the RANS equation (Olsen, 2017).

Firstly, assumption of incompressible Newtion fluid is made:

$$\frac{\partial u_i}{\partial x_i} = 0 \tag{3.22}$$

The velocity is then divided into a fluctating value u and the average value U. These parameters are intersteted in 3.21. By simplifiing the equation, the Navier-stokes for turbulence flow is expressed:

$$\frac{\partial U_i}{\partial t} + U_j \frac{\partial U_i}{\partial x_j} = \frac{1}{\rho} \frac{\partial}{\partial x_j} (-P\delta_{ij} + \rho \bar{u_i} \bar{u_j}) \tag{3.23}$$

The new term, to the right in 3.23 is Reynold's stress term:

$$-\rho \bar{u_i} \bar{u_j} = \rho v_T (\frac{\partial U_i}{\partial x_j} + \frac{\partial U_j}{\partial x_i}) - \frac{2}{3} \rho k \delta_i j \tag{3.24}$$

Here v_T is the eddy-viscosity. Inserting 3.24 in 3.23, the RANS equation is derived.

$$\frac{\partial U_i}{\partial t} + U_j \frac{\partial U_i}{\partial x_j} = \frac{1}{\rho} \frac{\partial}{\partial x_j} (-(P + \frac{2}{3} k)\delta_{ij} + \rho v_T (\frac{\partial U_i}{\partial x_j} + \frac{\partial U_j}{\partial x_i}) \tag{3.25}$$

There is a convective and transient term on the right side, and on the left, there is a pressure term, a diffusive term and the stress term derived from Reynold's stress term.

The k in this equation represents the kinetic energy. To solve this equation, there is a need for a turbulence model.

3.3.11 The k-ϵ turbulence model

The most commonly used turbulence model is the k-ϵ model (Jones and Launder, 1973). This model can be used to solve the stress term in 3.25. The eddy-viscosity is by the k-ϵ model expressed as:

$$v_T = c_\mu \frac{k^2}{\epsilon} \tag{3.26}$$

k is here the kinetic energy, which is defined as:

$$k = \frac{1}{2}\bar{u_i}\bar{u_j} \tag{3.27}$$

k is modelled by

$$\frac{\partial k}{\partial t} + U_j \frac{\partial k}{\partial x_j} = \frac{\partial}{\partial x_j}(\frac{v_T \partial k}{\sigma_k \partial x_j}) + P_k - \epsilon \tag{3.28}$$

where P_k is expressed as:

$$P_k = v_T \frac{\partial U_j}{\partial x_i}(\frac{\partial U_j}{\partial x_i} + \frac{\partial U_j}{\partial x_j}) \tag{3.29}$$

The dissipation of k is denoted ϵ, and the expression for the k-ϵ model is:

$$\frac{\partial \epsilon}{\partial t} + U_j \frac{\partial \epsilon}{\partial x_j} = \frac{\partial}{\partial x_j}(\frac{v_T \partial \epsilon}{\sigma_\epsilon \partial x_j}) + C_{\epsilon 1}\frac{\epsilon}{k}P_k + C_{\epsilon 2}\frac{\epsilon^2}{k} \tag{3.30}$$

The different constants that are being used in this model are the following (Olsen, 2017):

- $c_\mu = 0.09$
- $C_{\epsilon 1} = 1.44$
- $C_{\epsilon 2} = 1.92$
- $\sigma_k = 1.0$
- $\sigma_\epsilon = 1.3$

4 Modelling of the hydraulic jump

The hydraulic jump will only occur under a flow regime that transitions from super to subcritical. There are several ways to achieve this essential flow transition; one option is to increase the subcritical depth by removing sediments in Nidelva. Because of the challenges of scouring the river bed, Trondheim kommune has forbidden removing sediments under the bridge. There might be possible to remove sediments and increase the water depth by the Drop of Death because it is placed upstream of the bridge. However, it is desired to look most into decreasing the supercritical flow depth.

The decrease can be done by placing a weir on the river bed, illustrated in figure 4.1. The weir will force a supercritical flow. The water will transition through critical flow during the shut of the weir and eventually transition to subcritical flow as the depth increases.

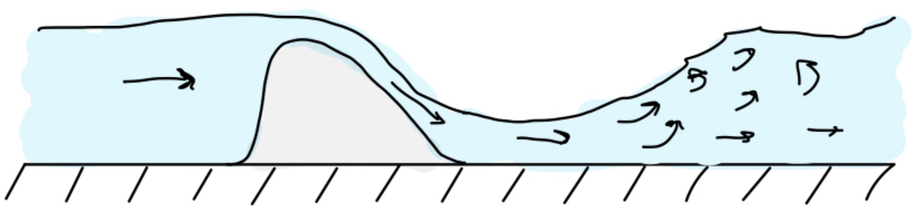

Figure 4.1: Illustration of a weir forcing the flow regime to transfer from supercritical to subcritical.

If the sub and supercritical water depths ratio are insufficient, a weir is essential to force a hydraulic jump (NEH, 2007). The main part of the experiment will be about monitoring how the hydraulic jump behaves and is induced for different water discharges. Secondly, a weir is modelled in the numerical model to examine how decreasing supercritical water depth will improve the hydraulic jump. The measurements that will be made are visual monitoring, velocity and depth measurements, and camera documenting.

4.1 Calibration

In 2020 Sweco Trondheim was engaged in a project examining and measuring the area around the Sluppen bridge as a mapping of the consequences of the filling in the river. They, therefore, conducted water depth measurements by the Drop of Death. The measurements were made right under the bridge over the drop. Their results are presented in table 4.1.

Q Nidelva	Q Drop of death	Water depth
289 m^3/s	67 m^3/s	2 m

Table 4.1: Measurements made by Sweco in 2020. Q Nidelva is collected from sildre.no

These data will be used to calibrate the physical and numerical model. As the table 4.1 shows, there is a difference between the total discharge in Nidelva and the quantitative water that flows through the Drop of Death. The ratio between these two discharges has been used when calculating the discharge over the Drop of Death for other discharges scenarios in Nidelva.

4.1.1 Discharge

To validate the assumptions made by looking at the 40th percentile of the discharge over the last nine years, a dialogue was established with Statkraft. Statkraft states that there is no "normal" discharge in Nidelva, but discharges between 40 m$^3/s$ and 200 m$^3/s$ are common. In addition to the more common discharges, a recommendation is to test for the typical value during the melting and flood period, respectively, spring and autumn, which is Q_{10}= 400 m$^3/s$. The discharges recommended by Statkraft are listed below in table 4.2 and do not vary much from the 40th percentile values.

Recomended discharge scenarios from Statkraft	
Value	Discharge [m^3/s]
Q_1	40.00
Q_2	140.00
Q_3	200.00
Q_4	400.00

Table 4.2: Flow duration in Nidelva, recomended from Statkraft.

The water level determines the downstream conditions in Nidelva. One of the challenges in this modelling is the varieties in discharge from the upstream power plants. Because it is desired to do the test with a controlled discharge, the discharge is defined after dialogue with Statkraft. The discharges that are to be tested are presented in table 4.3 and include the discharges from Statkraft including the discharge present when Sweco did measures in Nidelva.

Recomended discharge scenarios from Statkraft	
Value	Discharge [m^3/s]
Q_1	40.00
Q_2	140.00
Q_3	200.00
Q_4	289.00
Q_5	400.00

Table 4.3: Discharge in Nidelva, recomended from Statkraft.

The models will be tested under these five conditions.

4.2 Physical modelling

The physical modelling will involve building a scaled model of the desired area, the Drop of Death. The model will be built in Norges Hydrotekniske Laboriatorium at NTNU in Trondheim. Trondheim kommune will finance the building of the physical model, which will be used for further research on this topic after these measurements are done.

The physical model building will be simplified by using one of the flumes that already exists in the laboratory, as shown in figure 4.2. The experiments will be carried out in a rectangular flume that is 12.6 m long, 1 m wide and 1 m deep. The slope of the flume can be adjusted. The flume has transparent walls made of Plexiglas, making it easy to monitor and visually inspect the hydraulic jump. The see-through walls also make documenting the experiment easier because the flow is available for a camera.

The water in the flume is pumped into a closed system. There are two pumps in the system that have a capacity of approximately 260 l/s each. At the downstream end of the flume, there is a tailgate. By adjusting this, it is possible to change the water level in the flume.

Figure 4.2: The flume were the physical model will be built. The width of the flume is 1 m.

To validate that a wave is the desired oscillating wave, finding the velocity and depth that gives the desired Froude number is necessary. These parameters can be modelled by combining equation (3.2) and Chow's definition of the height of a hydraulic jump, equation (3.6).

The equation (3.6) is solved for the Froude number. The aim is to validate if the Froude number is in the desired interval (2.5 - 4.5). If not, the water depth is adjusted by a weir in the numerical model.

4.2.1 Bathymetry

There are two solutions to how the model of the river bed is to be constructed; one that is somewhat complex and one simplified solution. It is necessary to have detailed and up to date bathymetry of the desired area to build a model as accurate as possible. The bathymetry could then be modelled and scaled digital to be 3D-printed to match the physical model. Building the river bed and weir with gravel or more minor rocks is also possible. The experiment will eventually consist of the bathymetry placed in the flume with a realistic rock weir. Another option is to make a simplified river bed geometry.

The bathymetry is essential to understanding the geometry of the river bed. The bathymetry is plotted by creating a triangular model in HEC-RAS and importing satellite data. The cross-sections are drawn and scaled in AutoCAD.

The blue rectangular in figure 4.3 shows the part of the river built in the flume. The cross-sections are drawn for every 5 meters as in 4.4, and more often if there are significant elevation differences or changes in the river bed. The cross-sections are then placed in order, and the complete model can be shown as 4.5.

Figure 4.3: Illustration of the part of the river that is going to be modelled.

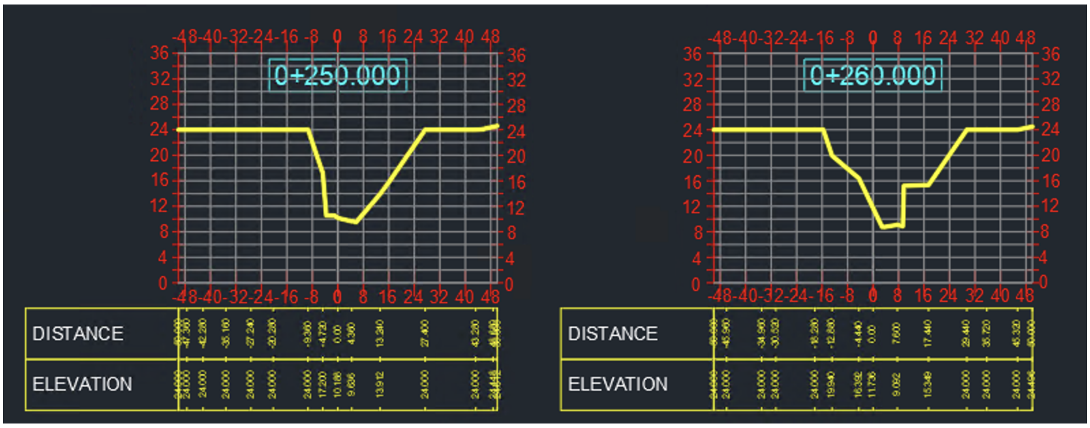

Figure 4.4: Cross sections drawn in AutoCAD of the area that is to be modelled.

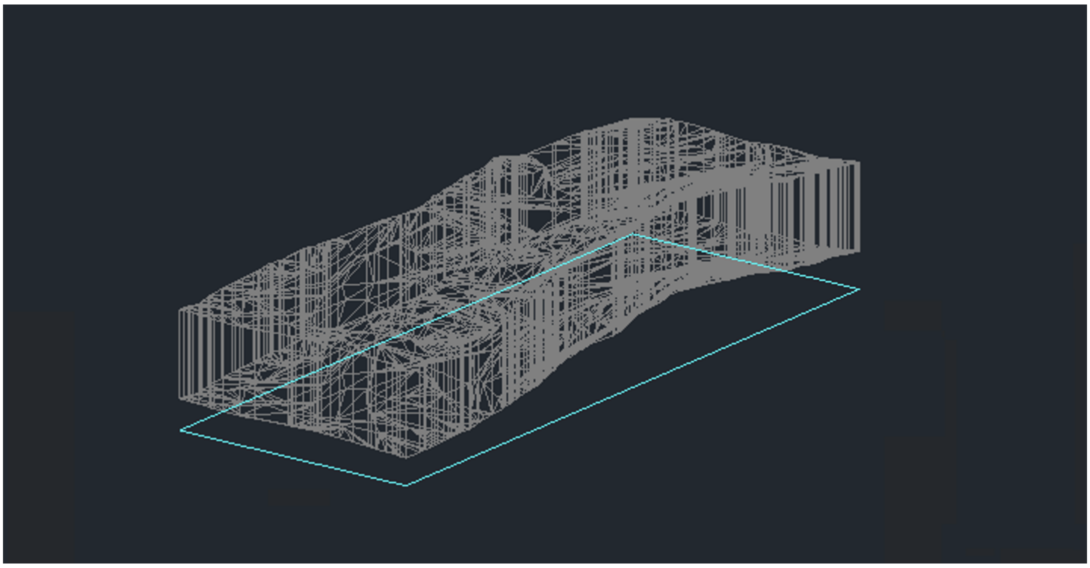

Figure 4.5: A 3D model of the physical model.

If it is desired to validate the bathymetry, a point of action could be to do new measurements of the environment where it is desired to place the weir. ADCP measurements could do the validation. If these measurements are necessary depends on whether the modelling depends on a true copy of the river geometry or if a simplified geometry is sufficient.

After discussing with experienced lab technicians and supervisors, it is decided that the model will be built with the actual bathymetry from the river but with a smooth surface. The bathymetry is 3D-modeled in AutoCAD. This model is then printed on high-density polyurethane foam, the river bed in the physical model in the flume. One of the river bed modules is shown in 4.6.

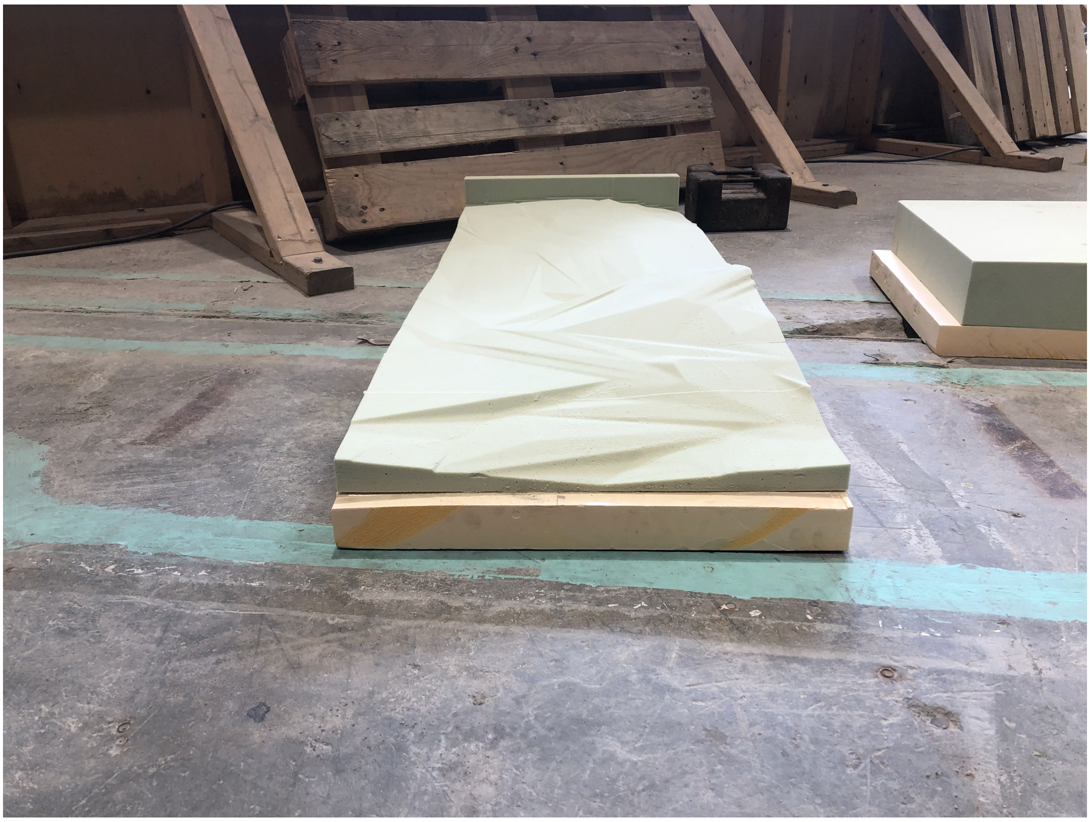

Figure 4.6: The finish result after printing the river bed on polyrethane.

The area between the two bridges has a complex geometry because the river turns at this point. The turning and the uneven river bed give a flow situation challenging to study in a physical model, like a flume. The study is challenging because when the river is modelled, the surroundings that do not fit in the flume are either neglected or simplified. Examining the flow situation when entering the modelled area is necessary to get a flow situation as accurately as possible. The flow situation is mapped and recreated in the physical model by examining the river.

4.2.2 Scaling by Froude similarity

When deciding the scaling of the model, two main parameters need to be weighed against each other. If the model is too small, it could cause significant scaling issues. At the same time, the costs increase as the model grows in size; here, the flume sets the boundary for the model's size. If the model is scaled less, less area will be modelled. Therefore the river is scaled by 1:50.

Froude similarity is the preferred model law because the dominant forces on the particles in the river are gravitational. To avoid significant scaling issues because of Reynolds similarity, the flow in the flume must be turbulent. In addition, a minimum water depth of 4-5 cm must be maintained due to the scaling issues of surface tension of water. By using Froude similarity, the scaling ratios presented in 4.4 are to be used (Heller, 2012),

Froude similarity	
Parameter	Froude scale ratio
Length	λ
Area	λ^2
Time	$\lambda^{1/2}$
Velocity	$\lambda^{1/2}$
Discharge	$\lambda^{5/2}$
Force	λ^3

Table 4.4: The scale ratio for different parameters according to Froude similarity

The discharges Statkraft recommended are the amount of water that will pass through the whole cross-section of the river. When the discharges are modelled in the flume, it is necessary to adjust them for the cross-section that is being modelled. The cross-section spans approximately 100 m. The part that is being modelled is more narrow. Therefore the discharge is multiplied by the ratio Sweco found between total and discharge over the drop. The scaling is calculated in python by Froude similarity as shown in 4.7. The results are presented in table 4.5.

```
In [5]:
#River values. Here we insert the values and dimensions from the river
#We multiply the discharge with the ratio from Sweco to get the correct discharge over the drop.

#Ratio from Sweco
R = 67/289

Q_real_1 = 40 * R
Q_real_2 = 140 * R
Q_real_3 = 200 * R
Q_real_4 = 289 * R
Q_real_5 = 400 * R


#Lab values. Scaling the data with Froude similarity. These are the values that should be used in the model.

Q_lab_1 = Q_real_1 * (1/sc_disch)
Q_lab_1_ls = Q_lab_1 * 1000
print('Q_lab_1:', "%.4f" % Q_lab_1, 'm3/s', "%.2f" %Q_lab_1_ls, 'l/s')
Q_lab_2 = Q_real_2 * (1/sc_disch)
Q_lab_2_ls = Q_lab_2 * 1000
print('Q_lab_2:', "%.4f" % Q_lab_2, 'm3/s', "%.2f" %Q_lab_2_ls, 'l/s')
Q_lab_3 = Q_real_3 * (1/sc_disch)
Q_lab_3_ls = Q_lab_3 * 1000
print('Q_lab_3:', "%.4f" % Q_lab_3, 'm3/s', "%.2f" %Q_lab_3_ls, 'l/s')
Q_lab_4 = Q_real_4 * (1/sc_disch)
Q_lab_4_ls = Q_lab_4 * 1000
print('Q_lab_4:', "%.4f" % Q_lab_4, 'm3/s', "%.2f" %Q_lab_4_ls, 'l/s')
Q_lab_5 = Q_real_5 * (1/sc_disch)
Q_lab_5_ls = Q_lab_5 * 1000
print('Q_lab_5:', "%.4f" % Q_lab_5, 'm3/s', "%.2f" %Q_lab_5_ls, 'l/s')

Q_lab_1: 0.0005 m3/s 0.52 l/s
Q_lab_2: 0.0018 m3/s 1.84 l/s
Q_lab_3: 0.0026 m3/s 2.62 l/s
Q_lab_4: 0.0038 m3/s 3.79 l/s
Q_lab_5: 0.0052 m3/s 5.25 l/s
```

Figure 4.7: Calculations and scaling performed in python to find the relevant discharge for the physical model.

Recomended discharge scenarios from Statkraft			
Value	Discharge $[m^3/\text{s}]$	Scaled discharge $[m^3/\text{s}]$	Scaled discharge $[l/\text{s}]$
Q_1	40.00	0.0005	0.52
Q_2	140.00	0.0018	1.84
Q_3	200.00	0.0026	2.62
Q_4	289.00	0.0038	3.79
Q_4	400.00	0.0052	5.25

Table 4.5: Discharge for physical model, given scaling 1:50.

4.2.3 Monitoring and measuring

The flow situation in the flume can easily be monitored by visualising through the walls made of plexiglass. Five cameras are mounted around the flume in the following set-up to document and monitor the flow situations obtained in the flume, as shown in 4.8, 4.9, 4.10 and 4.11.

Figure 4.8: Mounting of camera 1

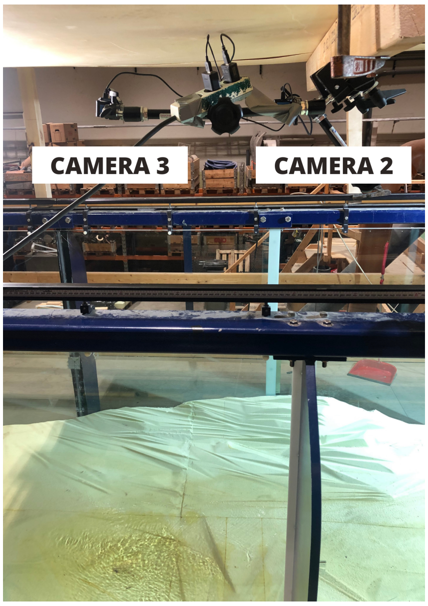

Figure 4.9: Mounting of camera 2 and 3

Figure 4.10: Mounting of camera 4

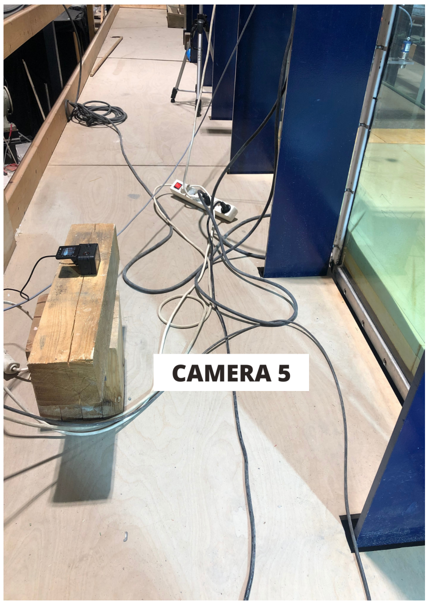

Figure 4.11: Mounting of camera 5

Documenting the flow situation with video cameras will make it easier to communicate the experiment results to stakeholders like Trondheim kajakklubb and kommunen. It will also be added colour drops in the water to better understand the flow situation.

When running the flume with discharges below 11 l/s, the discharge measurement mounted to the pipe system has difficulties reading the discharge. Therefore, to validate the velocity and discharge in the flume, a Vectrino ADV is mounted upstream of the model 4.13. Here the flow is approximately uniform, as shown in 4.12, so that it will give a good validation of the discharge running over the drop of death.

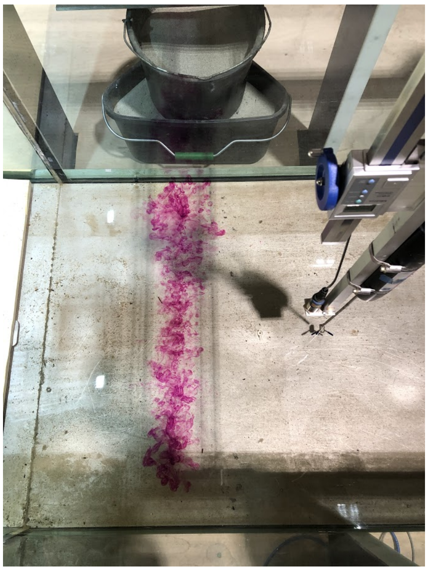

Figure 4.12: Flow situation by the Vectrino

Figure 4.13: The placing of the ADV, Vectrino

The Vectrino is an acoustic doppler velocity meter, ADV, with an accuracy of ±0.5 % of measured value ±1 mm/s (NORTEK, 2018)

The ADV instrument is shaped like a stick with four branches. The ADV is placed vertically in the water through the water surface. By using five transducers, the ADV determines the velocity of the water. The transmitter, one of the transducers, sends out a short acoustic pulse, and the other four transmitters record the echo of the pulse. The echo is processed to find the Doppler shift. Adjustments for the speed of sound in liquids are made, and the velocity is recorded on a computer.(NORTEK, 2018)

The other parameter measured during the experiments is the water depth, an essential parameter to validate the Froude number. Therefore, the inlet will measure the water depth to the model and where the flow is supercritical and subcritical. The water depth is measured with ultrasonic mic+ sensors. The instruments use ultrasonic technology to measure the distance to the water level, which is converted and documented in software. The first sensor is located at the inlet, the second is placed with the movable Vectrino, and the third is placed at the outlet. The degree of precision of the mic+ sensor is ±1 %. (Microsonic, 2020)

In addition to the digital instruments, the water depth is controlled manually using a ruler. This validation will minimise the failure and uncertainty of using digital instruments.

4.2.4 Experimental Procedure

The hydraulic jump in the Drop of Death will be monitored and studied by running different discharges. The aim is to better understand how the jump changes by different discharges and changes in the river bed. An example of a hydraulic jump in the flume is shown in 4.14. The aim is to run the physical model with representative discharges for the area in Nidelva studied. The final experimental set-up is shown in figure 4.15.

Figure 4.14: The hydraulic jump over the model for a random discharge.

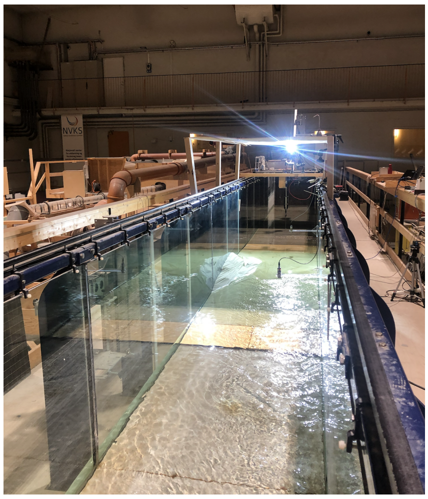

Figure 4.15: The flume where the experiment is conducted.

4.3 Numerical modeling

4.3.1 Software

The open-source finite volume software OpenFOAM was conducted for the numerical modelling of the Drop of Death. Olsen (Olsen, 2015) used OpenFOAM to model flow and water elevation over a weir with accurate results compared to a physical model. The simulations for this experiment were done with Reynolds-Averaged Navier-Stokes (RANS) equations, utilising the k-ϵ turbulence model. The specific solver used was interFoam, a volume of fluid (VOF) solver for multiphase flow.

4.3.2 Dimensions

Numerical modelling can be time-consuming. Choosing a one-dimensional model can save time but give a less accurate result than a 3D model. The one-dimensional model can present accurate models of hydraulic jumps, but only if they appear uniformly across the cross-section of the river. This is not the case in the Drop of Death. Hydraulic jumps that appear at weirs are localised and can therefore not be said to be uniform across the cross-section as the wave will follow the shape of the weir. (Gordon, 2016). A 3D model is chosen to achieve a comparable result with the physical model and as accurate as possible.

4.3.3 Geometry and bathyemtry

Several software is used to preprocess the model. The bathymetry is extracted from a raster file based on in-situ GPS measurements and satellite data. The profile lines are drawn before extracting to AutoCAD by loading the raster file in GIS. In AutoCAD, the profile lines are joined. AutoCAD is conducted to mesh the area between the profile lines. This software makes adjustments so that the topography matches the accurate site. The 3D surface of the bathymetry is then exported as a stereolithographic file (STL format), which can be utilised directly in OpenFOAM.

After the file is exported into OpenFOAM, a mesh of the flow domain is created. The tool blockMesh is used to create s structured grid of cells. These are defined in the blockMeshDict. The initial cell size are approximately 0.3 x 0.3 x 0.1 m, in X- Y- Z-direction respectively. Then the structured grid is snapped to the unstructured bathymetry STL file. The snapping is done by snappyHexMesh. The result is an unstructured mesh consisting of 2.0 10^6 cells.

4.3.4 Boundary conditions

While meshing the domain, the boundary conditions are defined. Regarding the velocity, the surfaces representing the river bed are given no-slip boundary conditions.

The outlet is defined by inletOutlet. This means a Dirichlet boundary condition handles outflow. The reverse flow is then defined as zero. variableHeightInFlowRate defines the inlet. This definition means inflow is defined as a fixed volumetric inflow rate. Here the water level is adjusted according to the calculated water level. The initial water level was set prior to start the simulation. The relevant wall functions were used for the riverbed for the Reynolds-Averaged Stress terms (k, ϵ, μt).

4.3.5 Solver

OpenFOAM allows discretisation to be set for each variable. As a default second-order Gaussian scheme is set. Whereas variables for the turbulence model, k-ϵ, are discretised by the first-order upwind scheme. The Courant number limited the timestep. For stability reasons, a Co-number under 0.3 is maintained. The VOF-equation is solved with the MULES algorithm. The velocity field is derived from the pressure field using the PIMPLE algorithm, combined with the SIMPLE and PISO method. This explanation can be summarised as an iterative solver that uses a guessed value for the pressure field and solving for the correct pressure and the velocity field.

The model was run for 100 seconds. A stable situation was found, and post-processing was conducted using Paraview, an open-source graphical data analysis tool well suited for handling results from OpenFOAM.

5 Results

The physical model was run with the different discharges. The different discharges were conducted through visual monitoring by cameras and water depth measurements. The water discharge was controlled by a Vectrino upstream of the model.

Because the changes and adjustments in the flume were made manually by turning a valve, it was challenging to achieve the proper discharge. Therefore the measured discharge often has a slight variation or deviation from the original discharge.

5.1 Calibration

To ensure that the model is tested for a realistic environment, the model was calibrated for the measurement data conducted by Sweco in 2020. To create a realistic environment, it had to be sure that both the discharge and water depth were correct, which, by the continuity equation (3.1) will give a realistically scaled velocity in the flume. The desired values are presented in table 5.1.

	Q Nidelva	Q Drop of death	Water depth
Real	289 m^3/s	67 m^3/s	2 m
Scaled	0,016 m^3/s	0,0038 m^3/s	0,04 m

Table 5.1: Data used to calibrate the model. Measurements made by Sweco in 2020. Q Nidelva is collected from the measurement station Rathe, from sildre.no.

Calibrating the physical model was an iterative process. First, the flume's system was filled with water, ensuring the water level was above the level of the pipes and pump. The water level needed to be monitored during the measuring process, ensuring no air entrainment in the pump system. When the water level was correct, the system was emptied for air. Air in the pumps would cause either inaccurate discharges or the pump stops as a safety measure.

Upstream the model, the Vectrino is mounted, measuring the water velocity. After several measurements and adjusting the inlet from the pump, the correct discharge that corresponds to 67 m^3/s is found. The correct discharge was found by starting the pump and the inlet to the flume; the system would then start pumping water with continuous discharge. The tailgate is adjusted, so the water flows over the gate to create a realistic environment. This way, the flume is outlet controlled. The tailgate is adjusted until the reference point measure the correct water depth, corresponding to 2 m.

5.2 Q = 40 m^3/s

Q = 40 m^3/s were supposed to be the lowest discharge tested in the physical model. This discharge corresponds to the minimum water flow in Nidelva. Experimenting showed that it was impossible to get this discharge in the flume. The scaled discharge is 0,5 l/s which is approximately 0,2 % of the maximum capacity of the flume. Several attempts were made to adjust the low discharge, but with no good results.

5.3 Q = 140 m^3/s

Q=140 m^3/s was the lowest discharge that was tested in the flume. The hydraulic jump seen from camera 5 is shown in figure 5.1.

Figure 5.1: Picture of the hydraulic jump induced for Q=140 m^3/s, seen from camera 5. Flow direction from right to left.

The equivalent discharges to Q = 140 m^3/s in Nidelva are presented in table 5.2.

Q Nidelva	Q Drop of Death	Q flume
140 m^3/s	32,46m^3/s	31m^3/s

Table 5.2: Real discharge in Nidelva and in the side channel, the Drop of Death and the discharge the experiment is conducted under.

The probes measured the following water depths when running the flume for this discharge. The water depths are presented in table 5.3.

Measure	Inlet	Supercritical flow depth	Subcritical flow depth
Probe [V]	4.7	0.62	2.8
Water depth [mm]	14	4.9	2.0

Table 5.3: Water depths for Q = 140 m^3/s from the physical model

From the visual inspection, the hydraulic jump can be seen as a smaller hydraulic jump. The wave height is significantly lower than for the more significant discharges, but there is a rough water surface and some small eddies occurring even though the discharge is low, as shown in 5.2 and 5.3.

Figure 5.2: The flow situation for Q=140 m^3/s seen from upstream, camera 1.

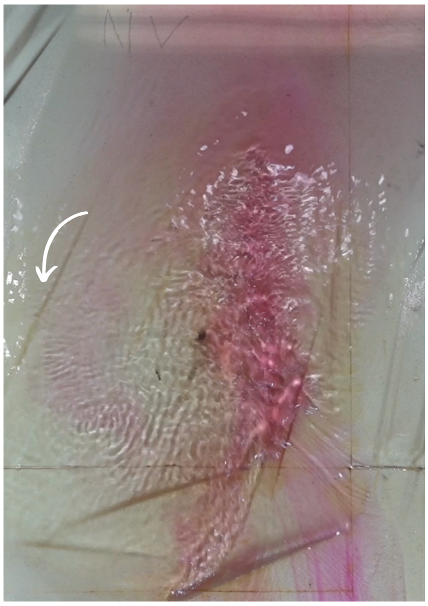

Figure 5.3: Picture of the hydraulic jump for Q = 140 m^3/s in Nidelva, seen from camera 3.

The numerical modelling in OpenFOAM shows that a hydraulic jump is induced for Q = m^3/s. The hydraulic jump seen from the same angle as camera 5 is presented in figure 5.4. Figure 5.5 shows the simulation of the hydraulic jump seen from upstream of the jump.

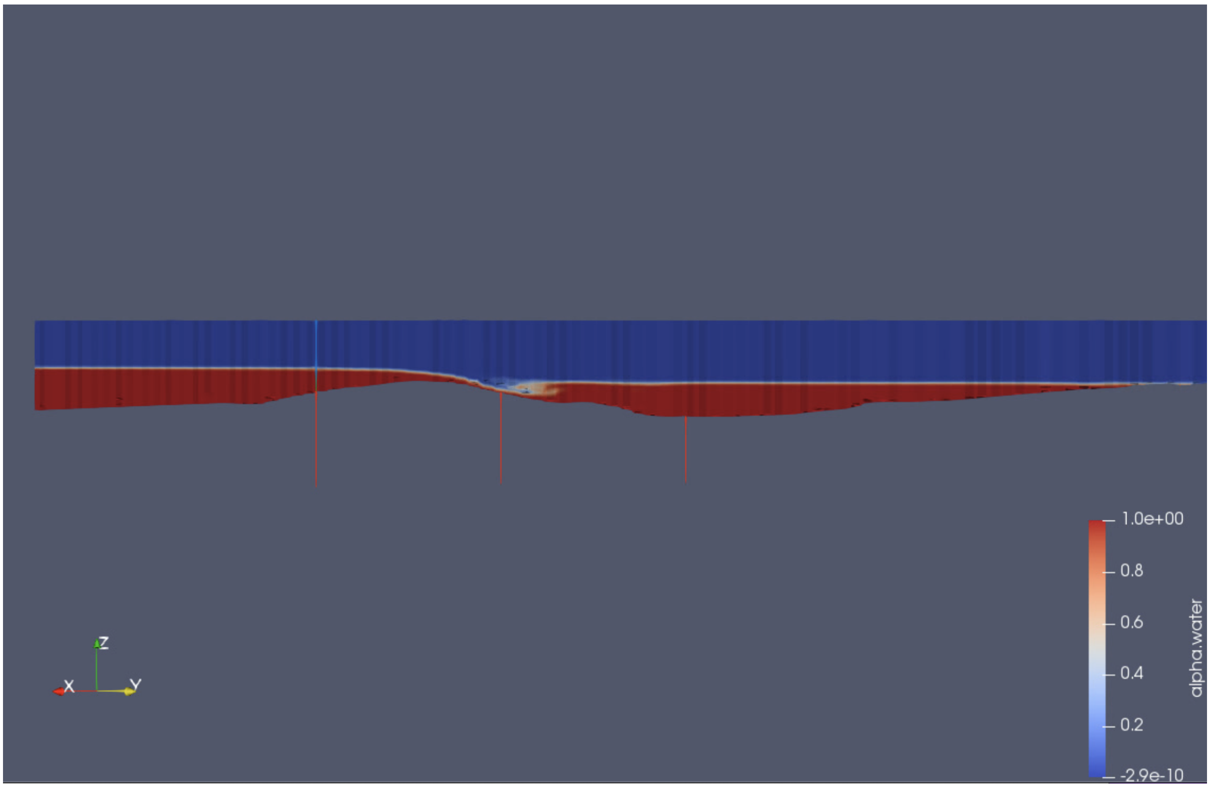

Figure 5.4: Numerical model of the hydraulic jump for Q = 140 m^3/s, seen from the side. Flow direction from left to right.

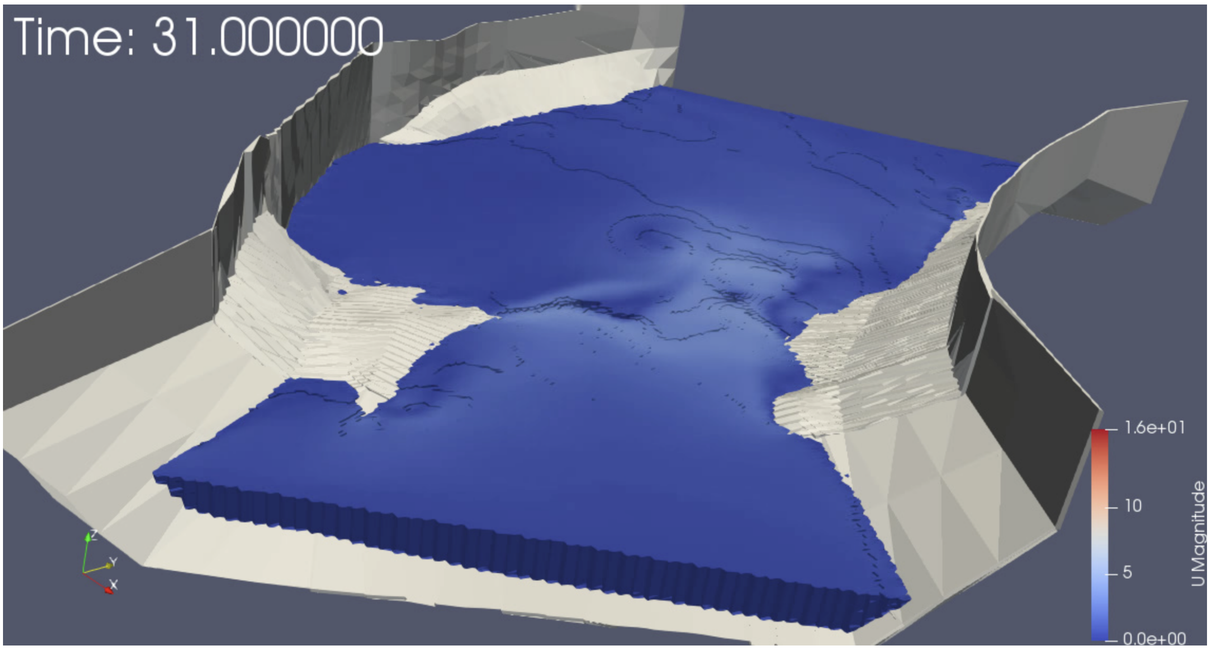

Figure 5.5: Numerical model of the hydraulic jump for Q = 140 m^3/s, seen from the top

The measured flow depths in the numerical model were taken in the hydraulic jump's super and subcritical flow regime. The data and the calculated and corresponding Froude

number, equation 3.2, are shown in 5.4.

Supercritical flow depth [m]	Subcritical flow depth [m]	Fr
0.29	1.87	2.62

Table 5.4: Water depths and Froude number, 3.2 for Q = 140 m^3/s, numerical model

5.4 Q = 200 m^3/s

Q=200 m^3/s is the second-lowest discharge situation tested in the flume. During this discharge, approximately 46 m^3/s runs over the drop of death in Nidelva. The hydraulic jump is more extensive than the lower discharge, the water surface is rougher, and it is a more significant trend for eddies formation - based on visual monitoring. The hydraulic jump is shown in 5.6

Figure 5.6: Picture of the hydraulic jump induced for Q=200 m^3/s, seen from camera 5. Flow direction from right to left.

The equivalent discharges to Q = 200 m^3/s in Nidelva are presented in table 5.5.

Q Nidelva	Q Drop of Death	Q flume
200 m^3/s	46,4m^3/s	46m^3/s

Table 5.5: Real discharge in Nidelva and in the side channel, the Drop of Death and the discharge the experiment is conducted under.

The probes measured the following water depths when running the flume for this discharge. The water depths are presented in table 5.6.

Measure	Inlet	Supercritical flow depth	Subcritical flow depth
Probe [V]	4.8	0.7	2.8
Water depth [mm]	16	7.1	2.0

Table 5.6: Water depths for Q = 200 m^3/s from the physical model

The flow situation and the hydraulic jump are documented and shown in 5.7 and 5.8.

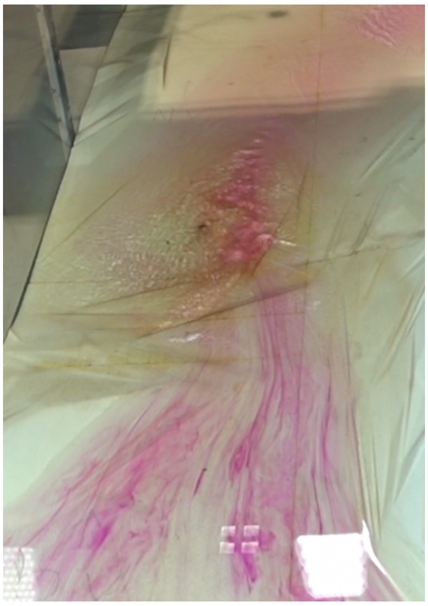

Figure 5.7: The flow situation for Q=200 m^3/s seen from upstream, camera 1.

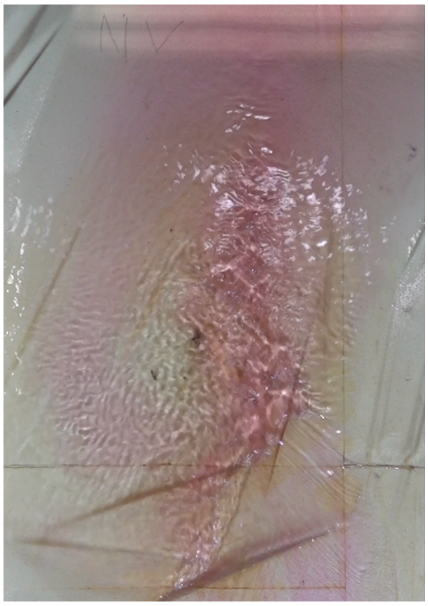

Figure 5.8: Picture of the hydraulic jump for Q = 200 m^3/s in Nidelva, seen from camera 3.

The numerical modelling in OpenFOAM shows that an hydraulic jump is induced for Q = m^3/s. The hydraulic jump seen from the same angle as camera 5 is presented in figure 5.9. Figure 5.10 shows the simulation of the hydraulic jump seen from upstream the jump.

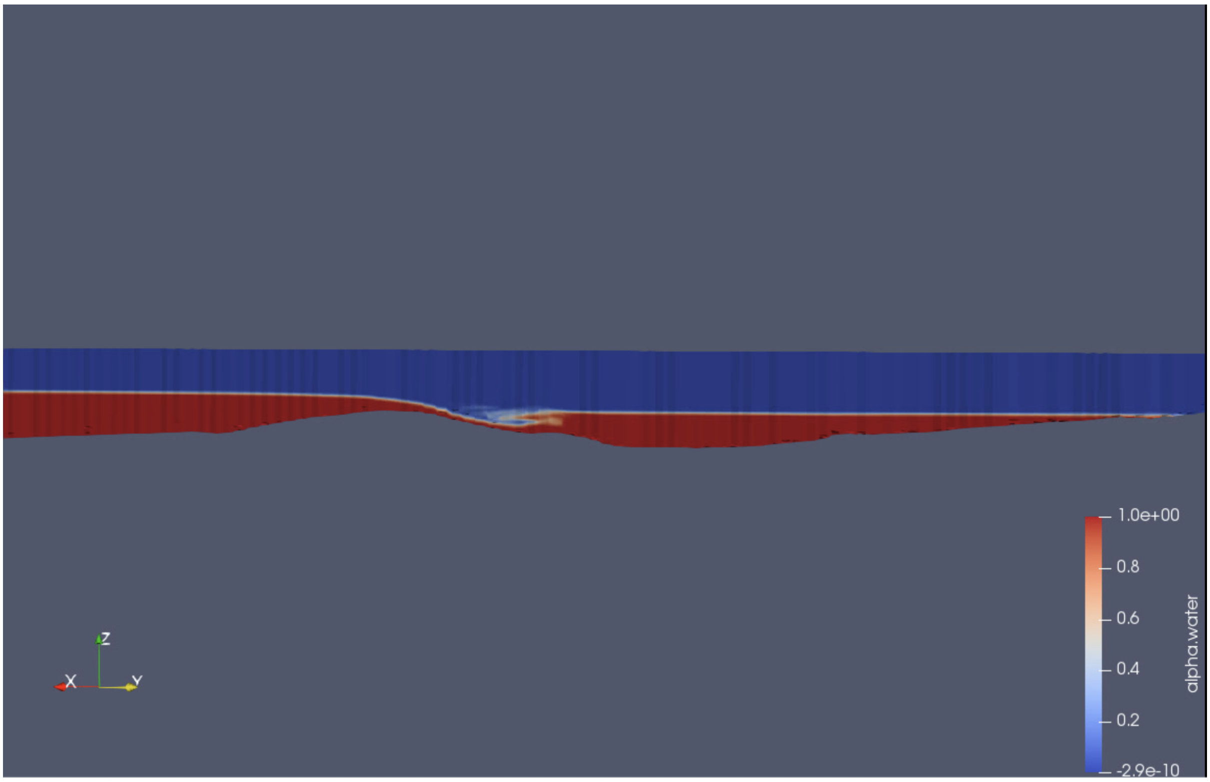

Figure 5.9: Numerical model of the hydraulic jump for Q = 200 m^3/s, seen from the side. Flow direction from left to right.

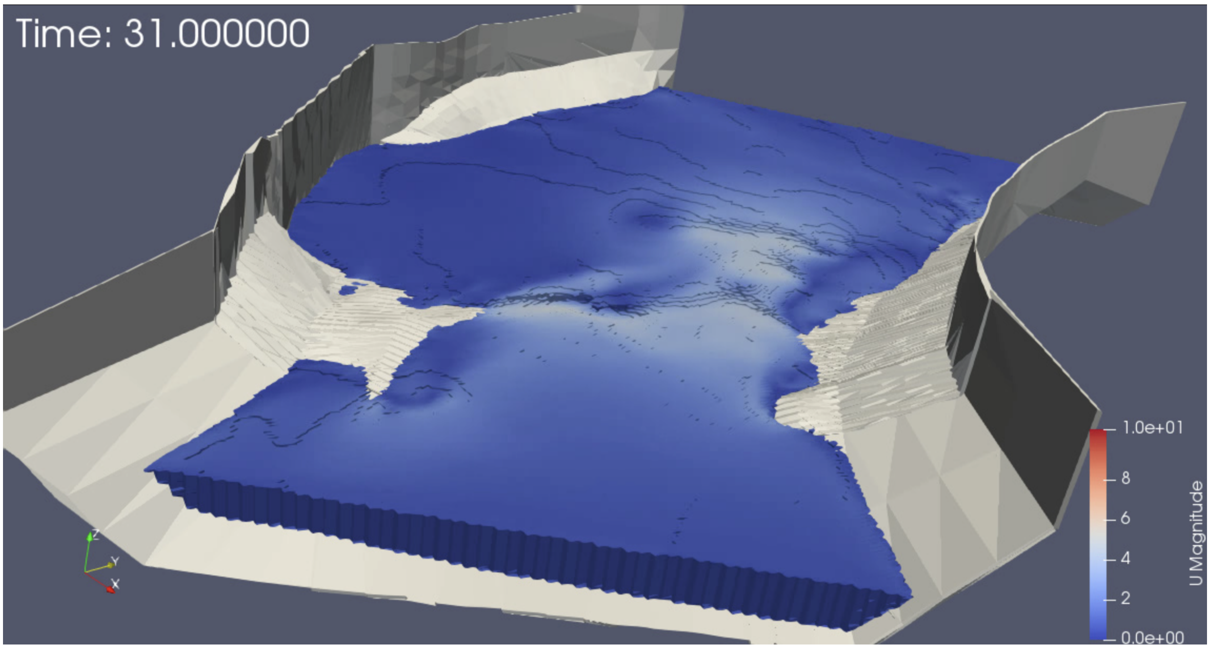

Figure 5.10: Numerical model of the hydraulic jump for Q = 200 m^3/s, seen from the top

The measured flow depths in the numerical model were taken in the hydraulic jump's super and subcritical flow regime. The data and the calculated and corresponding Froude

number, Equation 3.2, are shown in 5.7.

Supercritical flow depth [m]	Subcritical flow depth [m]	Fr
0.39	1.93	2.41

Table 5.7: Water depths and Froude number, 3.2 for Q = 200 m^3/s, numerical model

5.5 Q = 289 m^3/s

Q=289 m^3/s was the discharge used to calibrate the model, and because the relationship between water depth and discharge was known, it was decided to use the discharge for further testing.

Figure 5.11: Picture of the hydraulic jump induced for Q=289 m^3/s, seen from camera 5. Flow direction from right to left.

The equivalent discharges to Q = 289 m^3/s in Nidelva are presented in table 5.8.

Q Nidelva	Q Drop of Death	Q flume
289 m^3/s	67m^3/s	64m^3/s

Table 5.8: Real discharge in Nidelva and in the side channel, the Drop of Death and the discharge the experiment is conducted under.

The probes measured the following water depths when running the flume for this discharge. The water depths are presented in table 5.9.

Measure	Inlet	Supercritical flow depth	Subcritical flow depth
Probe [V]	6.8	1.8	3.0
Water depth [mm]	34.0	40.0	6.0

Table 5.9: Water depths for Q = 289 m^3/s from the physical model

From the visual inspection of the experiment, it can be seen a rougher water surface and higher wave height as the discharge increases. The flow situation and the hydraulic jump are documented and shown in 5.12 and 5.13.

Figure 5.12: The flow situation for Q=289 m^3/s seen from upstream, camera 1.

Figure 5.13: Picture of the hydraulic jump for Q = 289 m^3/s in Nidelva, seen from camera 3.

The numerical modelling in OpenFOAM shows that an hydraulic jump is induced for Q = 289 m^3/s. The hydraulic jump seen from the same angle as camera 5 is presented in figure 5.14. Figure 5.15 shows the simulation of the hydraulic jump seen from upstream the jump.

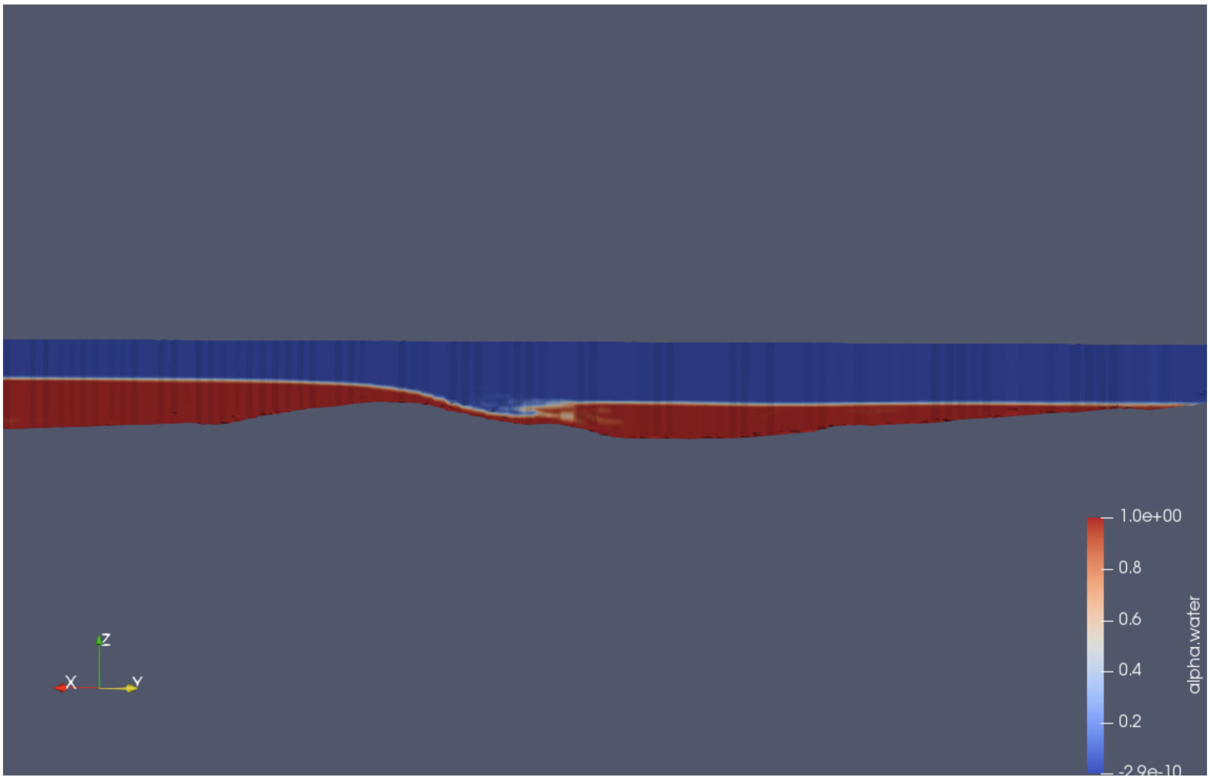

Figure 5.14: Numerical model of the hydraulic jump for Q = 289 m^3/s, seen from the side. Flow direction from left to right.

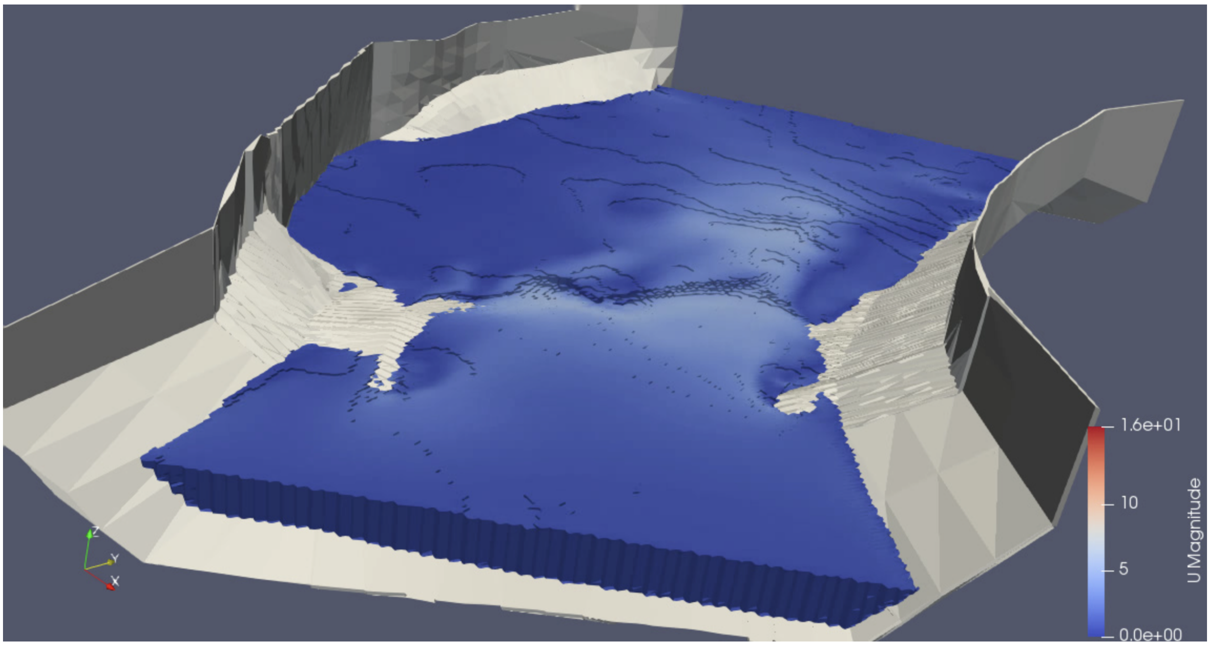

Figure 5.15: Numerical model of the hydraulic jump for Q = 289 m^3/s, seen from the top

The measured flow depths in the numerical model were taken in the hydraulic jump's super and subcritical flow regime. The data and the calculated and corresponding Froude

number, Equation 3.2, are shown in 5.10.

Supercritical flow depth [m]	Subcritical flow depth [m]	Fr
0.49	2.0	2.49

Table 5.10: Water depths and Froude number, 3.2 for Q = 289 m^3/s, numerical model

5.6 Q = 400 m^3/s

Q=400 m^3/s is the maximum discharge tested in the flume. It is a discharge that does not occur as often as the other discharges tested in the flume. Q=400 m^3/s is the Q_{10} in Nea-Vassdraget, which Nidelva is a part of (NVE, 2001).

Figure 5.16: Picture of the hydraulic jump induced for Q=400 m^3/s, seen from camera 5.Flow direction from right to left.

The equivalent discharges to Q = 400 m^3/s in Nidelva are presented in table 5.11.

Q Nidelva	Q Drop of Death	Q flume
400 m^3/s	92,7m^3/s	90m^3/s

Table 5.11: Real discharge in Nidelva and in the side channel, the Drop of Death and the discharge the experiment is conducted under.

The probes measured the following water depths when running the flume for this discharge. The water depths are presented in table 5.12.

Measure	Inlet	Supercritical flow depth	Subcritical flow depth
Probe [V]	5.7	1.3	3
Water depth [mm]	34.0	24.3	6.0

Table 5.12: Water depths for Q = 400 m^3/s from the physical model

The flow situation and the hydraulic jump for the maximum tested discharge are documented and shown in 5.17 and 5.18.

Figure 5.17: The flow situation for Q=400 m^3/s seen from upstream, camera 1.

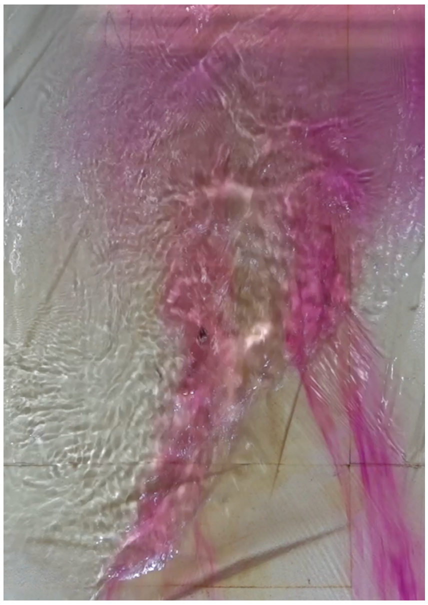

Figure 5.18: Picture of the hydraulic jump for Q = 400 m^3/s in Nidelva, seen from camera 3.

The numerical modelling in OpenFOAM shows that an hydraulic jump is induced for Q = 400 m^3/s. The hydraulic jump seen from the same angle as camera 5 is presented in figure 5.19. Figure 5.20 shows the simulation of the hydraulic jump seen from upstream the jump.

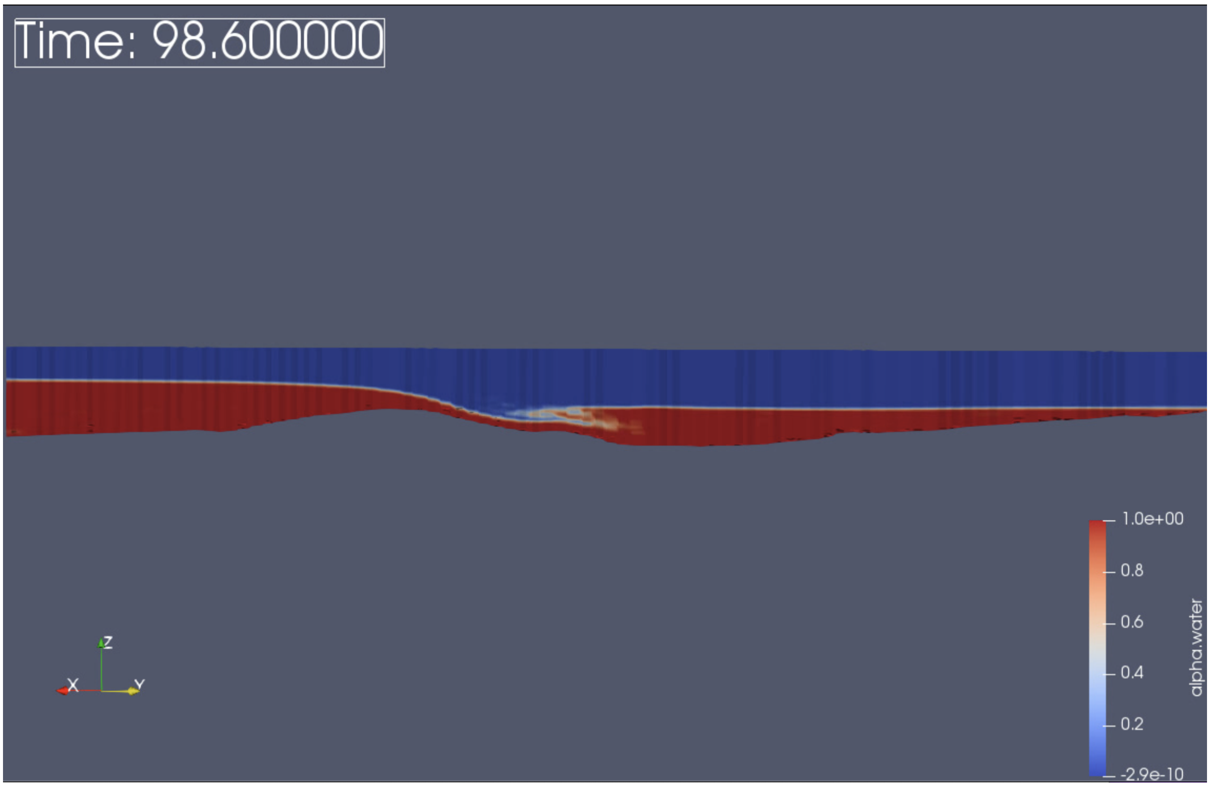

Figure 5.19: Numerical model of the hydraulic jump for Q = 400 m^3/s, seen from the side. Flow direction from left to right.

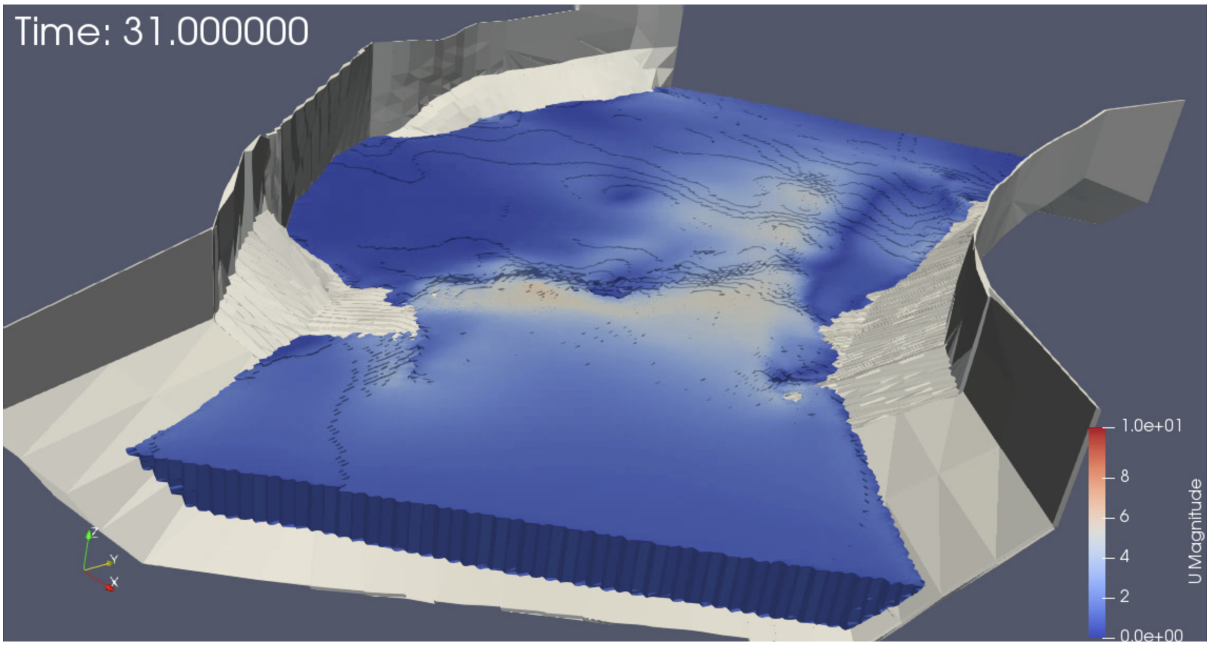

Figure 5.20: Numerical model of the hydraulic jump for Q = 400 m^3/s, seen from the top

The measured flow depths in the numerical model were taken in the hydraulic jump's super and subcritical flow regime. The data and the calculated and corresponding Froude

number, Equation 3.2, are shown in 5.13.

Supercritical flow depth [m]	Subcritical flow depth [m]	Fr
0.63	2.16	2.35

Table 5.13: Water depths and Froude number, 3.2 for Q = 400 m^3/s, numerical model

5.7 Summarize result

From the different results, it can be summarized to increase in three of the most important parameters for kayakers when increased discharge:

- Rougher water surface.
- Height and slope of hydraulic jump. The jump gets higher and steeper when discharge increases.
- Formation of eddies increases as discharge increases.
- The Froude number is satisfied for Q = 140 m^3/s

A comparison of the results from the heighest and lowest tested discharge is presented in figure 5.21, 5.22, 5.23 and 5.24.

Figure 5.21: Q = 140 m^3/s. Comparison of the highest and lowest water discharge tested in the flume. Flow direction from right to left.

Figure 5.22: Q = 400 m^3/s. Comparison of the highest and lowest water discharge tested in the flume. Flow direction from right to left.

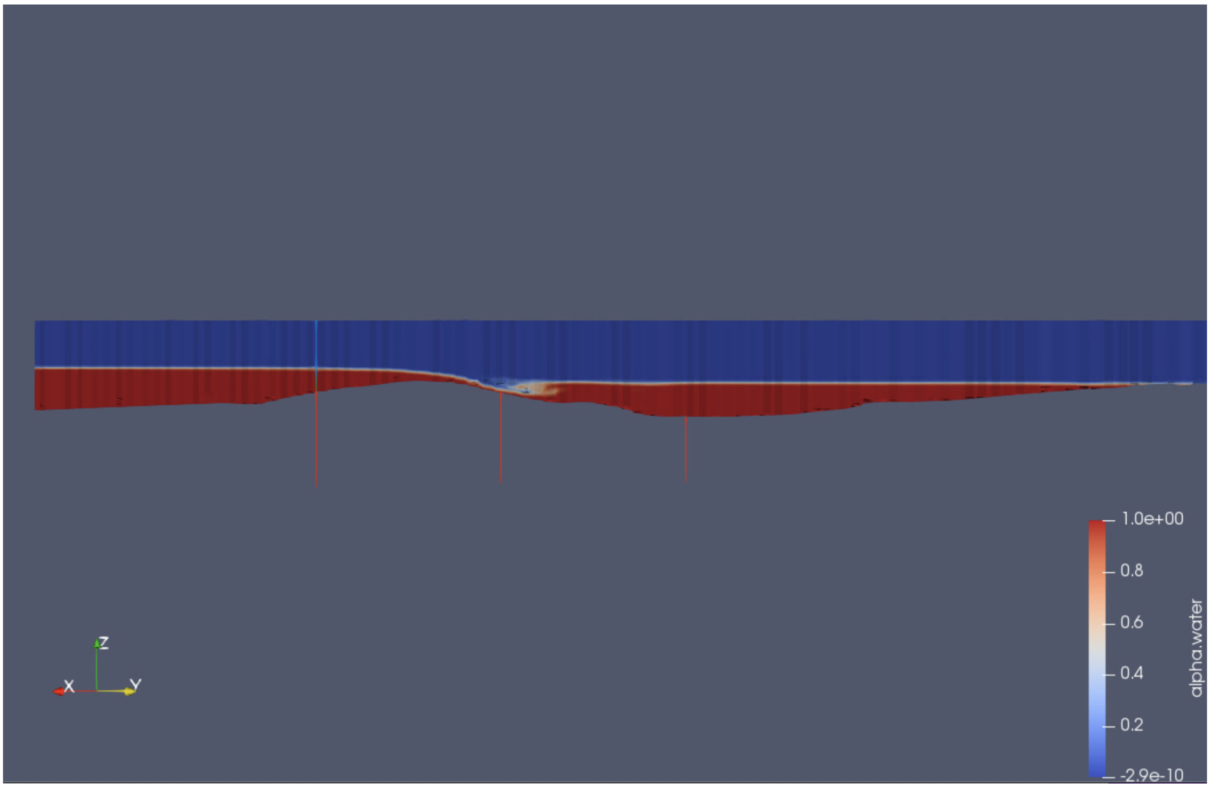

Figure 5.23: Q = 140 m^3/s. Comparison of the highest and lowest water discharge tested in the numerical model. Flow direction from left to right.

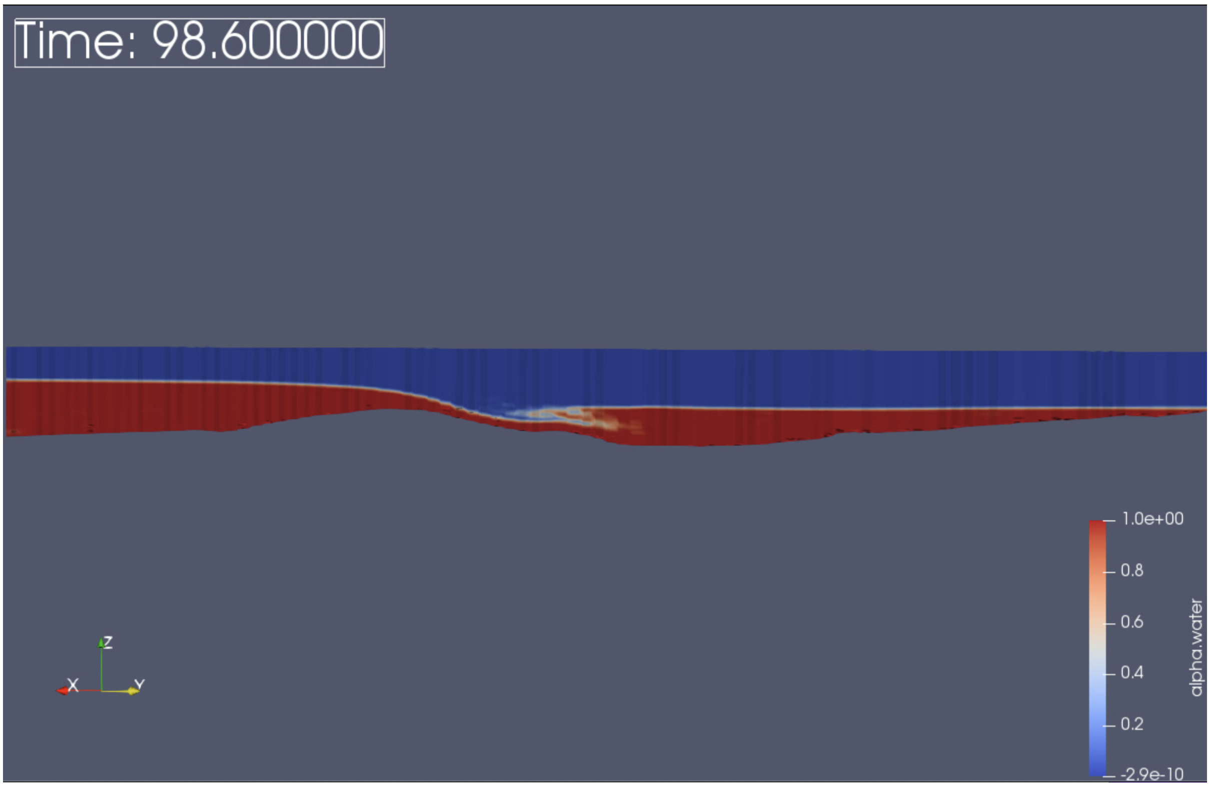

Figure 5.24: Q = 400 m^3/s. Comparison of the highest and lowest water discharge tested in the numerical model. Flow direction from left to right.

By looking at the Froude numbers calculated from the numerically measured water depths, it is found that for Q = 140 m^3/s, the form of the hydraulic jump is satisfying for the kayakers. It is, though, desired to optimize the waveform for the other discharges.

6 Discussion

6.0.1 Different discharges

To compare the nuemrical and physical model the footage from the experiments and simulations are compared to equivalent dishcarges in Nidelva. The two discharges documented in Nidelva, over the drop of death are Q = 102.4 m^3/s, as shown in figure 6.1, and Q = 200 m^3/s, as shown in figure 6.2. Here Q = 102.4 m^3/s is compared to Q = 140 m^3/s as tested in the lab and simulated in the Numerical model. Q = 200 m^3/s is compared to Q = 200 m^3/s.

Figure 6.1: Nidelva, The drop of death, Q = 102.4 m^3/s

Figure 6.2: Nidelva, The drop of death, Q = 200 m^3/s

As seen in the pictures taken from Nidelva, there is a visible difference in water quantity and surface roughness between the two discharges. The higher discharge has a white water effect, as the water breaks and the rough surface continues after the hydraulic jump; this effect is better seen in figure 6.6 and 6.9.

Figure 6.3: Camera 1, Physical model Q = 140 m^3/s

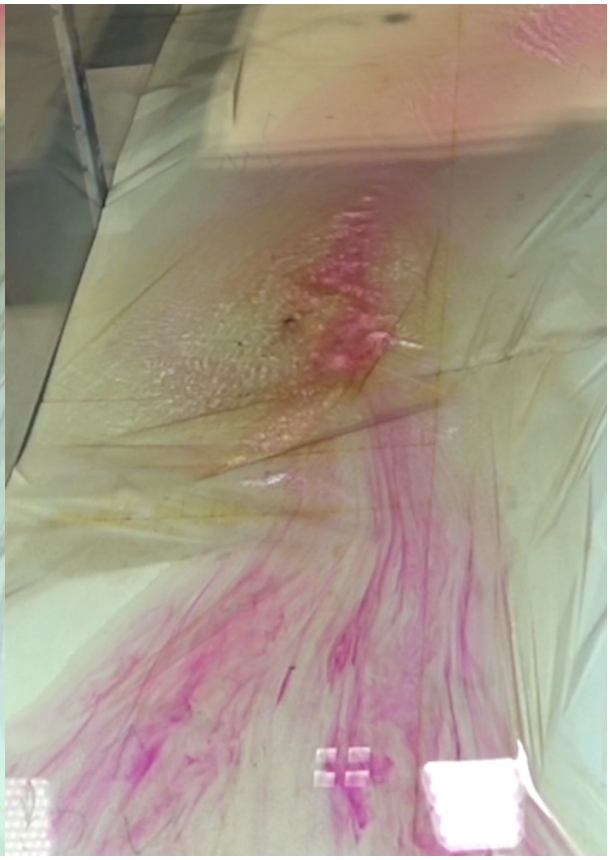

Figure 6.4: Camera 1, Physical model, Q = 200 m^3/s

When comparing the two water discharges from the physical model, visual differences are less than for the river. The water flow is approximately the same, forming the same patterns in the flume. The comparison is shown from upstream angle in figure 6.3 and 6.4.

The two discharges can be compared from the same angle in the three different environments in the following pictures. Discharge Q = 140 and 102 m^3/s is shown in the physical model 6.5, in situ 6.6 and in the numerical model 6.7. Discharge Q = 200 m^3/s is shown in the physical model 6.8, in situ 6.9 and in the numerical model 6.10.

Figure 6.5: Physical model, Q = 140 m^3/s. Flow direction from right to left.

Figure 6.6: Nidelva, The drop of death, Q = 102.4 m^3/s. Flow direction from right to left.

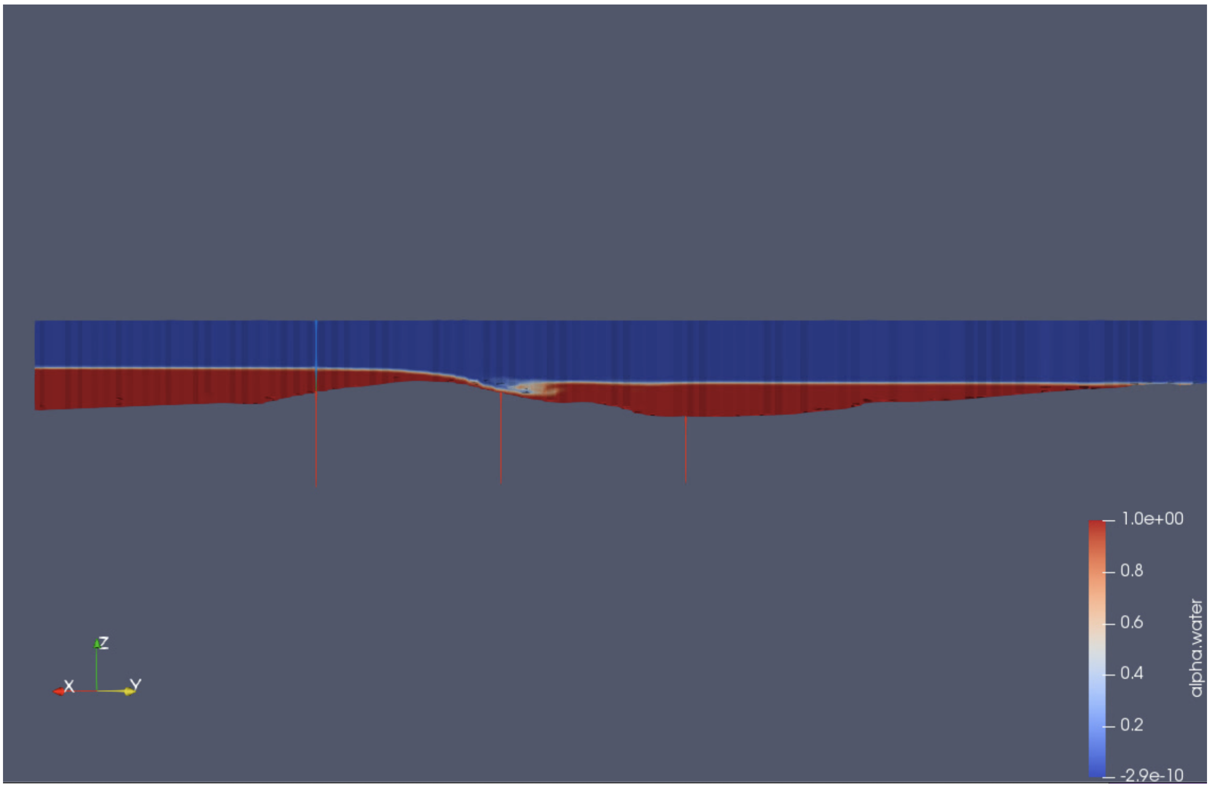

Figure 6.7: Numerical model, Q = 140 m^3/s. Flow direction from left to right.

Figure 6.8: Physical model, Q = 200 m^3/s. Flow direction from right to left.

Figure 6.9: Nidelva, The drop of death, Q = 200 m^3/s. Flow direction from right to left.

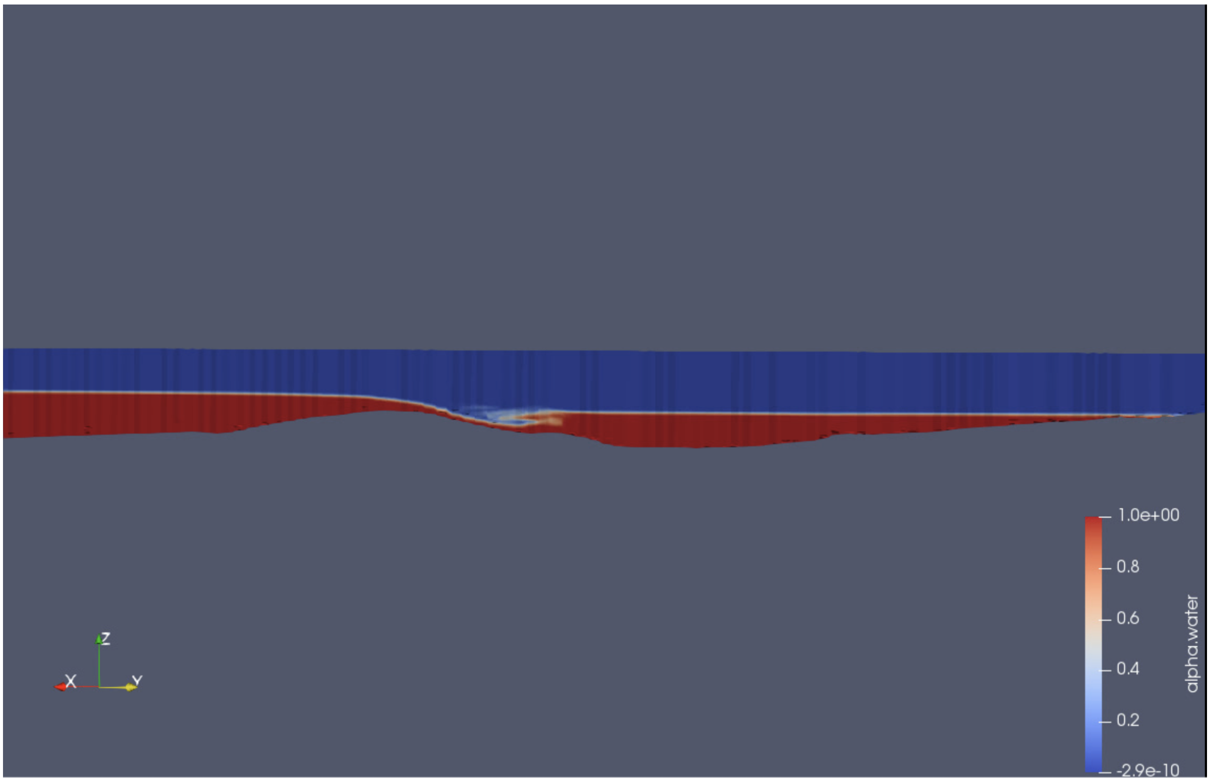

Figure 6.10: Numerical model, Q = 200 m^3/s. Flow direction from left to right.

6.1 Sources of error

6.1.1 Scale effects

Even though there are few visible scaling effects in the physical model, some might be present. The scaling issues often happen due to force errors, such as friction or surface tension. These forces are especially present when the water level is low, which is the case in the physical model in this experiment. The lowest measured water depth is 2 cm, below the recommended water depth (4-5 cm) to avoid significant scale effects Heller (2012). This limitation is set because friction forces and surface tension might not be correctly scaled and realistic for these water depths. An extreme version of this environment is when water is left on a blackboard after cleaning it. The water will stick to the board because the surface tension and friction forces are more potent than the gravitational. In the physical experiment, the gravitational forces are still dominating, but the friction forces and surface tension might be more present and influence than in situ.

According to Heller (2012), scale effects increase as the model decreases. Because the physical model is scaled relatively much, some scale effects could be avoided by looking at a minor part of the river. Less scaling is the best method for avoiding greater scaling issues.

When conducting the physical experiment, monitoring the flow situation and adjusting when visible scaling issues or other errors occurred was possible. Avoiding scaling issues would be more complicated if the flume were not equipped with Plexi glass walls.

6.1.2 Tilting

The river bed's slope is considered when designing and modelling the bathymetry in AutoCAD drawings. The first calibration could not achieve the desired discharge and water depth ratio. Because of this challenge, it was discovered that the flume was tilted, as shown in 6.11 and 6.12.

Figure 6.11: The tilting of the flume before adjustments were made.

Figure 6.12: The tilting of the flume after adjustmenst.

As the plaque on the spirit level says, the tilting still has an accuracy of ±0.003 mm/m even though the spirit level says the flume is levelled. Not propper levelling can affect the discharge or water depth through the flume, 3.4

6.1.3 Human errors

The intake to the flume is a pipe with a diameter of approximately 40 cm. The pump velocity is regulated on a panel, figure 6.14, and a valve regulates the quantitative of inlet water. When running as low discharges as was necessary for the physical experiment, the panel could not read the velocity or discharge. Therefore, the settings on the panel were left static, and the valve was used to adjust the discharge. The valve had to be operated manually by turning the wheel, as shown in figure 6.13.

Figure 6.13: The panel where the pump is operated from.

Figure 6.14: The valve that adjusts the inlet of the pump.

Because the experiment was done with discharges that are only 1% of the maximum capacity of the flume, the valve was almost closed for all time. Only minor adjustments were made to change the discharge in the flume. Even minor adjustments caused significant changes in discharges, which made the changes unpredictable. The Vectorino validated the discharge, but the data needed to be handled propper as the only validation.

6.1.4 Air in pump system

Because the flume was run with low discharges compared to the maximum capacity, there were repeated problems with air in the pumping system. To get the correct calibration of discharge and water depth, the water depth in the system was sometimes adjusted lower than the in- and outlet of the pipes, causing air entrainment in the system. An illustration of the challenges with air entrainment is shown in figure 6.15.

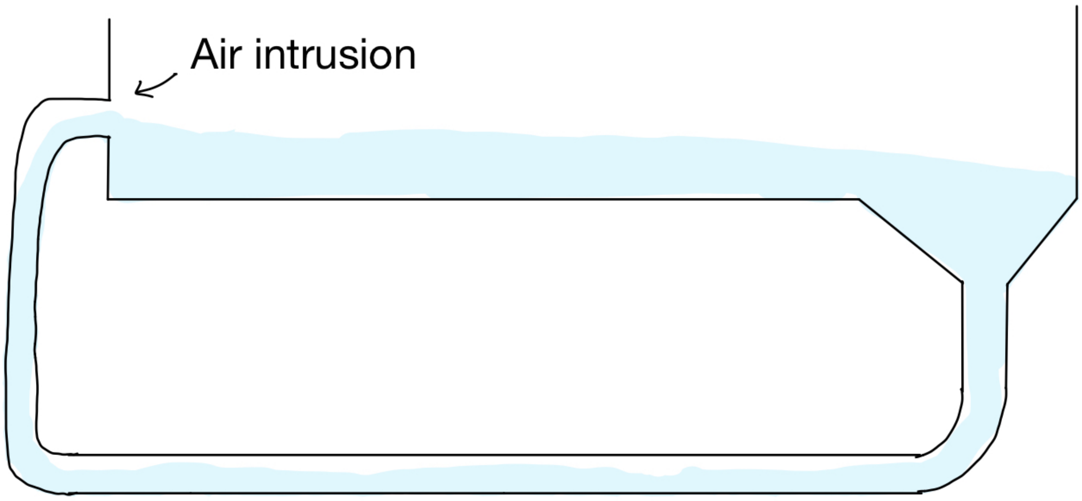

Figure 6.15: Illustration of the pumping system of the flume. The scaling or mounting of the system is not correct.

Air in the piping and pump system would cause inaccurate discharges, or the pump stops as a safety measure. The air issues were solved by emptying the air in the pumps and filling the system with water. If it was significant differences between the discharges delivered by the pump and what was measured, it was possible to expose the error. It is possible that more minor errors were delivered in measured and actual discharge as an effect of air in the pumping system.

6.2 Bathymetry and roughness

During an inspection of the river area, it was discovered that under the Sluppen bridge, the river bed is covered with rocks with a diameter of approximately 50 - 60 cm. The stones are course with roughness at about 10 cm, as illustrated in figure 6.16. These stones were placed on the river bed due to erosion challenges.

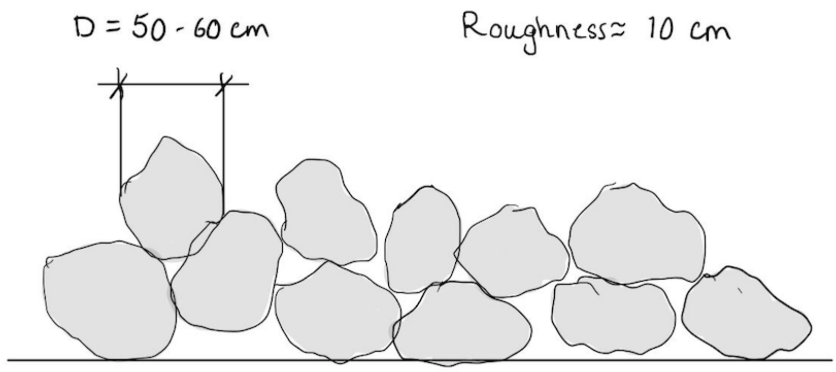

Figure 6.16: Illustration of rocks on the river bed under the Sluppen bridge .

For the physical experiment, a smooth riverbed surface printing the bathymetry on high-density polyurethane foam was chosen. The printing was more time-efficient than it would have been to build a replica of the accurate bathymetry and roughness. When choosing this simplification, the bathymetry remains realistic, but the river bed rocks' roughness and irregularities are not preserved. Manning's equation 3.4 shows that this simplification can affect the water depth and discharge ratio and thereby cause inaccuracies.

6.2.1 Instrument errors

The measuring instrument used in the experiment was mainly Vectrino and Mic+ sensor. The Vectrino has an accuracy of ±0.5 % of measured value ±1 mm/s (NORTEK, 2018), while the Mic+ sensor has a degree of precision of the mic+ sensor is ±1 %. These accuracies mean the instruments are relatively precise, but there is still room for errors. The most common error experienced during the experiments were either incorrect mounting of the instruments, causing them to have the wrong calibration or the disturbance of air bubbles. During experiments, small unsees by the human eye; air bubbles would attach to the sensor on the Vectrino, causing incorrect measurements. The error was only discovered when the Vectrino gave unrealistic data, for instance, when the valve was almost closed. The Vectrino said that the discharge in the flume was equivalent to the experiment's most extensive discharge. The air bubbles were removed by wiping the sensor with paper, and the Vectrino delivered accurate data.

6.3 Water depths

A significant discrepancy has been identified by studying the correspondence between the water depths and the experiments' film footage. The different measurements are plotted in figure 6.17.

Figure 6.17: A representation of the measured water depths from different discharges

The different probes are placed in the different stages of the hydraulic jump; the inlet, the supercritical flow and the subcritical flow. From literature and the physical experience, the changes in water depths should be something like illustrated in 6.18, (Chow, 1959):

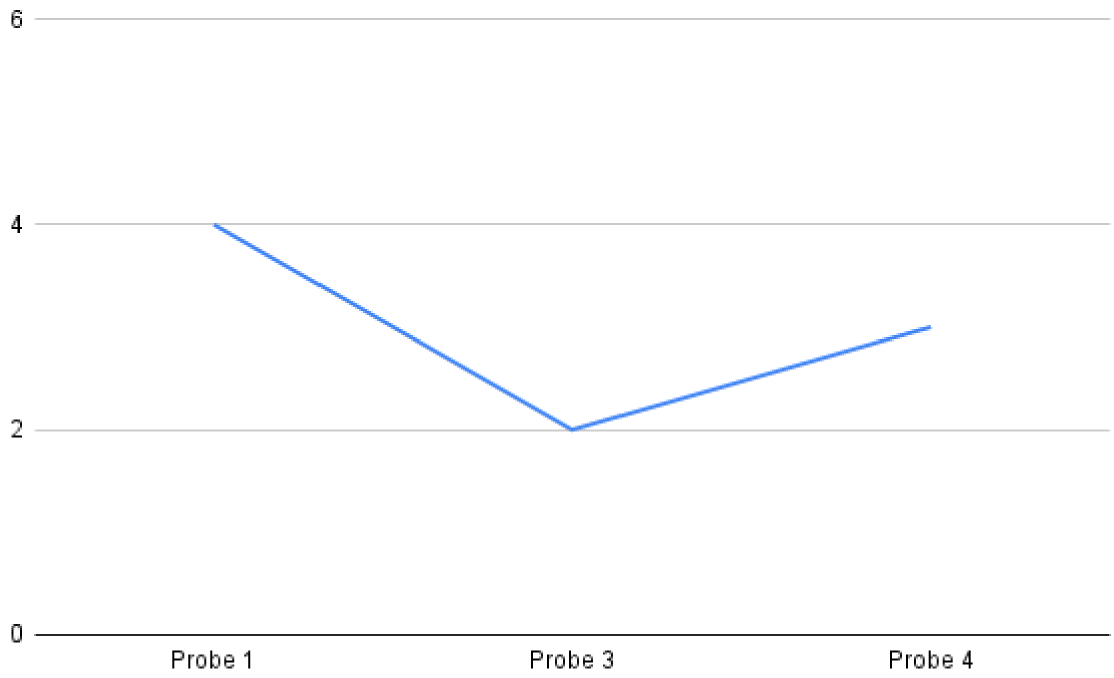

Figure 6.18: A biref representation of how the changes in water depths should be according to literature and physical experiments (Chow, 1959)

According to the laboratory technicians, there are probably technical errors with the sensors or the calibration of the sensors. A possibility is that all the sensors measure correct, but due to poor calibration, they do not read from the same heights levels, as if they do not speak the same language. They will therefore measure correct, but it is impossible to see the correspondence in the changes in water depths because it is impossible to compare the data.

Because the probes might measure correct, but the data is not comparable, it might be that the probe used for calibration of the flume, Probe 3, still gives accurate data. This means that the system is still calibrated, and the results will still be realistic. The greatest error will be if there are some technical errors with the sensors. Making all the results useless. Because the water depth manually was controlled with a ruler during the calibration, the essential measure is correct, validating the reliability of the other results. Because of this error, the water depts measured with the sensors will not be used to calculate the Froude number. Instead, the water depths from the numerical model will be used.

6.4 Comparing the numerical and physical model

The numerical and physical models are both calibrated with the same boundary conditions.

When deciding whether to build a physical model or do a numerical simulation, time and cost are the heaviest factors. Building a physical model is both time-consuming and expensive. Using a flume that already exists in the lab can save time, but calibrating and running the experiments demands a higher presence than a numerical simulation does. The physical experiment is also expensive, as it demands the use of expensive equipment and the engagement of employees.

Even though physical modelling is time-consuming and expensive, it is often preferred if the results are communicated to external people. In this case, Trondheim kommune will inspect the results. The modelling will present a visualisation of the hydraulic jump that will be implemented in the river, which has a great value when involving stakeholders that do not have a hydraulic background.

Numerical models are also time-consuming, requiring a significant understanding of the flow situation to simulate it. The simulations are often complex, which is demanding to calibrate and model. When the experiments are run, it can take several hours, depending on the complexity of the meshing and modelling. On the other hand, running the actual experiment might be more time consuming, but it does not demand supervision.

The numerical models are also expensive as they require expensive computers that can run great simulations.

Both models have pros and cons, but they give easy results to communicate and illustrate the actual situation.

6.5 Stakeholders

If changes are implemented, the aim should be to meet as many stakeholders' interests as possible. If Trondheim kommune, or others, are to make changes on the river bed in Nidelva, for instance, by introducing a weir, many stakeholders need to be kept in mind. When doing changes like this that will affect an established natural regime, several organisations, the public sector, industries, and private persons will or could be affected by the changes. The following stakeholders should be orientated or included in the project if changes are made.

6.5.1 Statens vegvesen

Suppose changes are to be done at the drop of death. In that case, Statens vegvesen is not an essential stakeholder because their area of responsibility is not likely to be affected by changes. However, if there are to be conducted changes under the Sluppen bridge, the changes in the flow regime could increase the scouring of the river bed and bridge pillars. Erosion like this can have fatal consequences. Therefore, it will be essential to calculate the erosion effect due to the hydraulic jump. Statens vegvesen should be included in this part of the project, as they will likely know the bridge's capacity.

6.5.2 Trondheim Omland Fiskeadministrasjon

Upstream the city centre in Trondheim, Nidelva is a popular area for practising sport fishing, especially is the river famous for its salmon fishing conditions despite the river being short. Trondheim Omland Fiskeadminsitrasjon, TOFA (Trondheim fish administration) is an organisation aiming to ensure good conditions for sports fishing and outdoors life in Nidelva. They are doing this by facilitating for the fish in Nidelva, ensuring their habitat is satisfying for the fish. (TOFA, 2021).

After dialogue with TOFA, changes in the river bed can affect the fish. These changes can force the fish to move further upstream and significantly influence the fish's spawning pattern. In an email correspondence with TOFA, they say that if protection against erosion is conducted by adding leftover rocks from tunnel extraction, the river bed can be compared with a "dead" river bed; there are no more plants or vegetation. To make specific changes to the river bed that are compatible with the fish and natural river pattern, TOFA should be included in the project.

6.5.3 Norges Vassdrags- og Energidirektorat

Norges Vassdrags- og Energidirektorat, NVE, represent the Govurenment, and are under the ministry of oil and energy production. They are responsible for managing and monitoring the watercourses in Norway. Because NVE monitors the rivers, they would be wise to include in the project because of their competence and experience. In addition to being essential to support the project, they could have information on other projects with development and construction in or along the river.

6.5.4 Trondheim kommune

Trondheim kommune has an ongoing project aiming to develop and urbanise the Sluppen area. (Trondheimkommune, 2020). Therefore they are already engaged and an important part of the project regarding reconstructing the kayak waves in Nidelva. Changes in the Sluppen area enabled changes on the river bed under the Sluppen bridge. By changing the transport pattern in the area, especially by moving vehicle transport away from the bridge, the demands regarding structural safety dimensions and scouring under the bridge are decreased, which means it will be possible making river bed changes.

Trondheim kommune is involved in most of the projects in the area and could be an essential stakeholder in optimising this project. They can also be an economic contributor if they find the project an excellent contributor to the local environment.

6.5.5 Surfers

Before the filling under the bridge, the wave downstream attracted surfers and kayakers. The induced hydraulic jump was not an oscillating wave but a standing wave. Whereas the kayaker's ideal wave has a Froude number between 2.5 and 4.5, the ideal surfing wave has an inlet Froude number at 1.7 (Famiglietti, 2010). The surfers should therefore be included in the project so that it could be possible also to satisfy their interests. Perhaps it could be possible to dedicate different areas in the river to different wave types.

6.5.6 Trondheim Kajakklubb

This project's main stakeholder is Trondheim kajakklubb and NTNUI Padling. These sports teams in Trondheim use Nidelva for recreation and leisure by practising whitewater kayaking. Early in the project, these groups were involved with dialogue and taking inceptions of the river and its current waves. The dialogue gave valuable information about their desires and the state of the river. As they spend much time in the river, they know it and its behaviour well. For further work, representations from these sports teams should inspect the solutions for improving the waves. They will provide helpful input for modifying or adjusting the wave to meet their needs.

All of the mentioned stakeholders should be addressed if there are changes on the river bed. How much they need to be directly involved in the project varies and is up to the project leader. It is easier to make the best solution on the first try by addressing these groups first.

6.6 The weir

By studying the different results from the physical and numerical modelling, it appears that a hydraulic jump is induced for every discharge tested. However, the Froude numbers tell that the hydraulic jumps can be improved and optimised to the kayaker's desires. The optimising can be done by placing a weir in the river and decreasing the supercritical water depth.

Because the inlet Froude number determines the outcome of the wave, it is desired to define an interval for the correlating supercritical depth, y_1.

$$
\begin{aligned}
Fr &= \frac{q}{\sqrt{gy_1}} \\
Fr &= \frac{\frac{Q}{y_1}}{\sqrt{gy_1}} \\
y_1 &= \frac{Q}{Fr\sqrt{g}}^{2/3}
\end{aligned}
\tag{6.1}
$$

The y_1 is solved for both $Fr_{min} = 2.5$ and $Fr_{max} = 4.5$. Giving an interval for the correlation y_1 shown in table 6.1.

Discharge	y_1 for Fr = 2.5	y_1 for Fr = 4.5
140 m^3/s	0.30	0.20
200 m^3/s	0.38	0.26
289 m^3/s	0.49	0.33
400 m^3/s	0.60	0.40

Table 6.1: y_1 must be inside these intervals for the correlating discharge to induce the desired hydraulic jump.

The height of the weir, Δh is calculated from the conservation energy equation. The intervals of y_1 are used for the different discharges.

$$\begin{aligned} E_1 &= E_c + \Delta h \\ y_1 + \tfrac{v^2}{2g} &= \tfrac{3}{2} y_c + \Delta h \\ \Delta h &= y_1 + \tfrac{v^2}{2g} - \tfrac{3}{2} y_c \end{aligned} \tag{6.2}$$

The critical water depth, y_c, is calculated from eq 3.7. q is found by dividing Q in the channel by the width of the channel, W = 25 m. The results are shown in table 6.2.

Discharge	y_c [m]
140 m^3/s	0.55
200 m^3/s	0.70
289 m^3/s	0.90
400 m^3/s	1.11

Table 6.2: The critical water depth for the different discharges

The equation for Δh 6.2 is solved with the minimum and maximum value of y_1 for each discharge. The results are shown in table 6.3.

Discharge	Δh for Fr = 2.5 [m]	Δh for Fr = 2.5 [m]
140 m^3/s	0.41	1.42
200 m^3/s	0.52	1.81
289 m^3/s	0.67	2.33
400 m^3/s	0.82	2.87

Table 6.3: The interval of the desired Δh for inducing the desired hydraulic jump.

The differences in values of Δh span from 0.41 m to 2.87 m. From 0.82 m to 1.42 m, the weir will, for all the four discharges, induce a hydraulic jump with a Froude number between 2.5 and 4.5.

If the weir is to be constructed in the river, it is desired to make it compatible with the environment. Therefore, the aim should be to use materials that imitate the sediments in the river. These materials will ensure that the changes influence the fish and the ecosystem as little as possible. The river bed's natural environment will be maintained using these materials.

The hydraulic jump over the rock weir could cause erosion and scouring. Therefore this must be taken into account. The USBR report on Rock weir hydraulics and failure mechanisms shows that the primary cause of rock weirs' instability and failure is scouring on the foundation and river bed. (Gordon, 2016) Therefore, it is necessary to calculate the bed shear stress and protect against scouring. Also, the guidelines from NVE regarding the construction of rock weirs must be followed during the design process 3.5

7 Further research

Further research aims to use these results to adjust the river bed as the desired wave is established.

The rived bed should be optimized in the numerical model before the physical model is used as a prototype. Relevant stakeholders should be invited to the laboratory to visualize the new hydraulic jump. It is also necessary to decide whether or not there is a need for new measurements of the water depths.

A hydraulic jump in a river could have side effects when scouring the river bed. Because scouring earlier has shown to be a problem under the Sluppen bridge, this effect must be considered when designing the hydraulic jump. This is done by controlling the bed shear stress the wave applies on the river bed. If the aim is to examine the scouring process, a geometry covered in gravel or smaller, scaled sediments will better understand the process. There must, therefore, be considered how much time is valuable to invest in building the model.

For further research, it would also be interesting to look at other popular parts of the river, like the Sluppen bridge. The idea is that the distance between the bridge piers could be modelled individually and optimized for different discharges. By doing this, there will be a hydraulic jump under the bridge for every discharge in Nidelva.

8 Conclusion

This thesis aims to study the possibility of reconstructing the river's kayak wave in The Drop of Death area. After changes in the river bed in Nidelva, due to safety measures due to erosion, two of the popular kayak waves were affected. The study was conducted using a numerical model and a physical model.

A hydraulic jump was induced for every discharge tested for the physical and numerical model. From the different results, it can be summarized by the following; there is an increase in three "kayak-parameters" when the discharge is increased:

- Rougher water surface.
- Height and slope of hydraulic jump. The jump gets higher and steeper when discharge increases.
- Formation of eddies increases as discharge increases.

The Froude number varied depending on the discharges but was satisfying for Q = $140 m^3/s$.

The decided solution is to design a weir to achieve a wave with the desired Froude number. The calculated weir height shows that a weir with a height of $0.82 < \Delta\text{h} < 1.42$ will induce a wave for discharges from Q = 140 m^3/s to 400 m^3/s with a Froude number between 2.5 and 4.5. What should be done next is to measure the current step in the physical and numerical model. The step should be adjusted so that the height is between the minimum and maximum height of the interval inducing the desired hydraulic jump.

References

Asiaban, P., Rennie, C. D., and Egsgard, N. (2021). Sensitivity analysis of adjustable river surf waves in the absence of channel drop. *MDPI.*

Aufleger, M. and Neisch, V. (2018). Stationary surf waves in rivers. *Hydrolink number 2, 2018.*

Babaali, H., Shamsai, A., and Vosoughifar, H. (2015). Computational modeling of the hydraulic jump in the stilling basin with convergence walls using cfd codes. *Arabian Journal for Science and Engineering.*

Bayon, A. and López-Jiménez, P. A. (2015). Numerical analysis of hydraulic jumps using openfoam. *Article in Journal of Hydroinformatics.*

Borman, D., Sleigh, A., Coughtrie, A., and Horton, L. (2014). Hydraulic free-surface modelling with a novel validation approach. *White Rose Resaerch Online.*

Chow, V. T. (1959). *Open-channel hydraulics.* Kogakusha Company, LTD.

Christodoulo, G., Papathanassiadis, T., Georgakopoulou, C., and Kapetanaki, M. (2004). Physical vs. mathematical modelling of the canoe kayak slalom watercourse for the athens 2004 olympic games. *National Technical Uniervsity of Athens.*

Famiglietti, J. (2010). Kayaking-surfing wave for a wide range of flows. Master's thesis, Universita di' Pisa.

Fang, Y. and Jawitz, J. W. (2019). The evolution of human population distance to water in the usa from 1790 to 2010. *Nature Communications.*

Fuchs, H. (2017). Effect of adjustable flaps on river surf waves at abrupt drops. *ETH Zürich.*

Fujita, I., Muste, M., and Kruger, A. (1998). Large-scale particle image velocimetry for flow analysis in hydraulic engineering applications. *Journal of Hydraulic Research.*

Gaboriault, D. (2009). Topscholar® vietnamese water puppet theatre: A look through the ages.

Ghaderi, A., Dasineh, M., Aristodemo, F., and Ghahramanzadeh, A. (2020). Characteristics of free and submerged hydraulic jumps over different macroroughnesses. *Journal of Hydroinformatics.*

Gordon, E. (2016). *Rock Weir Design Guidance.* USBR Technical Service Center.

Heller, V. (2012). Froude similarity. *Comprehensice Renewable Energy.*

Jones, W. and Launder, B. (1973). The calucation of low-reynolds-number phenomena with a two-equation model of turbulence. *International Journal of Heat and Mass Transfer.*

Lane, S. N., Biron, P. M., Bradbrook, K. F., Butler, J. B., Chandler, J. H., Crowell, M. D., Mclelland, S. J., Richards, K. S., and Roy, A. G. (1998). Three-dimensional measurement of river channel flow processes using acoustic doppler velocimetry. *University of Cambridge.*

Lemmin, U. and Rolland, T. (2005). Acoustic velocity profiler for laboratory and field studies. *ASCE*.

Lester, B., Guelph, C. , and Kelly, S. (2012). Whitewater park design principles: An integrated approach for multiple user groups in partial fulfilment of requirements for the degree of master of landscape architecture. Master's thesis, Universita of Guelph.

Martin, S. A. (2019). Surfing the eisbach river wave in downtown munich, germany. *StevenAMartin.com*.

Microsonic (2020). mic+130/d/tc. *Microsonic*.

NEH (2007). Stream hydraulics. *National Engineering Handbook, Part 654*.

Nickel, R. H. (1996). The development of a filming technique for the eskimo roll in kayaking. Master's thesis, University of Manitoba.

NORTEK (2018). Comprehensive manual 2. *NORTEK*.

NVE (2001). Flomsonekartprosjektet flomberegning for nea-nidelvvassdraget. *NVE*.

NVE (2020). Retningslinjer for flomløp til §4-6 og §4-13 i forskrift om sikkerhet og tilsyn med vassdragsanlegg. *NVE*.

Olsen, N. R. B. (2015). Four free surface algorithms for the 3d navier-stokes equations. *Journal of Hydroinformatics*.

Olsen, N. R. B. (2017). *Numerical Modelling and Hydraulics*. Department of Hydraulic and Environmental Engineering, The Norwegian University of Science and Technology.

SurfLakes (2020). Surf lake with five waves prototype. *raisedwaterreasearch.com*.

Sweet, S. (2009). Physical modeling of wave generation for the boise river recreation park in the center for ecohydraulics stream. *Academia*.

TOFA (2021). Nidelva. *Trondheim Omland Fiskeadministrasjons webpage, www.tofa.no*.

Trondheimkommune (2020). Kommunedelplan for sluppen. *Trondheim kommune*.

Walls, M. (2016). Frozen landscapes, dynamic skills: an ethnoarchaelogical study of inuit kayaking enskilment and the perception of the environment in greenland. *University of Toronto*.

9 Appendix

A1 Discharge data the last nine years

			Discharge in Nidelva. Data from Rathe measuring station, NVE							
			All the yellow cells were missing data. "Calibrated" by looking at average values.							
Date	**2011**	**2012**	**2013**	**2014**	**2015**	**2016**	**2017**	**2018**	**2019**	**2020**
1-Jan		46.99	170.38	62.97	40.23	75.77	119.31	37.53	57.99	138.96
2-Jan		97.81	249.66	76.00	69.12	75.33	172.09	91.91	70.04	135.75
3-Jan		84.62	169.91	72.90	64.16	75.48	185.68	79.25	81.55	138.53
4-Jan		87.13	240.15	74.23	64.29	75.77	174.34	105.69	93.90	124.00
5-Jan		89.39	226.20	64.02	130.31	75.62	186.24	91.93	96.79	130.31
6-Jan		87.37	224.19	56.58	101.63	75.91	168.57	80.56	73.60	131.55
7-Jan		94.09	277.75	61.26	125.20	77.97	110.55	62.13	109.85	132.59
8-Jan		97.57	297.05	70.54	97.46	82.97	111.14	68.66	110.79	134.27
9-Jan		145.38	228.37	67.17	110.86	92.41	120.84	70.65	108.50	130.10
10-Jan		158.26	93.72	72.07	100.05	75.48	109.87	115.98	116.68	110.49
11-Jan		160.66	129.10	68.62	99.88	66.95	99.50	119.67	124.80	127.43
12-Jan		128.87	113.81	0.00	121.81	101.98	99.44	118.76	130.87	121.41
13-Jan		96.25	105.83	142.93	147.75	115.20	110.72	89.61	126.97	79.02
14-Jan		76.19	138.77	166.35	126.42	121.81	110.07	65.28	124.65	76.64
15-Jan		94.51	142.59	163.40	95.59	129.48	110.76	65.21	125.70	123.80
16-Jan		133.91	137.95	113.48	90.76	120.63	159.19	79.54	114.98	121.61
17-Jan		135.24	139.40	111.77	90.43	120.43	135.01	95.32	116.36	124.40
18-Jan		117.08	114.14	102.29	90.43	120.82	113.42	112.11	117.88	150.23
19-Jan		101.07	83.51	52.08	122.21	120.23	120.24	118.07	118.44	153.19
20-Jan		98.10	71.59	61.56	112.36	120.63	120.59	110.59	114.79	155.27
21-Jan		46.10	93.20	62.38	122.80	121.61	130.87	111.81	116.44	147.97
22-Jan		48.40	115.10	97.64	132.59	120.04	148.66	123.38	116.37	146.85
23-Jan		109.38	126.14	105.05	123.40	121.41	154.72	117.08	118.41	151.82
24-Jan		117.70	125.74	93.42	90.60	121.02	159.78	66.00	116.48	150.68
25-Jan		105.14	124.45	42.03	98.49	121.61	147.29	71.58	115.71	126.42
26-Jan		80.01	83.23	59.11	88.81	95.08	151.75	108.47	114.02	133.22
27-Jan		123.02	83.46	64.90	84.21	84.21	159.32	100.75	101.08	129.27
28-Jan		90.67	85.00	72.57	78.87	93.57	161.36	68.39	113.58	125.61
29-Jan		72.84	80.00	73.02	77.09	98.66	158.83	73.40	107.79	130.10
30-Jan		118.23	70.62	72.89	83.28	75.33	155.78	103.44	115.71	129.69

Discharge in Nidelva. Data from Rathe measuring station, NVE

All the yellow cells were missing data. "Calibrated" by looking at average values.

Date	2011	2012	2013	2014	2015	2016	2017	2018	2019	2020
31-Jan		140.43	42.20	56.98	71.76	96.09	177.16	81.48	116.51	78.27
1-Feb		149.98	78.81	75.01	71.20	95.93	186.68	73.30	120.51	37.12
2-Feb		162.26	64.92	65.60	87.05	90.27	182.33	110.23	124.14	84.99
3-Feb		158.39	42.69	68.26	120.23	98.15	144.35	102.42	127.24	135.12
4-Feb		142.94	67.30	69.49	139.61	92.41	136.97	93.03	133.10	152.96
5-Feb		76.45	67.00	91.93	110.49	100.58	148.54	121.20	121.59	124.60
6-Feb		134.35	80.00	84.06	74.32	64.16	139.69	125.76	117.64	147.30
7-Feb		159.05	90.00	60.14	38.61	39.08	163.22	125.22	110.28	98.49
8-Feb		155.50	109.25	39.69	61.58	61.58	172.11	130.69	103.58	56.62
9-Feb		139.74	83.30	39.92	79.02	74.03	171.38	82.47	81.33	54.95
10-Feb		132.75	67.68	65.60	72.04	95.25	165.19	86.21	97.32	58.82
11-Feb		79.85	95.54	67.12	73.60	93.57	85.77	81.10	114.38	42.50
12-Feb		51.50	123.23	65.24	98.49	99.53	111.03	84.65	107.87	41.80
13-Feb		97.14	113.95	40.37	83.59	79.92	134.81	123.67	105.05	150.68
14-Feb		86.21	103.33	45.66	80.98	76.79	157.87	127.51	108.29	150.46
15-Feb		63.71	103.52	40.37	46.21	101.45	166.83	79.13	95.11	101.10
16-Feb		118.63	69.56	40.19	66.95	117.70	151.78	125.83	102.63	38.70
17-Feb		95.38	67.38	62.06	73.03	107.18	152.85	137.35	110.29	38.61
18-Feb		42.67	79.40	65.97	67.76	136.81	121.89	112.60	128.42	41.11
19-Feb		40.81	68.00	93.41	71.06	109.20	86.26	140.54	117.98	127.02
20-Feb		75.26	88.45	93.59	72.18	60.31	98.36	146.73	135.42	80.07
21-Feb		90.66	120.88	71.85	76.94	57.10	106.77	143.66	135.49	127.76
22-Feb		77.29	117.21	53.55	76.21	70.22	76.24	139.16	107.23	40.59
23-Feb		80.01	68.43	42.95	82.51	67.76	107.89	126.23	88.81	81.96
24-Feb		78.22	64.02	66.36	75.48	70.22	116.35	84.85	100.10	123.20
25-Feb		81.63	78.05	66.25	73.17	127.23	102.30	84.81	99.72	129.89
26-Feb		81.23	80.03	71.62	67.76	126.82	94.35	125.93	121.84	125.24
27-Feb		137.54	87.22	79.63	67.62	99.18	114.33	127.48	99.01	127.66
28-Feb		130.84	88.05	60.43	54.59	103.93	91.20	132.42	130.51	123.94
1-Mar		148.79	85.00	76.46	36.03	102.69	97.53	141.45	128.00	38.45

			Discharge in Nidelva. Data from Rathe measuring station, NVE							
			All the yellow cells were missing data. "Calibrated" by looking at average values.							
Date	**2011**	**2012**	**2013**	**2014**	**2015**	**2016**	**2017**	**2018**	**2019**	**2020**
2-Mar		141.70	68.04	54.60	64.82	82.20	115.81	137.70	126.93	78.36
3-Mar		138.91	59.05	66.22	67.08	130.51	126.26	103.98	87.23	38.03
4-Mar		130.22	104.49	69.77	68.30	116.35	80.56	88.61	104.86	37.75
5-Mar		132.76	94.22	92.55	79.47	77.23	75.76	131.36	121.15	79.02
6-Mar		137.95	74.43	73.57	78.57	76.21	126.75	131.73	134.04	126.60
7-Mar		135.02	73.45	40.13	40.52	111.61	141.14	131.49	115.67	80.60
8-Mar		138.35	72.76	39.84	42.20	113.87	131.29	109.85	108.18	38.59
9-Mar		152.93	77.00	40.13	72.61	106.27	124.93	79.91	129.98	65.88
10-Mar		125.49	80.00	61.65	71.48	99.53	112.50	77.72	122.83	87.69
11-Mar		99.41	126.78	82.56	87.85	103.04	112.07	47.43	135.28	38.70
12-Mar		136.17	134.85	68.55	95.76	94.91	102.64	104.03	140.76	79.02
13-Mar		148.00	139.00	51.09	66.81	81.28	124.45	115.22	137.07	98.84
14-Mar		133.79	143.68	47.07	56.14	90.27	89.96	130.12	137.28	128.66
15-Mar		150.20	136.57	41.22	59.94	82.20	86.08	118.43	114.78	37.30
16-Mar		158.52	75.12	41.78	59.07	81.59	91.07	103.39	111.63	127.43
17-Mar		154.28	45.97	41.41	76.21	94.57	84.30	80.03	109.45	81.28
18-Mar		143.84	87.43	60.73	103.93	85.46	83.24	79.41	116.96	130.31
19-Mar		149.55	91.66	41.87	93.90	85.31	82.61	112.53	125.65	82.35
20-Mar		155.50	110.64	64.70	90.43	61.71	101.92	115.47	116.06	128.86
21-Mar		161.60	120.87	39.58	48.35	80.82	90.48	102.47	113.19	121.22
22-Mar		167.94	85.00	46.77	63.64	92.08	126.71	95.12	110.32	36.75
23-Mar		178.90	40.34	41.31	72.75	81.74	139.77	106.41	108.67	124.20
24-Mar		187.73	38.52	67.28	78.27	80.37	144.23	44.13	120.02	81.73
25-Mar		184.26	72.59	59.58	89.62	79.47	96.50	42.79	122.04	120.20
26-Mar		190.82	58.30	65.71	80.37	66.95	97.68	79.62	115.39	123.99
27-Mar		202.69	63.93	72.18	92.90	49.12	140.11	74.62	125.31	122.75
28-Mar		331.30	76.30	75.41	78.12	47.06	143.07	80.53	127.95	71.25
29-Mar		389.47	42.28	61.49	62.73	85.94	147.04	51.09	138.27	65.95
30-Mar		300.32	36.34	62.08	80.98	111.24	149.35	40.79	124.77	121.22
31-Mar		287.56	36.81	0.00	80.98	115.58	145.91	38.10	114.95	123.00

Date	2011	2012	2013	2014	2015	2016	2017	2018	2019	2020
			Discharge in Nidelva. Data from Rathe measuring station, NVE							
			All the yellow cells were missing data. "Calibrated" by looking at average values.							
1-Apr		279.43	36.61	126.35	65.35	131.97	125.06	36.03	123.11	123.60
2-Apr		241.38	66.91	109.17	49.12	101.45	129.82	36.13	119.65	142.21
3-Apr		204.03	45.51	117.67	49.45	103.22	151.15	92.63	124.48	143.75
4-Apr		202.28	105.02	90.12	49.67	132.80	136.96	77.91	124.76	115.57
5-Apr		203.68	129.64	74.53	38.89	137.03	118.54	93.60	122.25	119.90
6-Apr		202.48	69.49	78.64	45.26	113.87	135.92	73.65	121.95	144.79
7-Apr		201.16	35.26	88.68	74.18	125.20	148.20	60.19	119.51	89.73
8-Apr		200.85	78.14	69.27	76.64	125.00	144.96	43.40	122.35	81.05
9-Apr		202.98	68.00	43.03	85.94	125.00	102.56	79.59	115.96	117.24
10-Apr		202.21	71.00	105.96	85.94	126.62	110.51	70.83	117.72	103.01
11-Apr		205.97	55.56	92.28	81.59	132.17	121.08	74.31	108.01	123.25
12-Apr		204.30	40.23	49.43	61.45	131.76	133.56	78.12	97.79	126.75
13-Apr		197.32	35.35	42.90	83.12	133.85	135.85	49.06	79.84	41.17
14-Apr		191.59	37.64	68.76	109.57	136.18	138.23	40.92	79.81	123.15
15-Apr		189.45	46.70	79.66	104.83	131.13	143.09	41.99	91.52	150.36
16-Apr		185.48	60.77	86.57	110.68	100.58	145.75	74.42	91.43	162.03
17-Apr		179.67	46.58	59.04	112.17	100.40	144.29	70.95	93.19	156.29
18-Apr		177.33	46.17	67.51	86.57	96.78	138.16	95.83	91.61	159.73
19-Apr		175.69	55.56	59.34	84.52	87.53	131.08	120.54	78.02	161.20
20-Apr		180.24	93.38	39.99	102.69	109.75	128.07	70.90	79.05	163.27
21-Apr		177.77	94.00	61.48	103.22	90.27	133.23	53.06	76.87	163.03
22-Apr		176.90	101.69	65.11	94.74	99.53	148.41	50.77	69.06	158.53
23-Apr		180.26	64.44	75.82	102.16	108.28	147.23	50.40	70.32	116.35
24-Apr		181.58	75.48	107.22	130.51	92.41	148.93	56.75	76.81	160.89
25-Apr		176.75	87.49	95.46	101.80	127.84	149.35	60.08	94.74	159.67
26-Apr		180.07	104.15	77.99	104.65	136.39	149.91	57.37	105.23	169.41
27-Apr		186.26	80.89	59.46	70.50	137.24	150.22	47.83	46.16	166.63
28-Apr		186.99	75.33	61.44	114.63	143.75	149.78	39.55	65.95	162.20
29-Apr		184.33	72.97	110.58	115.01	113.30	145.06	39.20	102.64	163.27
30-Apr		184.82	62.95	139.67	112.36	129.69	140.00	38.60	107.19	163.21

			Discharge in Nidelva. Data from Rathe measuring station, NVE							
			All the yellow cells were missing data. "Calibrated" by looking at average values.							
Date	**2011**	**2012**	**2013**	**2014**	**2015**	**2016**	**2017**	**2018**	**2019**	**2020**
1-May		174.34	57.32	76.61	38.14	113.87	126.15	38.31	79.37	158.68
2-May		163.12	69.81	91.49	38.42	136.81	133.71	47.35	110.01	158.21
3-May		180.20	96.37	78.18	38.42	142.00	133.52	47.74	90.79	161.91
4-May		180.73	99.56	82.80	38.70	145.30	131.08	76.96	72.65	158.03
5-May		171.49	76.42	148.05	37.77	135.12	101.53	73.84	76.30	139.24
6-May		173.40	114.67	144.45	37.58	61.07	74.42	63.74	102.58	72.09
7-May		177.61	115.06	146.24	36.12	65.48	67.75	110.97	102.50	70.24
8-May		179.95	109.24	125.02	44.53	56.98	48.14	143.53	92.55	157.51
9-May		172.94	111.88	107.91	36.66	119.84	38.10	153.47	72.63	154.85
10-May		177.79	88.37	38.81	36.48	105.37	88.79	145.28	65.97	97.75
11-May		184.12	113.94	40.96	51.92	107.18	126.41	153.31	44.80	106.09
12-May		186.24	131.57	39.86	45.89	106.45	105.08	217.30	60.23	101.45
13-May		184.34	141.19	39.85	38.23	63.64	73.29	202.25	136.88	118.67
14-May		178.72	130.75	40.35	37.58	36.39	64.01	182.40	181.40	114.25
15-May		187.75	125.58	39.65	37.21	36.48	104.95	176.46	138.64	113.87
16-May		183.26	112.01	69.22	37.12	36.12	79.33	140.79	177.68	103.58
17-May		179.93	126.15	40.74	37.77	82.04	103.09	113.70	177.92	102.87
18-May		186.65	132.59	40.71	76.35	97.63	103.19	82.26	178.42	144.63
19-May		187.63	120.00	41.52	60.69	164.70	122.64	37.90	178.96	141.34
20-May		184.14	134.14	99.35	70.22	159.47	89.76	37.67	178.60	145.74
21-May		173.41	153.11	64.67	62.99	142.43	101.54	37.60	172.60	132.59
22-May		180.76	138.89	101.54	42.30	137.67	162.24	60.78	177.69	163.74
23-May		182.14	181.83	175.76	37.67	150.23	172.95	58.85	183.95	164.94
24-May		181.02	170.55	194.66	37.30	173.51	173.28	37.58	202.75	159.00
25-May		179.27	49.64	188.13	38.89	175.25	176.35	37.62	194.87	161.83
26-May		182.75	41.41	194.50	79.17	175.75	176.96	37.81	187.86	173.51
27-May		183.80	130.19	191.35	96.09	171.03	171.67	38.53	175.71	171.28
28-May		183.49	124.17	179.49	102.33	163.74	170.98	67.01	170.13	179.03
29-May		183.49	130.06	145.31	131.34	164.70	176.30	51.82	160.59	178.53
30-May		184.83	96.53	151.95	182.35	157.36	174.63	65.25	129.18	172.02

Discharge in Nidelva. Data from Rathe measuring station, NVE

All the yellow cells were missing data. "Calibrated" by looking at average values.

Date	2011	2012	2013	2014	2015	2016	2017	2018	2019	2020
31-May		176.86	83.19	83.28	188.06	172.76	173.13	38.49	143.79	182.61
1-Jun		184.99	88.69	65.48	197.37	167.85	175.77	38.54	165.84	185.45
2-Jun		182.35	110.00	123.92	205.88	145.08	175.40	38.48	174.96	189.90
3-Jun		184.66	134.05	119.52	207.39	143.31	136.98	38.44	176.66	211.45
4-Jun		186.69	120.00	100.28	207.39	109.20	171.51	38.58	178.03	230.81
5-Jun		186.82	180.00	99.20	208.41	86.09	171.68	38.73	192.11	266.00
6-Jun		183.80	166.54	79.84	208.66	125.00	151.51	62.47	137.03	299.13
7-Jun		185.01	176.61	40.60	209.93	128.45	153.12	67.40	187.82	322.33
8-Jun		180.94	137.63	56.23	207.65	114.06	181.25	70.06	198.10	355.49
9-Jun		159.65	142.82	99.65	203.37	96.95	190.76	38.84	235.44	346.72
10-Jun	130.59	142.62	180.00	96.32	206.38	105.19	195.39	44.70	194.54	342.22
11-Jun	147.8938	158.3223	175.0001	111.8787	210.1793	67.6209	196.8999	45.8935	177.4815	335.9391
12-Jun	157.4316	158.6383	141.2934	131.8321	205.8804	59.18932	198.9242	39.05598	146.9512	329.4064
13-Jun	143.3758	105.981	152.0842	180.24485	208.4055	86.56934	261.7185	45.20669	148.5707	327.6325
14-Jun	138.032	90.0266	137.3394	88.35	205.8804	113.6804	264.5393	38.73746	164.778	329.7025
15-Jun	150.5756	95.30408	137.5348	100.9186	207.6468	113.1136	198.9659	38.69865	147.2221	338.3253
16-Jun	158.6171	58.26321	93.4887	120.7007	206.8891	117.1201	190.4272	34.99877	139.5325	309.4942
17-Jun	154.2872	58.16596	148.0841	115.0336	201.9979	101.4521	190.2724	35.10542	137.8318	183.8964
18-Jun	155.612	134.6365	146.9661	115.3858	205.6283	36.20691	191.5004	35.10694	135.7127	176.5075
19-Jun	154.9937	160.8087	143.2617	94.05741	200.6293	45.88938	203.1353	35.79138	136.9222	172.0193
20-Jun	103.9634	166.2289	161.0244	120.2499	173.2586	104.2909	245.2777	35.30178	76.70632	118.5824
21-Jun	120.2774	160.4335	112.7274	130.226	180.0501	97.97434	242.1385	35.2127	76.91959	134.5614
22-Jun	104.5732	160.7618	43.7314	194.7152	151.3642	105.91	224.4623	36.57292	69.05987	175.0032
23-Jun	91.22121	159.3342	57.98651	212.4526	135.3267	122.0076	197.3537	36.91232	74.86863	163.7438
24-Jun	47.94717	160.6092	97.73023	191.0852	121.8097	65.47798	191.3316	35.92729	103.695	162.549
25-Jun	36.44392	134.8901	100.7297	188.0314	117.5063	48.57248	192.3693	35.61339	115.1931	164.4635
26-Jun	38.5955	141.1483	102.4702	161.8651	134.9034	36.20691	192.0091	35.47562	112.2084	174.0047
27-Jun	38.42062	140.0603	69.16536	158.2642	66.81213	51.46825	190.3507	35.50354	103.6596	137.4146
28-Jun	75.51186	141.9247	69.38992	104.3763	74.75236	109.7508	182.7835	35.84121	114.3462	76.32948
29-Jun	56.01128	158.8484	48.81532	86.90506	130.9259	120.037	169.4858	34.94489	73.1686	127.2284

Discharge in Nidelva. Data from Rathe measuring station, NVE

All the yellow cells were missing data. "Calibrated" by looking at average values.

Date	2011	2012	2013	2014	2015	2016	2017	2018	2019	2020
30-Jun	60.34646	186.291	39.66241	128.8568	156.1943	99.52959	166.5461	36.53848	74.34991	44.63623
1-Jul	61.53571	184.799	39.58435	131.1714	134.0597	61.96206	136.8674	36.49712	132.2026	80.67258
2-Jul	72.44157	185.4756	39.44495	140.9983	137.6694	34.51521	116.9852	42.32217	146.9299	118.8647
3-Jul	54.70698	185.8635	39.604	110.1043	137.0278	37.67226	111.8367	41.89508	163.2147	144.1912
4-Jul	60.37477	186.558	40.80012	103.5688	84.99156	55.65841	82.3669	36.16191	162.85	59.18932
5-Jul	74.75828	184.1933	40.04237	71.24954	118.2813	39.94123	80.59277	36.01547	136.8804	60.56544
6-Jul	95.66272	177.481	40.02278	46.42059	138.0981	35.39908	82.21263	36.01719	60.167	103.5765
7-Jul	75.8134	177.8174	40.00594	66.92219	130.9259	35.48821	98.59425	37.18229	47.86504	102.5107
8-Jul	78.09988	182.6703	39.85008	64.978565	90.10705	43.91555	82.49053	37.0422	44.44856	88.6488
9-Jul	76.00266	182.2144	39.40605	77.14	41.40316	35.22117	73.39642	37.01989	73.51324	58.57051
10-Jul	73.90524	157.1977	39.86467	83.25655	51.92347	36.29734	80.68545	36.59879	91.70398	102.157
11-Jul	71.808	160.2442	40.41552	75.10358	121.0197	35.22117	80.37008	37.14003	80.79905	56.90368
12-Jul	69.66836	130.1358	43.49182	87.43328	125.8089	38.89069	79.35316	37.08562	110.1868	103.393
13-Jul	63.86506	77.0619	35.84713	77.92381	142.433	72.60684	103.8056	35.72979	88.54508	102.203
14-Jul	67.94313	54.71947	36.20587	76.55325	146.8547	56.73919	132.096	35.8145	77.83784	59.37579
15-Jul	68.07928	43.13955	46.35138	69.12124	145.5191	36.75198	178.1259	34.99641	81.26117	57.44774
16-Jul	78.19269	49.80587	63.35145	80.27287	157.5923	35.75665	178.4518	35.02771	79.95984	38.07063
17-Jul	53.1909	42.15112	49.99998	71.4945	137.2415	36.93484	120.123	35.02197	80.71294	38.20992
18-Jul	55.32796	41.63733	40.50371	71.46079	70.22382	41.50177	109.0736	35.97312	81.44237	79.09028
19-Jul	66.91962	43.244	40.74649	69.94237	134.2704	40.81428	92.58321	35.37657	80.89768	81.57209
20-Jul	65.73035	43.59245	40.32551	57.06291	145.9634	59.31351	135.1876	35.21566	77.48334	82.04496
21-Jul	100.2761	42.45008	40.02498	48.37417	148.648	63.89989	151.4776	35.51546	55.00454	81.89167
22-Jul	75.41017	42.03166	45.3302	51.17587	141.559	49.2312	126.646	35.98557	71.58698	84.67825
23-Jul	41.74405	43.51318	64.40586	66.94373	87.04642	36.11653	101.0331	35.51495	78.70576	74.32
24-Jul	41.8661	41.76939	55.00002	73.6824	85.62043	44.53277	115.5557	34.4827	68.82882	128.4535
25-Jul	42.03194	41.38191	70.00002	72.56199	61.32477	87.36536	107.3303	34.37861	39.42372	133.8492
26-Jul	41.64978	40.78224	69.34492	69.03593	65.61066	66.00951	62.36384	35.49732	38.39653	71.33888
27-Jul	42.89908	40.56417	46.79082	62.04967	116.158	67.89188	40.50565	35.37775	36.96997	167.8487
28-Jul	41.65969	43.82507	47.00002	37.77647	116.7346	66.94643	46.8066	35.93509	37.30022	100.5753
29-Jul	41.94826	43.24787	77.09181	65.86412	81.73871	67.35061	39.60966	35.83727	37.15257	68.0277

			Discharge in Nidelva. Data from Rathe measuring station, NVE							
			All the yellow cells were missing data. "Calibrated" by looking at average values.							
Date	**2011**	**2012**	**2013**	**2014**	**2015**	**2016**	**2017**	**2018**	**2019**	**2020**
30-Jul	41.51815	43.7693	59.88783	70.9472	59.18932	46.95085	39.89761	35.45375	35.77179	39.94123
31-Jul	40.50788	42.93719	43.46775	95.48539	58.32419	36.84338	68.56427	35.48506	35.49749	40.13418
1-Aug	41.57875	43.32102	70.00002	90.0398	56.61851	93.23631	68.04546	35.66904	35.76913	83.58746
2-Aug	40.49694	40.4898	97.99992	51.85386	55.5391	88.97151	61.51786	35.71116	36.23209	81.12828
3-Aug	65.83951	59.74297	115.4383	74.71657	58.20122	96.7756	36.65099	35.76272	36.23753	84.05373
4-Aug	62.91464	70.29141	116.0001	69.82135	66.54394	122.4042	36.3894	35.79266	36.24814	79.16513
5-Aug	55.00182	68.43465	126.3063	79.64415	92.90369	130.9259	36.80041	37.24075	36.20881	80.97624
6-Aug	60.60752	104.1728	75.61446	83.61204	116.7346	74.17619	36.84382	36.56546	36.1155	134.2704
7-Aug	51.00431	64.88475	83.11551	99.24197	89.45708	68.57248	61.89536	37.69349	36.11274	84.5218
8-Aug	40.26702	97.46478	105	106.6698	39.84494	84.67825	39.35608	36.26247	36.18415	83.89817
9-Aug	68.33261	65.17608	90.00006	73.916745	57.83343	108.6444	35.95045	36.58672	36.29311	125.4053
10-Aug	51.26832	81.03207	67.13046	73.52351	79.91656	128.8634	60.31661	39.72453	36.16433	135.115
11-Aug	47.57393	93.23186	65.00005	61.72363	58.44721	121.8097	35.06934	58.11995	36.06353	137.8835
12-Aug	82.98671	99.96435	85.96115	100.010175	114.0592	78.71644	35.81715	51.55465	39.36272	130.9259
13-Aug	111.8806	123.7269	93.54217	100.635085	107.728	43.60898	36.0104	54.68998	41.82511	40.42477
14-Aug	58.0369	127.7197	100.3632	94.506	88.6488	45.15566	36.09441	52.14032	37.77053	40.42477
15-Aug	71.47831	129.0014	125.3691	96.427415	67.48573	85.30563	36.01727	67.42349	36.41008	39.94123
16-Aug	113.2119	96.19827	97.38522	72.49022	47.59522	105.3684	38.9882	67.78428	36.90944	40.23093
17-Aug	230.2131	142.6405	123.8808	93.69501	63.50922	113.4913	75.72492	64.80598	39.54655	41.50177
18-Aug	387.2766	118.0187	87.60448	78.293725	68.98297	126.2134	49.35663	38.36331	40.05839	41.99739
19-Aug	300.5986	68.41034	102.8593	101.45545	100.0516	118.2813	60.59093	39.09203	39.26142	40.71672
20-Aug	184.9579	76.84515	102.1811	114.50145	126.8218	68.0277	108.7009	52.42814	39.70193	39.26678
21-Aug	178.6312	84.12548	77.15067	67.86059	58.57051	68.98297	123.2224	63.93897	39.57924	41.21707
22-Aug	177.994	80.80614	104.891	72.99952	41.10804	101.2763	125.6314	38.51468	44.39533	41.21707
23-Aug	177.7326	74.6424	98.77859	68.179105	37.57962	105.3684	100.0323	67.9078	37.67792	41.80666
24-Aug	142.8259	98.11723	70.54657	82.476595	94.40662	77.52802	66.22307	79.32025	42.92574	41.79871
25-Aug	147.0656	102.3274	68.43752	58.55971	48.6819	99.18263	103.4384	81.57399	36.43172	41.50177
26-Aug	142.1781	47.48769	117.5699	84.34928	51.12866	100.226	110.7321	144.0176	70.26588	41.40316
27-Aug	150.2279	95.21181	115.3299	79.266165	43.20243	65.87643	101.8703	155.5391	71.21191	85.77819
28-Aug	146.2962	92.68331	114.4875	87.337785	60.18807	70.22382	57.90019	125.4507	64.42937	41.79871

Discharge in Nidelva. Data from Rathe measuring station, NVE

All the yellow cells were missing data. "Calibrated" by looking at average values.

Date	2011	2012	2013	2014	2015	2016	2017	2018	2019	2020
29-Aug	129.1072	103.291	107.9469	74.38059	40.81428	99.18263	103.9837	107.5438	70.09416	126.2318
30-Aug	141.4862	113.5137	84.18835	63.847755	43.50716	96.94634	105.1663	99.56935	71.19189	87.40054
31-Aug	106.1211	89.87687	42.74428	72.89349	103.0427	56.13708	88.37592	103.7632	44.02034	138.9581
1-Sep	76.88383	62.46801	39.01742	64.80701	90.5966	71.33888	81.34883	103.4948	41.07444	124.8013
2-Sep	77.05418	59.1628	76.02242	83.227795	90.43317	91.25191	74.91743	76.14972	64.17339	128.4535
3-Sep	106.7972	67.90741	110.6506	105.61295	100.5753	93.56969	64.40749	93.9763	68.99879	124.6005
4-Sep	78.47836	65.2038	112.3711	109.77575	107.1804	80.82424	96.76829	106.9854	67.24562	84.83474
5-Sep	88.68324	66.89104	103.4031	69.71474	36.02638	116.158	85.43554	108.3019	67.77718	120.8229
6-Sep	91.60629	53.79082	60.76205	48.304245	35.84644	96.09492	76.78152	104.5313	67.05316	82.04496
7-Sep	84.117	56.95033	50.17733	55.68754	61.19775	109.3812	92.33224	68.7487	70.26112	127.4322
8-Sep	105.4602	46.39488	46.16311	56.152995	66.14288	115.9661	71.01698	63.89778	78.77026	41.51072
9-Sep	103.1433	44.1536	114.9999	99.061315	83.12273	123.3993	66.6321	59.60011	75.91404	83.40912
10-Sep	86.13878	61.39132	110.8483	116.13125	121.4142	96.7756	52.43898	68.1589	71.3083	39.48059
11-Sep	60.02385	84.31017	97.54242	93.49975	89.45708	55.18239	61.88329	73.78407	76.2137	82.33509
12-Sep	58.72332	108.7965	94.53282	65.369865	36.20691	119.45	35.92934	50.53721	94.73019	39.98268
13-Sep	59.74618	108.0426	99.41882	67.587735	35.75665	129.2742	38.13765	85.16041	100.0602	39.52839
14-Sep	37.93958	47.07037	57.83985	50.319095	42.79834	120.4295	37.44596	65.01489	112.0812	83.64016
15-Sep	50.50759	52.38402	42.86628	39.177245	35.48821	111.9853	36.07178	39.1974	119.6499	39.48059
16-Sep	44.25276	81.9257	108.2883	71.666025	35.04375	95.92516	36.23925	64.22181	127.8435	44.21832
17-Sep	39.20929	88.54354	69.15188	52.320045	35.48821	60.31373	36.26661	72.30389	147.4098	40.92477
18-Sep	39.90459	105.7912	61.86976	49.219735	36.56971	64.68577	64.51773	65.77522	183.116	41.1188
19-Sep	59.01244	105.3241	61.41108	51.210505	41.00993	91.41628	73.53204	38.87191	193.7142	41.21707
20-Sep	60.02839	129.1531	58.32313	49.422505	40.52188	89.61921	75.81702	45.16571	263.1988	41.65894
21-Sep	60.26088	125.1991	46.76407	42.63857	38.51307	91.08788	67.49462	75.3595	353.2543	41.69954
22-Sep	59.46389	77.52266	40.00769	54.770175	69.53266	91.41628	73.6273	66.00633	227.826	75.76742
23-Sep	60.80795	74.09429	46.32104	61.629645	76.93825	83.89817	75.69841	134.4677	181.5685	41.00993
24-Sep	61.03961	87.88269	68.81107	69.6477225	70.484375	61.32477	62.94359	132.7748	168.4624	107.5452
25-Sep	63.35046	100.9701	85.30698	74.66874	64.0305	44.01809	65.43325	84.75857	163.9875	100.226
26-Sep	86.06546	134.1001	63.10601	68.713005	74.32	63.63931	93.37485	41.95537	149.3465	104.6493
27-Sep	118.837	138.5399	56.32738	66.485915	76.64445	62.60372	89.91859	70.71741	155.5935	104.4701

Discharge in Nidelva. Data from Rathe measuring station, NVE

All the yellow cells were missing data. "Calibrated" by looking at average values.

Date	2011	2012	2013	2014	2015	2016	2017	2018	2019	2020
28-Sep	160.3139	129.5199	39.92516	51.39336	62.86156	35.84644	73.45114	84.41736	128.0389	103.2203
29-Sep	104.2987	56.34596	36.95144	49.84204	62.73264	34.51521	57.8213	60.03149	95.23982	36.11653
30-Sep	118.837	44.38618	59.94334	61.27353	62.60372	36.56971	37.36081	55.14177	128.3285	38.13791
1-Oct	160.3139	62.2177	68.62823	79.148695	89.66916	90.92387	38.29372	81.37995	137.4548	36.84338
2-Oct	150.5482	66.01065	51.18482	83.95971	116.7346	81.43305	37.54262	83.19501	113.1126	63.12021
3-Oct	147.0907	47.36134	47.83727	80.475435	113.1136	71.05908	37.74183	70.06484	99.20478	55.65841
4-Oct	103.3689	65.69069	42.70513	59.3091	75.91307	86.88731	37.84581	93.90003	87.19963	39.2706
5-Oct	80.99451	59.35278	37.12662	55.79523	74.46384	100.226	57.97728	94.58827	117.7392	41.10804
6-Oct	82.02668	98.97784	36.63257	54.83266	73.03275	105.5488	52.36914	82.62222	97.91828	39.17535
7-Oct	78.10229	83.25375	67.13792	70.44202	73.74612	97.6309	47.41592	95.50152	130.0842	79.46512
8-Oct	67.90055	100.2315	56.34986	64.40752	72.46518	78.41827	53.64944	75.25117	125.7022	70.36263
9-Oct	74.02846	94.87755	41.59808	57.315415	73.03275	73.60303	74.37584	80.40168	105.81	104.8288
10-Oct	86.88898	121.4585	38.17788	55.605315	73.03275	113.1136	68.75443	73.03248	103.5972	102.5107
11-Oct	103.8195	149.0565	37.37428	55.203515	73.03275	118.2813	92.74882	75.41003	85.65921	103.3983
12-Oct	146.4165	102.2445	44.20321	58.61798	73.03275	147.3017	64.40886	68.80363	77.25317	105.5488
13-Oct	164.6253	55.33657	37.8664	55.734715	73.60303	148.873	82.24514	39.99804	79.85131	57.34546
14-Oct	180.9582	56.4773	70.00002	71.801525	73.60303	91.41628	72.55064	47.2218	103.6674	105.3684
15-Oct	187.2947	112.2972	50.09594	62.136065	74.17619	35.39908	95.15694	113.2171	125.086	104.4701
16-Oct	187.232	122.5305	37.56169	56.084855	74.60802	35.39908	72.13759	137.9038	117.0998	105.5488
17-Oct	187.1525	109.8936	65.62827	69.90223	74.17619	50.45362	69.13996	132.6705	89.17133	103.7547
18-Oct	186.7852	73.94735	68.22572	71.99657	75.76742	61.19775	71.98201	128.3654	84.2169	104.8162
19-Oct	181.8654	56.00442	93.70792	84.08588	74.46384	59.06517	60.00831	107.8057	55.12186	108.8282
20-Oct	182.2105	75.038	69.18147	71.822655	74.46384	104.6493	53.05086	99.3867	64.49031	126.2134
21-Oct	185.6675	79.6136	79.8424	77.44193	75.04146	86.56934	37.38211	94.49597	84.34946	129.0686
22-Oct	181.5055	100.8654	69.28053	72.81596	76.35139	46.52432	37.3815	113.83	39.68116	128.2487
23-Oct	110.6372	114.8093	61.92474	69.652555	77.38037	44.94744	70.65353	80.12418	66.35686	126.4161
24-Oct	97.48717	135.4098	60.39948	68.30227	76.20506	111.4239	101.2259	89.40498	63.62926	121.217
25-Oct	138.4924	138.9238	64.49306	70.642195	76.79133	117.6996	104.7489	94.05294	51.27393	115.9661
26-Oct	87.41683	132.2146	40.19457	58.41951	76.64445	115.392	108.39	95.6088	39.35507	126.6188
27-Oct	144.5123	128.3018	39.369	58.006725	76.64445	96.43488	112.3822	71.88987	46.24486	129.6859

Discharge in Nidelva. Data from Rathe measuring station, NVE

All the yellow cells were missing data. "Calibrated" by looking at average values.

Date	2011	2012	2013	2014	2015	2016	2017	2018	2019	2020
28-Oct	149.5806	138.3444	42.55049	59.524125	76.49776	56.86016	124.2452	69.76102	83.64712	125.4053
29-Oct	130.4794	127.2255	36.81052	56.28897	75.76742	40.81428	127.1636	69.76379	100.5442	125.6069
30-Oct	125.014	134.2389	39.15812	54.00202	68.84592	64.94923	163.252	64.50734	103.7117	126.0112
31-Oct	64.67223	132.7581	63.67469	69.79388	75.91307	108.2773	185.4637	76.13955	102.181	101.1009
1-Nov	116.32	87.69787	71.96293	73.285475	74.60802	104.1119	174.1575	83.56261	122.1841	99.18263
2-Nov	98.66259	86.76294	66.75414	72.73529	78.71644	99.52959	175.0965	81.93563	128.5078	82.19829
3-Nov	126.0125	89.38644	43.473	63.06634	82.65968	149.5498	177.8767	80.62081	107.63	82.65968
4-Nov	113.7963	81.3766	65.22789	70.77986	80.3695	142.433	178.5812	67.51073	123.6008	68.0277
5-Nov	103.3689	130.2357	81.77343	76.49776	81.12828	82.04496	177.9567	78.43347	141.7242	70.36263
6-Nov	80.99451	131.2017	69.21658	68.84592	81.43305	82.19829	180.8013	128.278	152.5015	39.74889
7-Nov	82.02668	96.71429	80.04256	80.52095	88.16607	147.3017	168.2417	125.9539	149.3226	40.13418
8-Nov	78.10229	110.8084	80.91956	71.47898	83.12273	156.8922	163.4393	129.0596	148.1898	80.52095
9-Nov	100.6753	118.2622	74.24156	70.08531	85.14842	157.5923	137.3887	89.92077	99.5387	71.90061
10-Nov	94.81219	76.02841	77.41164	63.12021	89.13322	156.4266	139.6623	50.09562	107.7145	113.3023
11-Nov	112.962	82.97551	55.15138	73.60303	90.10705	163.2653	98.56346	50.41027	143.8988	140.2547
12-Nov	108.8553	97.43913	72.25795	65.34547	89.61921	152.0481	120.0965	68.18744	104.8521	81.43305
13-Nov	105.7674	114.2583	74.42458	65.34547	89.13322	112.3606	161.2557	98.86663	94.51295	82.19829
14-Nov	101.7301	104.0233	84.29231	63.89989	89.29498	138.0981	170.2643	69.344	104.4398	68.16357
15-Nov	94.05022	54.51012	70.00002	51.80939	87.68504	124.3997	164.7177	69.26009	94.78346	70.22382
16-Nov	117.1226	79.42144	79.48403	43.71105	89.29498	115.201	155.0417	65.26067	78.72626	39.84494
17-Nov	137.6238	77.29297	47.3436	46.31205	87.20586	102.6879	125.0869	63.94046	78.26968	77.38037
18-Nov	125.312	64.64828	80.78501	61.19775	87.20586	102.3338	105.0007	58.93824	128.7026	40.42477
19-Nov	104.4962	68.87987	70.66827	67.48573	87.36536	83.58746	83.68843	91.43212	134.0083	41.40316
20-Nov	111.2014	73.22714	96.15113	66.41003	76.20506	82.50565	117.9313	89.59258	139.8481	101.1009
21-Nov	120.0578	74.33879	78.61456	63.12021	75.91307	85.46286	66.95232	100.1611	96.37873	106.2719
22-Nov	147.4167	96.27689	116.2876	56.49787	75.47638	90.43317	35.42747	99.03478	85.961	146.4086
23-Nov	132.3049	96.76585	99.37876	33.73206	75.76742	100.5753	35.01379	96.89928	62.82869	90.10705
24-Nov	134.6816	131.9624	68.9997	60.06269	76.35139	115.201	34.76006	80.82816	81.3023	141.3412
25-Nov	136.0424	102.5772	117.2312	64.94923	76.20506	119.2547	35.28236	80.85625	101.0333	143.0906
26-Nov	94.85362	125.6787	134.0053	88.16607	76.05904	58.57051	34.75099	92.90765	123.5442	110.3067

Discharge in Nidelva. Data from Rathe measuring station, NVE

All the yellow cells were missing data. "Calibrated" by looking at average values.

Date	2011	2012	2013	2014	2015	2016	2017	2018	2019	2020
27-Nov	95.73508	168.0562	150.5278	83.12273	81.28065	65.34547	34.64537	125.662	109.4322	135.5385
28-Nov	69.60917	143.7022	130.8356	46.95085	79.01534	98.14644	35.24854	77.80421	120.8574	128.8634
29-Nov	127.2671	165.5853	144.0725	68.43609	76.49776	90.43317	34.58306	68.55633	122.2634	70.22382
30-Nov	136.3844	170.1659	143.7205	63.89989	76.64445	89.78168	34.79055	71.97932	106.6253	127.6359
1-Dec	97.4705	166.5558	144.8024	73.03275	78.56734	74.60802	34.60868	49.215	117.4444	71.05908
2-Dec	69.06026	159.9907	162.0802	76.79133	77.67599	120.2332	35.25888	49.31957	137.2803	105.0084
3-Dec	104.2619	194.1425	140.7141	91.74546	76.79133	56.853875	36.91642	68.84853	146.3691	68.43609
4-Dec	67.01762	210.5966	105	98.66374	75.91307	56.20427	36.49547	70.74106	126.309	84.05373
5-Dec	62.14569	173.7773	119.9171	66.14288	76.79133	174.2541	35.84301	80.9313	81.44019	127.6359
6-Dec	120.0617	171.8666	137.2876	69.67059	77.23277	172.2666	35.3443	106.8038	63.37632	83.74265
7-Dec	126.4041	170.987	126.7295	44.32641	79.91656	188.5814	35.52704	61.34646	64.86954	73.88925
8-Dec	123.6833	198.0453	143.7629	68.70918	86.25229	222.48	62.27654	33.44995	60.3894	82.96815
9-Dec	108.8797	210.3695	143	72.89056	87.20586	356.7106	44.28693	35.88132	71.64765	39.2706
10-Dec	90.23199	214.7362	133.3348	65.61066	87.36536	440.0186	60.02134	83.89535	83.05566	79.46512
11-Dec	58.48222	215.1588	89.54771	67.35061	86.25229	310.3638	99.67144	96.10157	69.98458	122.4042
12-Dec	65.86793	215.2679	76.54221	68.43609	86.88731	175.7542	87.05523	98.51196	72.89435	120.2332
13-Dec	112.3796	215.1122	110.0001	64.42312	86.72823	167.8487	77.62434	86.68278	73.40649	81.73871
14-Dec	109.2649	214.0181	90.8745	56.61851	87.52518	172.2666	92.42411	88.68922	63.62318	83.29449
15-Dec	99.48669	259.3051	78.16349	61.96206	87.68504	179.7957	113.8506	55.43665	62.93066	126.2318
16-Dec	110.1231	276.8988	93.27998	68.29974	85.77819	171.0319	110.0766	46.06816	75.24385	141.6048
17-Dec	106.0257	328.4109	120.7231	89.13322	86.09412	122.6029	93.50732	87.28163	82.02698	119.6982
18-Dec	63.49137	335.1811	135	80.06731	85.46286	127.0249	105.5108	73.38405	96.064	107.8811
19-Dec	65.30736	351.2525	125.0372	63.89989	88.00564	149.3239	104.2274	55.80958	106.9122	107.39665
20-Dec	112.8179	323.3957	96.72942	42.19669	88.16607	172.762	114.6963	42.47904	104.8636	106.130125
21-Dec	123.1751	300.0386	65.13891	45.78405	168.824	179.2871	83.57001	64.14357	84.66169	95.3959075
22-Dec	124.4869	281.0396	61.49614	58.81751	149.0984	178.7796	93.29587	61.76575	99.54499	97.47044875
23-Dec	105.503	242.4482	71.34516	56.13708	104.2909	182.6085	62.56898	74.86532	91.49517	94.48280938
24-Dec	85.91233	261.8336	62.18896	57.10248	83.58746	183.1229	68.69249	61.10886	88.22153	91.35216969
25-Dec	52.1257	222.0641	63.87663	62.86156	84.36554	161.8347	68.75052	41.47569	113.6533	102.5027348
26-Dec	38.89078	231.247	78.98951	67.48573	85.77819	127.2284	65.3927	64.22893	100.558	101.5303674

			Discharge in Nidelva. Data from Rathe measuring station, NVE							
			All the yellow cells were missing data. "Calibrated" by looking at average values.							
Date	**2011**	**2012**	**2013**	**2014**	**2015**	**2016**	**2017**	**2018**	**2019**	**2020**
27-Dec	43.64389	233.8362	73.01498	71.33888	75.76742	156.4266	99.82936	64.33672	111.4761	106.5032337
28-Dec	67.55135	251.2778	67.28292	100.9254	75.76742	111.4239	110.2308	71.4937	104.4894	105.4963169
29-Dec	61.57082	189.7752	69.82478	114.2491	75.62181	130.7188	72.64671	64.51422	71.81645	88.65638343
30-Dec	38.42107	171.5142	70.94415	82.35194	75.91307	117.6996	37.53371	68.18186	75.35937	82.00787671
31-Dec	72.84451	170.8795	70.00002	72.04155	76.79133	118.8647	54.96998	65.50175	111.0248	96.51633836

A2 Water depth measurements in numerical model

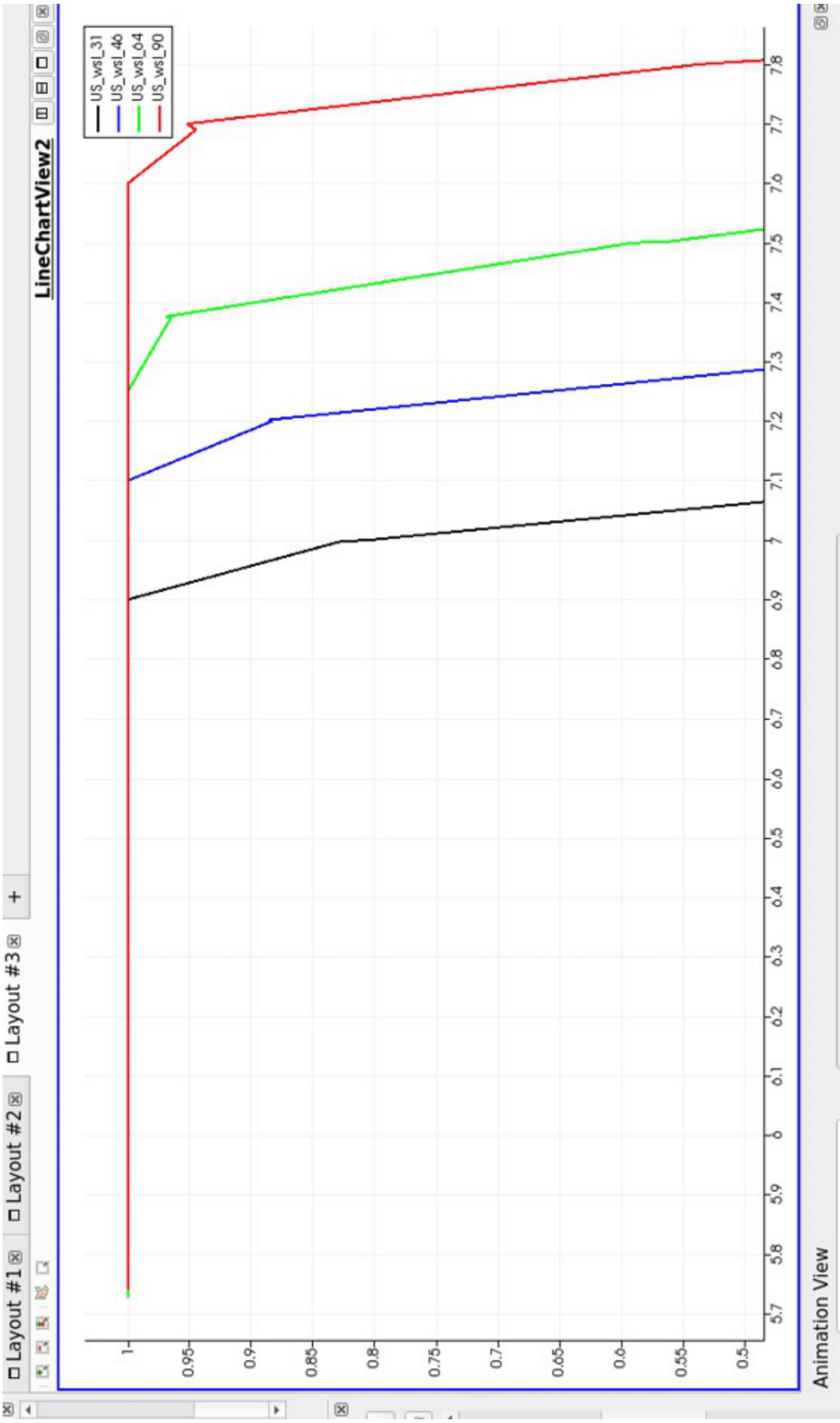

Figure A2.1: Water depth measured at place 1, upstream the jump.

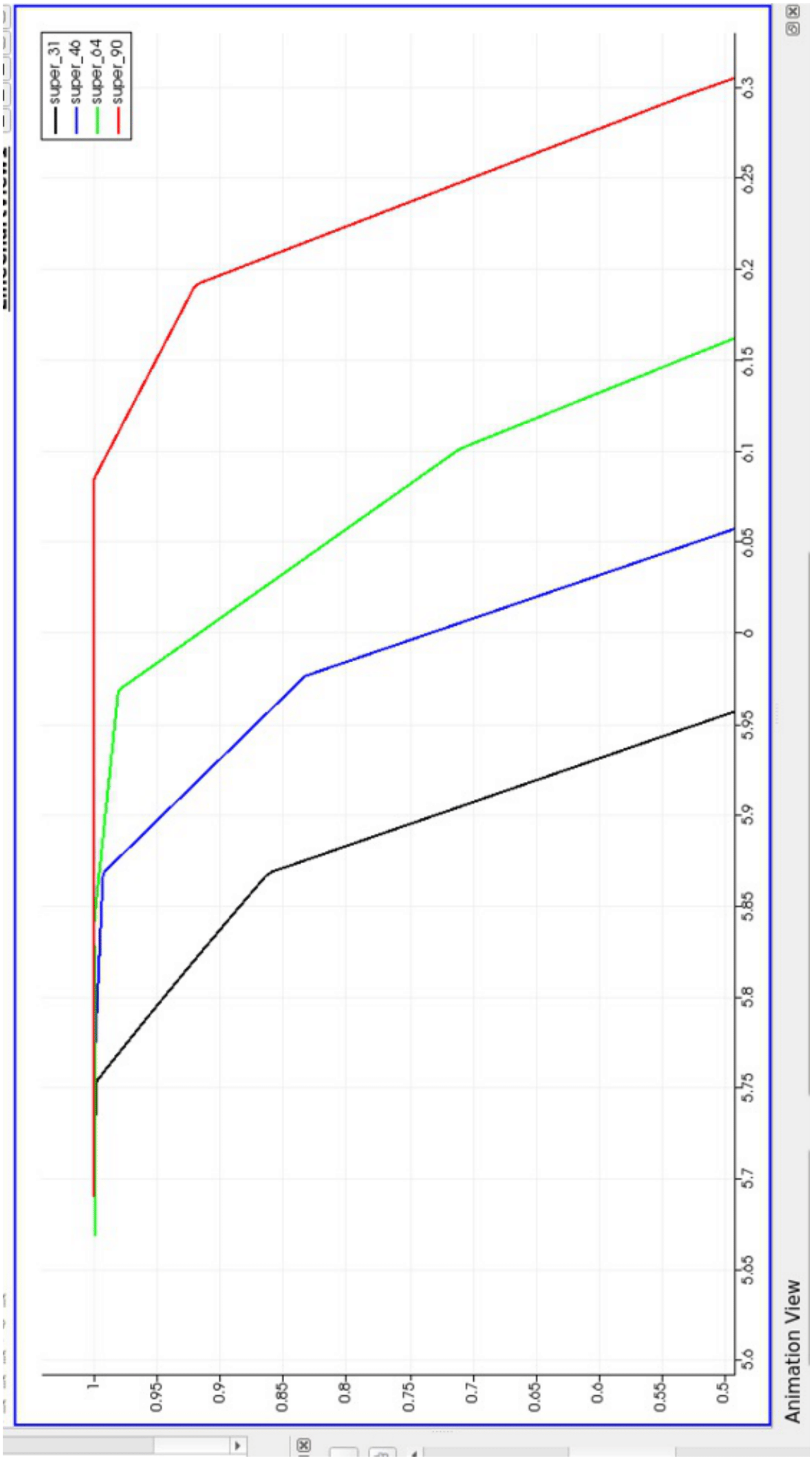

Figure A2.2: Water depth measured at place 2, supercritical.

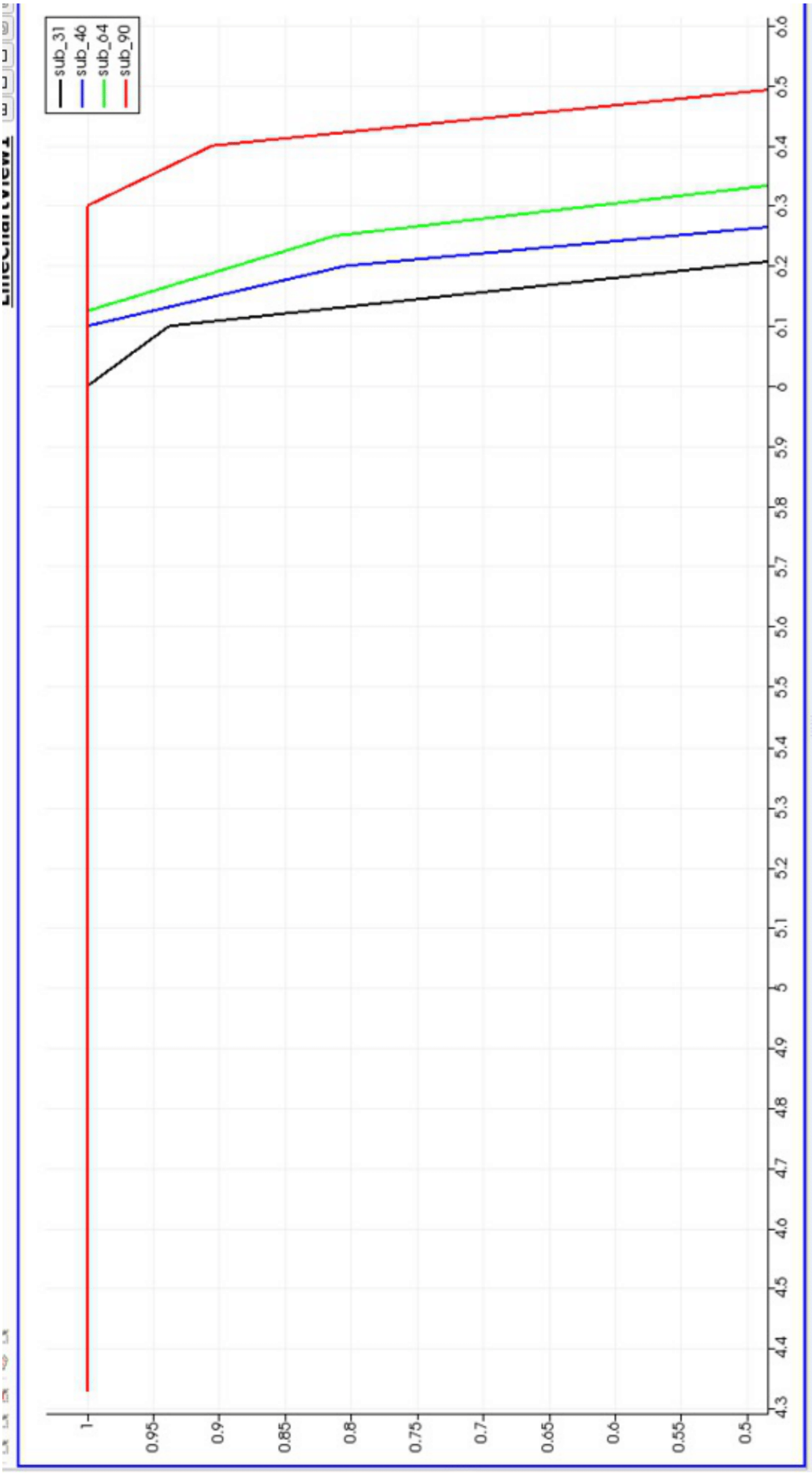

Figure A2.3: Water depth measured at place 3, subcritical.

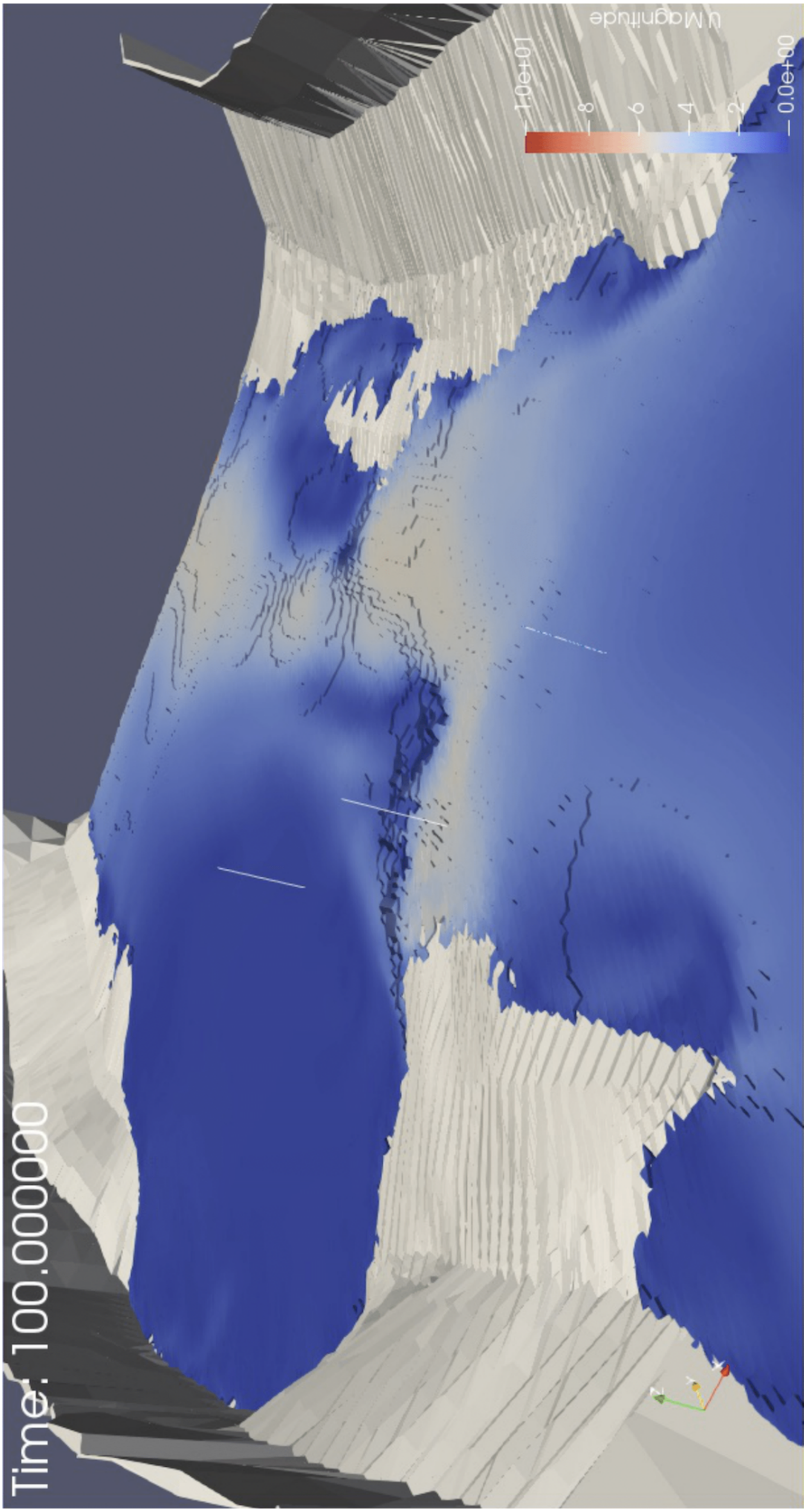

Figure A2.4: Placing for water depth measurements. Seen from upstream; place 1 (upstream), 2 (supercritical) and 3 (subcritical).

A3 Place for slicing the numerical model

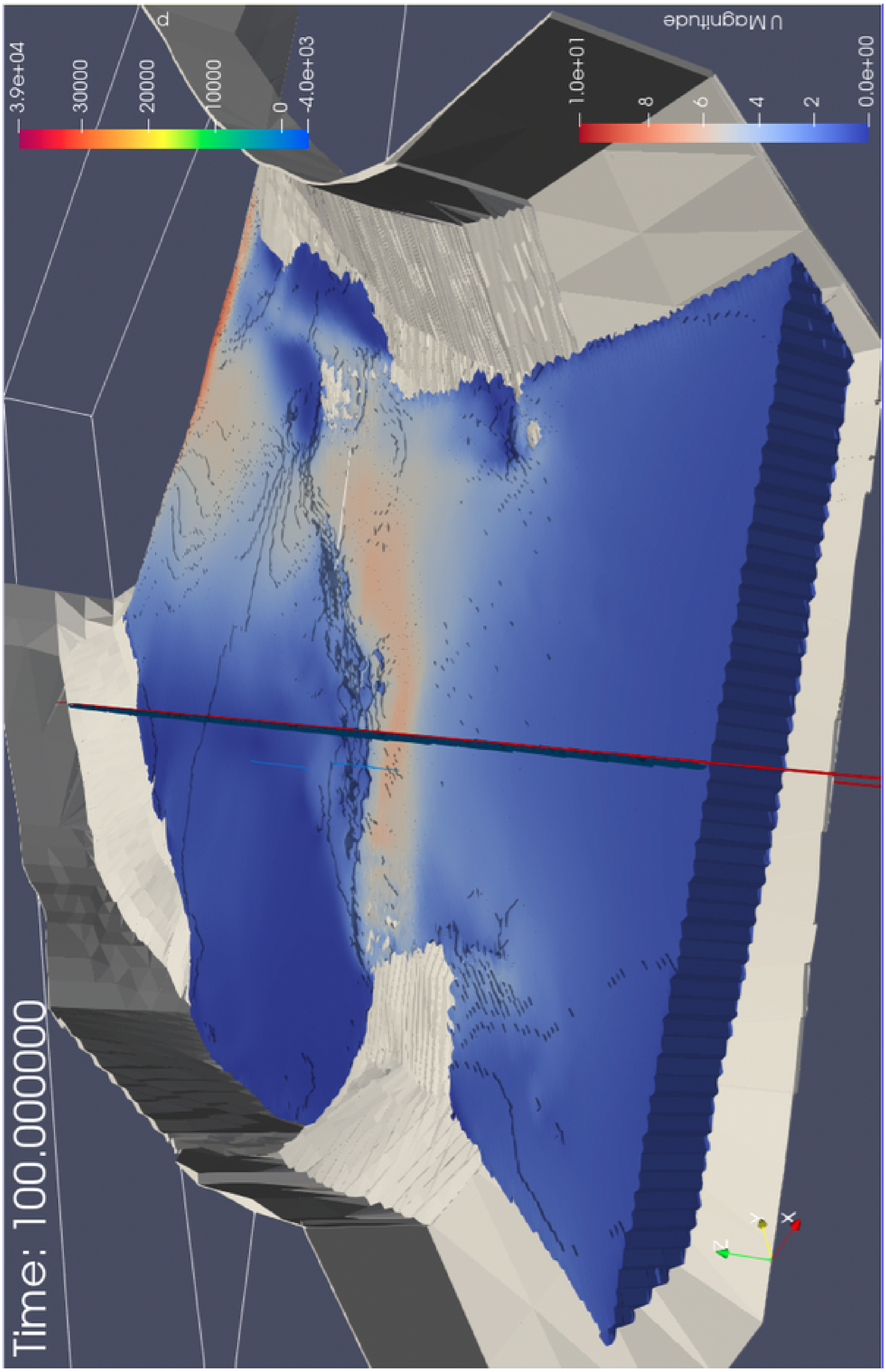

Figure A3.1: Placing for slicing the numerical model to get a view orthogonal on the hydraulic jump

Maren Johanne Mood

Reconstruction of whitewater kayak waves in Nidelva

NTNU
Kunnskap for en bedre verden